Real option analysis in resilient energy networks

Blair, J.W.

2013

MIMS EPrint: **2013.46**

Manchester Institute for Mathematical Sciences
School of Mathematics

The University of Manchester

Reports available from: http://eprints.maths.manchester.ac.uk/
And by contacting: The MIMS Secretary
School of Mathematics
The University of Manchester
Manchester, M13 9PL, UK

ISSN 1749-9097

REAL OPTION ANALYSIS IN RESILIENT ENERGY NETWORKS

A thesis submitted to the University of Manchester
for the degree of Master of Philosophy
in the Faculty of Engineering and Physical Sciences

2013

James Blair
School of Mathematics

Contents

Word count 31113

List of Tables

List of Figures

The University of Manchester

James Blair
Master of Philosophy
Real Option Analysis in Resilient Energy Networks
April 13, 2013

The resilience of future power systems are being challenged in three fronts: (i) decarbonising energy supply will alter supply mix; (ii) shift of previous non-electric demand onto the energy network will require the system to work at higher capacity; and (iii) expected changes in climate will alter demand and performance of electrical network components. This thesis quantitatively assesses the impact of future climate change on the resilience of a power system, in secure and hazardous conditions. This is done through the use of reliability indices and probabilistic security assessment. Dynamical thermal ratings of circuits are used throughout this thesis given their potential for increased capacity over the standard static ratings. The first finding is that the predicted future climate scenarios will result in components with lower thermal ratings then if used currently. Due to this, it is found that the reliability of the system decreases under further climate scenarios. In order to keep a satisfactory level of reliability in the system, a method of temporary overloaded circuits is introduced which doesn't result in a higher risk of component failure. The temporary overload method allows for the rating constraint to be violated provided the temperature constraint isn't. Applying this to the system, and assessing the results under various climate scenarios, it is found that the method is beneficial in terms of economical cost and system reliability. When applied to hazardous conditions, it is found the method has a higher potential to strengthen the reliability of the system in comparison to when used on the 'safe' system.

An approach is taken to aid the system operator in decision making under uncertain conditions. A scenario is devised in which an operator wants to plan the power dispatch for a future time period. This is done through the use of stochastic optimisation, where the uncertainty is encapsulated by the conductor ratings which are calculated using dynamical thermal ratings in which the weather parameters are stochastic. This is developed for a one and two period model, in which the two period model has the first and second period coupled through the addition of a ramp rate constraint in the optimisation. System adequacy indices and probabilistic security indices are added as constraints so the system operator can control the reliability of his system.

Declaration

No portion of the work referred to in the thesis has been submitted in support of an application for another degree or qualification of this or any other university or other institute of learning.

Copyright Statement

Acknowledgements

I would like to thank my supervisor, Dr John Moriarty, for his help and guidance during this project. I would also like to thank other members of the probability group in the School of Mathematics, notably Dr Jonathan Bagley for his many discussions and advice throughout the project. This thesis would not of been possible without the help of them and also fellow members of the RESNET project, all of whom I owe a thank you to. I would especially like to thank Prof. Ian Cotton and Xiaolong Wu for their help with engineering along with Dr Lucy Manning for her help with introducing me to the weather generator and the UKCP09 climate scenarios. Another group of academics I owe a thank you to are to those at the Department of Mathematics at the University of Limerick. It was there I studied my undergraduate degree and where my admiration of mathematics evolved. Had they not been so inspirational then I may not have ended up in Manchester writing this thesis. I would also like to thank the administrative and IT staff in the School of Mathematics at the University of Manchester, whom were always helpful when required.

I would like to thank my parents, and my brother and sister for there support throughout my education, especially through the last few months of this thesis. They have always been there for me through many skype conversations, phone calls, emails and text messages. They have helped me integrate into a new city and country, a journey which would have been a lot more difficult if I didn't have their support to rely on.

Lastly, I would like to thank my friends. For all those who support me back home through phone calls and skype and for all the new ones I've made here in Manchester, in and out of the department. There are too many to name but I'm sure you know who you. You have all made my time here in Manchester an enjoyable one.

Chapter 1

Introduction

1.1 Project Information

The research completed for this thesis was for part of a multi-disciplinary project between the University of Manchester and Newcastle University and comprised of members from the School of Electrical and Electronic Engineering (Manchester), the School of Mathematics (Manchester), the Tyndall Centre for Climate Change Research (Manchester) and the School of Civil Engineering and Geosciences (Newcastle) and was funded by the EPRSC and National Grid. The aim of the project is to examine the future of the resilience of Great Britain's electrical energy network [1]. It is believed that the following will be the main obstacles that will need to be examined:

- Policies aimed at reducing GHG emissions through decarbonising energy supply will alter the existing supply mix.
- Decarbonising of the energy system will involve considerable shift of previously non-electric energy demand onto the electricity network with accompanying changes in how much electricity is needed and when it is needed.
- The expected mean changes in climate will alter the electricity demand and performance of electricity infrastructure, and increased severity and frequency of extreme weather events will impact on the electrical network and distribution systems.

To deal with these challenges, the RESNET project has came up with the following work packages (WP):

1) Spatial scenarios of future climate: WP1 will produce future climate scenarios for three key weather variables: temperature, rainfall and wind, where changes in average characteristics can impact on the operational resilience of the network and changes in extremes can impact the infrastructural resilience of the network.

2) Electricity demand and supply scenarios: WP2 will develop electricity demand and supply scenarios, consistent both with the climate change impact scenarios from WP1 and levels of decarbonisation required to meet policy targets.

3) Network performance analysis: WP3 will couple the hazard model from WP1 with demand and supply scenarios from WP2 with a dynamic, spatially explicit, power systems simulation model.

4) Quantified analysis of resilience and the effectiveness of adaptation: WP4 will use the model to quantify the potential impacts of future climate upon the day to day resilience and resilience to extreme events of the overall GB electricity transmission system and case study distribution networks, and to test the effectiveness of a wide range of adaptation options for improving the overall resilience of the energy system.

5) Social responses to adaptation measures: WP5 will assess the impact of the future vulnerability of the network upon organisations and households, taking into account climate change impacts, and consider how these may adapt.

This thesis was part of the work for WP4.

1.2 Background

The study of energy networks is a highly researched area due to our reliance on electricity, and other forms of energy, both commercially and residentially. Given the focus of this project the energy network we will focus on is the electrical energy network, also known as a power system. A power system is a network of electrical components used to supply, transmit and use electrical power. The basic function of a power system is to provide electric energy to its customers at the lowest possible cost and at an

acceptable risk level [2]. As users of electricity we each make up part of that power system and as such we have a reliance on the other sections of the power system to provide us with energy. On the other side of the network energy suppliers also have a reliance on the system as they require their power to be transported to the user when demanded. A resilient network is defined as a network which has the ability to provide and maintain an acceptable level of service in the face of faults and challenges to normal operation [3]. Due to our reliance on energy, and the cost associated with blackouts, it is beneficial, if not necessary, for a power system to be a resilient network.

Since the energy sector became unregulated companies have to compete against each other for market share. While in competition they want to provide the consumer with a low price which still deems the company profitable. To provide a low cost for the consumer they must achieve a low operating cost for themselves. To minimise costs, competitors could minimise the amount invested into power system components and maintenance. However, this would result in a very unreliable power system. On the handy hand, if a power system is over invested, and over secure, money is being spent that necessarily need not be [4].

Reliability has a very wide range of meanings and cannot be associated to a specific definition. As such, we will use the term in a general sense, to indicate the overall ability of the system to perform its task [5].

It is predicted that in the future people will rely more on electrical energy than at current times [6]. This is partly due to the depletion of fossil fuels. Appliances that rely on fossil fuels such as heating and vehicles are being replaced by electrical heating and electric vehicles (EV). To cope with this increased demand measures should be taken to increase the capacity of the power system. One method would be to purchase new components. However, this method is quite expensive. Another method that is popular in current research is using dynamical thermal ratings. The term dynamical thermal rating (DTR) is defined as using real time or forecasted meteorological weather conditions to, when favourable, allow more current to pass through a conductor than is previously stated by the static rating [7]. It has been shown that this method can be more efficient and less expensive than other methods examined [8]. As such, we will include dynamical thermal ratings in our modelling throughout this thesis.

As mentioned above, it is expected that energy demand will increase in the future.

This is generally accepted but to what extent is still in debate, and is currently being examined by WP2. The future of climatic conditions, coupled with using dynamical thermal ratings, and the future of demand results in a lot of uncertainty for future power system modelling. Real Option Analysis is defined as decision making under uncertainty [9]. To help us make decisions in these uncertain conditions we shall use quantitative methods.

1.3 Power Systems

As mentioned above, the primary function of an electrical power system is to provide electrical energy to its customers as economically as possibly and with an acceptable degree of continuity and quality. Modern society has come to expect that the supply of electricity is continuous. However, this is not possible due to the random faults of components in the power system.

A power system is divided into three function zones [10]. The functional zones consist of:

1. Generation Facilities.
2. Transmission Facilities.
3. Distribution Facilities.

and can be seen in figure 1.1(a). Generation facilities consist of the generating units in a power system. Transmission facilities consist of the high voltage, long distance, bulk transmission components. Distribution facilities consist of the lower voltage transmission lines, along with the consumer load points. This division occurs because utilities usually divide the power system into these subgroups for the purpose of organisation, planning, operation and analysis.

In system analysis, it is also possible to combine the functional zones into hierarchical levels, shown in figure 1.1(b). Hierarchical levels include the function zone above it. This means that system analysis on the transmission facilities includes system analysis on the generation facilities, and system analysis on the distribution zone includes system analysis all three function zones. The basis of this project is to focus on modelling the transmission network of Great Britain's electrical system. We will

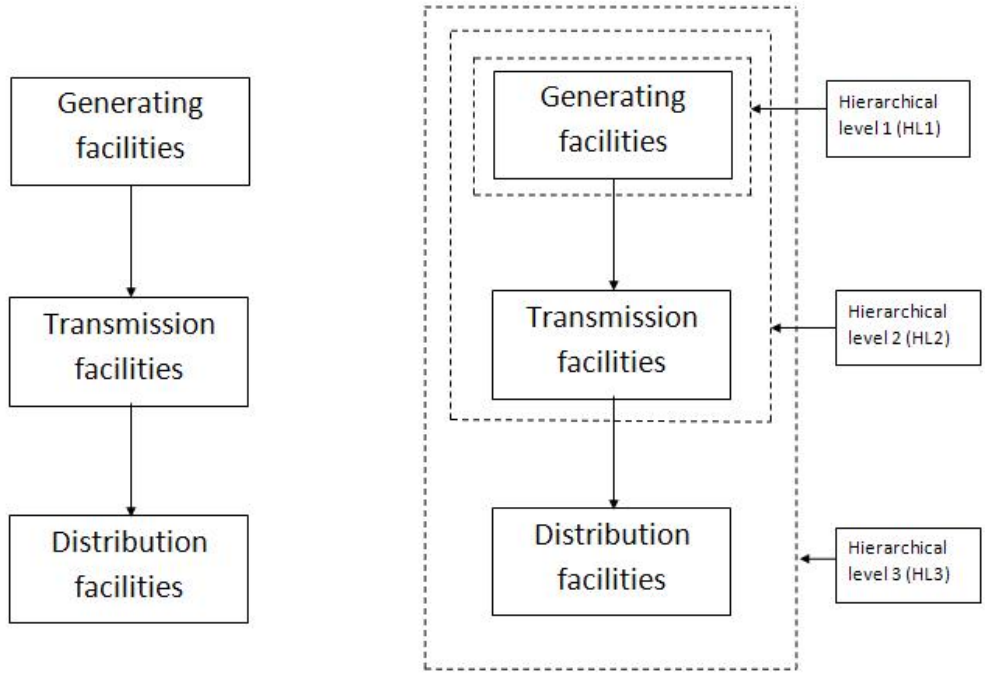

(a) Functional Zone Diagram. (b) Hierarchical Level Diagram.

Figure 1.1: Figure 1.1(a) is the function zone diagram. Figure 1.1(b) is the hierarchical level diagram.

therefore focus on hierarchy level two while assuming adequate generation is continuously available. This is a common assumption made when assessing the transmission network [5].

1.3.1 Optimal Power Flow

The objective of the power system is to transport the required power from the generators to the load points, through the transmission circuits. This is defined as a power flow [11].

The classical optimal power flow is a power flow problem in which certain controllable variables are to be adjusted to minimise an objective function, such as cost of power or power losses, while satisfying physical and operating limits on various controls, dependent variables and functions of variables [12].

An Alternating Current (AC) optimal power flow is defined as:

$$\min_{\underline{P}_g} \sum_{i=1}^{N_B} f_i(P_{gi})$$

subject to

$$\begin{aligned}
P_i = &\quad \sum_{j=1}^{N} |V_i||V_j|(G_{ij}\cos(\delta_i-\delta_j)+ \quad B_{ij}\sin(\delta_i-\delta_j)) \\
Q_i = &\quad \sum_{j=1}^{N} |V_i||V_j|(G_{ij}\sin(\delta_i-\delta_j)- \quad B_{ij}\cos(\delta_i-\delta_j)) \\
P_{gi,min} &\quad \leq P_{gi} \quad \leq P_{gi,max} \\
Q_{gi,min} &\quad \leq Q_{gi} \quad \leq Q_{gi,max} \\
V_{i,min} &\quad \leq V_i \quad \leq V_{i,max} \\
&\quad |F_{ij}| \quad \leq F_{ij,max}
\end{aligned} \tag{1.1}$$

where N_B is the number of buses in the system. $\underline{P}_g$ is the set of generator power outputs with $P_{gi} \in \mathbb{R}^+$ is the power generated from generator $i \in \{1,\ldots,N_B\}$ with $\mathbb{R}^+ := [0,\infty)$. The function $f_i : \mathbb{R}^+ \to \mathbb{R}$ is the cost function for generator i. This function in practice takes the form of either a continuous polynomial of varying degree or a linear piecewise function. $P_i \in \mathbb{R}$ is the real power injection with $P_i = P_{gi} - P_{di}\, \forall i \in \{1,\ldots,N_B\}$, where $P_{di} \in \mathbb{R}^+$ is the demand at bus i. $Q_i \in \mathbb{R}$ is the reactive power injection with $Q_i = Q_{gi} - Q_{di}$, where $Q_{gi} \in \mathbb{R}^+$ is the reactive power output of generator at bus i and $Q_{di} \in \mathbb{R}^+$ is the reactive power demanded at bus i. $V_i \in \mathbb{R}^+$ is the voltage at bus i. $G_{ij} \in \mathbb{R}^+$ is the conductance of the circuit between bus i and bus j. $B_{ij} \in \mathbb{R}^+$ is the susceptance of the circuit between bus i and bus j. $\delta_i \in [0,\pi]$ is the voltage angle at bus i. $P_{gi,min} \in \mathbb{R}^+$ and $P_{gi,max} \in \mathbb{R}^+$ are the minimum and maximum real output power of generator i. $Q_{gi,min} \in \mathbb{R}^+$ and $Q_{gi,max} \in \mathbb{R}^+$ are the minimum and maximum reactive output power of generator i. $V_{i,min} \in \mathbb{R}^+$ and $V_{i,max} \in \mathbb{R}^+$ are the minimum and maximum voltage at bus i. $F_{ij} \in \mathbb{R}$ is the power flow between bus i and bus j. $F_{ij,max} \in \mathbb{R}^+$ is the maximum safe amount of power that can flow through the circuit connecting bus i to bus j. This is also known as the circuit rating. A derivation of (1.1) has been included in appendix B.1.

(1.1) is a non-linear optimisation problem. We want to minimise the sum of the $f_i : \mathbb{R}^+ \to \mathbb{R}$ for $P_{gi} \in \mathbb{R}^+$ for $i \in \{1,\ldots,N_B\}$. The equality constraints in (1.1) are non-linear and the cost function $f_i : \mathbb{R}^+ \to \mathbb{R}$ is generally linear or linear piecewise but can be non-linear also. The inequality constraints consist of $P_{gi} \in [P_{gi,min}, P_{gi,max}]$, $Q_{gi} \in$

$[Q_{gi,min}, Q_{gi,max}]$, $V_i \in [V_{i,min}, V_{i,max}]$ and $F_{ij} \in [-F_{ij,max}, F_{ij,max}]$.

(1.1) is usually solved using iterative methods such as the Newton-Raphson method or Gauss-Seidel method. Power systems can comprise of thousands of buses and circuits and for these (1.1) can be computationally expensive. For this reason linear approximations of (1.1) have been developed which we will discuss further in the thesis, see section 2.2.1.

1.3.2 Per-Unit Systems

Power transmission lines are operated at voltage levels where the kilovolt (kV) is the most convenient unit to use. For large transmissions of power, the units kilowatt (kW), megawatt (MW) or gigawatt (GW) are used. It is easier to express these units, as well as amperes and ohms, as a percent, or "per-unit" of a base or reference value specified for each parameter. The per-unit (p.u.) value of any quantity is defined as the ratio of the quantity to its base expressed as a decimal [13]. For example, consider a base voltage of 400kV, then the voltages 380, 400 and 420kV become 0.95, 1.0 and 1.05 per-unit respectively. Through-out this thesis we will express voltage and power in per-unit, with the base units being 400kV and 400MW respectively.

1.4 Dynamical Thermal Ratings

As mentioned before, one of the constraints in the optimal power flow, (1.1), is the branch flow constraint:

$$|F_{ij}| \leq F_{ij,max} \tag{1.2}$$

with $F_{ij,max}$ as the circuit rating. A circuit rating is the maximum amount of power that can safely flow through the circuit at a given time.

1.4.1 Static Ratings

Currently the National Grid use static ratings [14]. These consists of three ratings for each seasonal period, with spring and autumn sharing the same ratings. The ratings which are specified for each season are the normal (pre-fault), and long term emergency and short term emergency (post-fault). The normal rating is the maximum

safe amount of power which can continuously flow through the circuit. This is specified at 84% of the long term emergency. The long term emergency rating is normally used for 6-24 hours after a fault. The short term rating can be used for time spans of less than an hour depending on the specific conductor, and can be set at 10% above the long term rating.

These ratings are calculated using a very conservative method [15]. This is done to obtain a low probability of faulting via voltage overload or thermally overheating. When a component overheats it can sag and this could result in flashover with trees or similar objects and would cause a fault. If a component sags too low it wouldn't meet the necessary minimum clearance condition and would have to be switched off by the system operator. Overheating can also lead to annealing which over time can damage the conductor to a state of beyond repair which would result in a very high replacement cost. Using this conservative method results in having a power system which is on average under utilised and as a result not economical to its full potential.

In [8] the authors examine introducing using dynamical thermal ratings against other reinforcement alternatives. The motivation behind this paper was the result of [6] which found that an increase in the UK's electricity network capacity was needed in order to meet government regulations. The results concluded that introducing dynamical thermal ratings would have the greatest increase in the capacity of the network, more than doubling that of the static network. It was also the lowest costing solution, with line re-tensions and line replacements as the other options. The weather data the authors used to calculate the ratings was estimated from UK weather data from Valley, Wales.

In [16] the authors examine temporarily overloading the conductor rating by examining its temperature constraint rather than its current constraint. A current violation may not necessarily result in a temperature violation due to the time lag of the conductor's temperature, as defined by the thermal time constant. The authors examine this method for a static rating and how the component could be better utilised from an engineering perspective, rather than an economical perspective. In section 2.3.3 we implement this method to a power system using dynamical thermal ratings and examine the potential economical and reliability benefits of using the method in a future power system.

1.4.2 Calculating Dynamical Thermal Ratings

The equation governing overhead line temperature is the steady state heat balance equation [17]:

$$Q_c(\theta_a, \theta_c, W_s, \phi) + Q_r(\theta_a, \theta_c) = Q_s + I^2R(\theta_c) \tag{1.3}$$

$Q_c : \mathbb{R} \times \mathbb{R} \times \mathbb{R}^+ \times [0, \pi] \to \mathbb{R}$ is forced convection, $Q_r : \mathbb{R} \times \mathbb{R} \to \mathbb{R}$ is the radiated heat loss, Q_s is the solar heat gain and $I^2R(\theta_c)$ is the heat gained from the current flow.

$Q_c : \mathbb{R} \times \mathbb{R} \times \mathbb{R}^+ \times [0, \pi] \to \mathbb{R}$ is the loss of heat due to the wind and the ambient air temperature. This function is dependent on the wind speed (W_s), the angle at which the wind meets the conductor (ϕ), and the difference between the conductor temperature (θ_c) and ambient air temperature (θ_a). It is calculated as:

$$\begin{aligned} Q_{cl}(\theta_a, \theta_c, W_s, \phi) &= \left[1.01 + 0.0372\left(\frac{D\rho_f W_s}{\mu_f}\right)^{0.52}\right] k_f K_{angle}(\theta_c - \theta_a) \\ Q_{ch}(\theta_a, \theta_c, W_s, \phi) &= \left[0.0119\left(\frac{D\rho_f W_s}{\mu_f}\right)^{0.6} k_f K_{angle}(\theta_c - \theta_a)\right] \\ Q_{cn}(\theta_a, \theta_c) &= 0.0205\rho_f^{0.5} D^{0.75}(\theta_c - \theta_a) \\ Q_c(\theta_a, \theta_c, W_s, \phi) &= \max(Q_{cl}, Q_{ch}, Q_{cn}) \end{aligned} \tag{1.4}$$

where $Q_{cl} : \mathbb{R} \times \mathbb{R} \times \mathbb{R}^+ \times [0, \pi] \to \mathbb{R}$ is used during low wind speeds, normally less than 1.5m/s, and $Q_{ch} : \mathbb{R} \times \mathbb{R} \times \mathbb{R}^+ \times [0, \pi] \to \mathbb{R}$ is used for wind speeds higher than this. $Q_{cn} : \mathbb{R} \times \mathbb{R} \to \mathbb{R}^+$ is used in zero wind speed conditions and is the natural convection. D is the diameter of the conductor, ρ_f is the density of air, μ_f is the dynamic viscosity of air, k_f is the thermal conductivity of air, K_{angle} is the wind direction factor.

$Q_r : \mathbb{R} \times \mathbb{R} \to \mathbb{R}$ is the radiated heat loss due to the difference between the conductor and ambient temperature.

$$Q_r(\theta_a, \theta_c) = 0.0178D\epsilon\left[\left(\frac{\theta_c + 273}{100}\right)^4 - \left(\frac{\theta_a + 273}{100}\right)^4\right] \tag{1.5}$$

where ϵ is the emissivity of the conductor.

Q_s is the solar heat gain which is due to radiation from the sun and is defined as:

$$Q_s = \alpha Q_{se} A \sin\left(\arccos[cos(H_c)cos(Z_c - Z_l)]\right) \tag{1.6}$$

where α is the solar absorbability of the conductor, Q_{se} is the total solar and sky radiated heat flux rate elevation corrected, A is the area of conductor per unit length, H_c is the altitude of the sun, Z_c and Z_l is the azimuth of the sun and the line respectively.

$I^2R(\theta_c)$ is the heat gained from the current I passing through the wire, known as the joule heating effect. $R : \mathbb{R} \to \mathbb{R}$ is the resistance which varies with the conductor temperature.

$$R(\theta_c) = R(\theta_s)(1 + \beta(\theta_c - \theta_s))$$

where θ_s is a temperature in which $R(\theta_s)$ is known, usually specified by the manufacturer of the component and β is the temperature coefficient of resistance and is specified for each type of material (i.e. copper, aluminium etc).

We can now calculate the ratings of a conductor using (1.3). Every conductor has a maximum safe operator temperature. This would be specified by the manufacturer and is based on the chemical composition of the conductor's alloy. Knowing this value, denoted $\theta_{c,max}$, we can calculate $Q_c(\theta_a, \theta_{c,max}, W_s, \phi)$, $Q_r(\theta_a, \theta_{c,max})$ and $R(\theta_{c,max})$. We can then find I_{max} by rearranging (1.3) as:

$$I_{max} = \Big(\frac{Q_c(\theta_a, \theta_{c,max}, W_s, \phi) + Q_r(\theta_a, \theta_{c,max}) - Q_s}{I^2R(\theta_{c,max})}\Big)^{\frac{1}{2}}. \tag{1.7}$$

I_{max} corresponds to the normal rating of the conductor which is safe to be used continuously. Since this is the normal rating, which is 84% of the maximum, we shall denote it I_N, rather than I_{max}.

1.4.3 Previous Research in Dynamical Thermal Ratings

Most of the current literature is focused primarily on examining the dynamical thermal ratings of overhead lines, known as dynamical thermal line ratings (DTLR). Overhead line temperatures are highly impacted by the current weather conditions. This is primarily due to the wind speed and the surrounding air temperature [17]. Although the majority of the work concentrates on overhead lines, a smaller proportion of literature is available on the use of dynamical thermal ratings on other circuit components such as cables and transformers, see for example [18]. For the rest of this thesis we will concentrate only on the dynamical thermal line ratings of overhead lines so this is implied when using the term dynamical thermal ratings.

When considering dynamical thermal ratings we must make a realisation about the design and operation of a power system. Design and operation require two very different perspectives. The designer is concerned on economic optimisation while using averages and expectations of risks and frequencies, of say, a non 100% operational power system. To minimise risks and frequencies he uses static ratings which are quite conservative. The designer is not concerned about the normal conductor conditions but rather the 'worst case', very infrequent occurrences. The operator on the other hand works in real time. He would like to take advantage of the under utilisation that exists in the system due to the use of static ratings. Therefore, to satisfy both parties, methods must be developed that allow the operator to utilise the highest allowable amount of efficiency in the system, while keeping the operational resilience of the system. From a system operators point of view, forecast ratings would be much more beneficial as it would give the system operator time in advance to plan the optimal dispatch and transportation of power in the system.

Real Time Ratings

The following examine using real time weather conditions to calculate dynamical thermal ratings. [19] investigates the critical spans of overhead lines using overhead line temperature measurement apparatus and weather stations located at various distances from the components. Critical spans are defined as the hottest spots in the transmission system and as such these points are used to calculate the circuit ratings. Comparing the results from both measurements, it was found that weather-based ratings were within 7°C of the measured conductor temperatures 90% of the time when the weather stations were in the immediate vicinity of the test span. However, it was shown that this error increased to 17°C if the measurements were made 1 mile away.

In [20] the authors compare weather calculated dynamical thermal ratings with tension-based line ratings. Tension based line ratings are approximated from the conductor sag while the weather calculated line ratings are calculated using weather data read from nearby stations. He concludes that in some instances weather calculated ratings are more accurate while in other instance tension based ratings are more accurate.

In [18] the authors develop their method in [20] by applying dynamical thermal

ratings to various components of the circuits rather than just overhead lines. They develop a software which will output the rating of the entire circuit which comprises of various components.

In [21] the authors develop the methods used in [20] by proposing a more accurate method of measurement. The authors propose a method of using GPS to calculate conductor sag and from this the rating can be calculated. Using the rating they calculate the errors associated with using weather based dynamical thermal ratings. From this they conclude that extremely accurate weather variables are needed as a wind speed error of 0.3m/s can yield a 37% inaccuracy in conductor ratings. Finally, [22] estimates real time environmental conditions from measured conditions. They do this by interpolating the measured weather variables to points on the line away from the measurement apparatus. They do this by using the inverse distance interpolation technique together with two meteorological stations at the end of the monitoring line. The inverse distance interpolation technique is defined as:

$$Z_k = \frac{\sum_i \frac{Z_i}{d_{ik}}}{\sum_i \frac{1}{d_{ik}}} \tag{1.8}$$

where Z_k represents the unknown environment, Z_i represents the known environment d_{ik} represents the distance between locations i and k. The authors concluded that this technique had potential to provide more accurate results than other standard models and were in the process of testing a real time experiment on an actually power system.

Forecasted Ratings

In [23] the authors use sampled weather forecasts to calculate dynamical thermal ratings and assess the accuracy of them. They do this by first predicting the accuracy of the forecasts by using previous forecast data against real time data. They calculate the minimum, maximum, average and standard deviation for each 6 hour time step of the rating forecast. The first results they find are that as time from the reference increases so too does the error of the forecast ratings. They also find that at one point, 18:00hr, which coincides with the highest daily demand, the forecasted minimum thermal rating is below the static rating. Using this forecast the system operator can evaluate the probability of the thermal rating being lower than the static and make control decisions regarding the dispatch of power as to avoid load curtailment. Load curtailment is the

failure of the supplier to meet the full power demands of the consumer.

In [24] the authors use affine arithmetic to obtain bounds for parameters and functions and using these calculate the forecasted dynamical thermal ratings. Affine arithmetic is a development of interval arithmetic but keeps track of the correlations between the input and computed quantities. For an unknown quantity x, its affine arithmetic value $\hat{x}$ is represented as:

$$\hat{x} = x_0 + x_1\tau_1 + x_2\tau_2 + \cdots + x_n\tau_n \tag{1.9}$$

where x_0 is the central value and the x_i's represent partial deviations. The symbols τ_i are call the noise symbols and take a value in the interval $[-1, 1]$. Each τ_i stands for an independent source of uncertainty in the quantity x_i. For example, consider the parameter that represents the emissivity of the conductor, ϵ, in (1.5). This parameter takes a value between 0.23 (new conductor) and 0.98 (old conductor), depending on conductor surfaces, aging and pollutant emission levels [17]. We can write this in affine arithmetic as:

$$\hat{\epsilon} = \epsilon_0 + \tau_{age}\epsilon_{age} + \tau_{pol}\epsilon_{pol}. \tag{1.10}$$

Here τ_{age} and τ_{pol} range in value between $[-1, 1]$ and stand for the uncertainty in the quantity $\hat{\epsilon}$. The authors use this method on the uncertain parameters used in calculating (1.7) and from this calculates a minimum and maximum bound for the ratings. They use extrapolated climate data to calculate minimum and maximum forecasted thermal ratings using affine arithmetic and compares these results to that of interval arithmetic and Monte Carlo simulation. It is found the affine arithmetic is less conservative than using interval arithmetic and less of a computational task than Monte Carlo simulations, given the number of simulations needed to obtain accurate results.

Adaptations and Applications

Adaptations to that of (1.3) have also been developed. In [25] the authors expand the mathematical heat balance equation for modelling conductor temperatures, (1.3), by including the cooling effective of snow and rain. The authors conclude that precipitation does have a significant cooling effect and thus increased ratings with its presence. However, a real world test is necessary to verify this conclusion.

[26] is a study of the effect of wind on the cooling of overhead lines and thus the increase of ratings, in comparison to the wind generation obtained from wind turbines using the same wind data. This study is particularly relevant for overhead lines that connect wind turbines to the grid. These are normally located in windy coastal areas so the variation in the ratings would be large and would fluctuate quite rapidly. It was shown that the overhead lines using dynamical ratings can be significantly overloaded, in excess of 70% of their static rating, by the wind power generated from the same wind. Therefore, the inclusion of dynamical thermal ratings in a power system is highly beneficial.

In [27] the authors do statistical analysis of weather data at 10 different locations to calculate the probability of a conductor rating overheating using the steady state heat equations, (1.3), with the parameters calculated using ieee conductor standard values, as defined in [17]. Given the percent of overheating that occurs, they make a correction for wind speed bias and reassess the ratings using the weather data under this correction, while keeping the probability of overheating fixed to the value found previously. The bias correction they make is that of the anemometer to detect low wind speed thus giving reading of zero wind speeds when it is in fact not the case.

1.5 Power Systems Reliability/Risk

The words risk and reliability often have various meanings and considerable overlap. Previously we defined reliability, from a power systems perspective, as the ability of the system to performs its task. It can be assumed that risk and reliability have identical implications [2]. Higher risk means lower reliability and vice versa. The probabilistic behaviour found in power systems is the root origin of risk. Random outages of system components are outside the control of the power systems operator. Forecasted dynamical thermal ratings are calculated on the basis of predicted weather values which have no certainty of occurrence. This is just to name a few and is not an exhaustive list.

To manage risk we must perform at least the following three tasks:

1. Perform quantitative risk evaluation.

2. Determine measures to reduce risk.

3. Justify an acceptable risk level.

In this thesis quantitative methods are used to examine risk and methods of reducing risk are developed. Justifying an acceptable risk level is outside the scope of this thesis and is part of the work being done by WP5 at time of writing.

System reliability can be divided into the two basic aspects of system adequacy and system security [28]:

System Adequacy: relates to the existence of sufficient facilities within the system to satisfy consumer demand while satisfying operational constraints.

System Security: relates to the ability of the system to respond to disturbances, planned or unplanned, arising within a system.

1.5.1 System Adequacy

To perform system adequacy assessment indices have been developed which help quantify the reliability of the system [29]. Hierarchy level two's indices include:

1. PLC - Probability of Load Curtailment:

$$PLC = \sum_{i \in S} p_i \mathbb{1}_{\{l_i < L\}} \tag{1.11}$$

where p_i is the probability of being in system state i and S is the set of all system states. A system state depends on a combination of the state of each component. A simple component state is either up or down. If up, when using dynamical thermal ratings, we must include at what rating it is working. $\mathbb{1}_{l_i<L}$ is the indicator function and is defined as:

$$\mathbb{1}_{l_i<L} = \begin{cases} 1 \text{ if } & l_i < L \\ 0 \text{ if } & \text{otherwise} \end{cases} . \tag{1.12}$$

L is the demand in the system and l_i is the demand supplied in system state i.

2. EDLC - Expected Duration of Load Curtailment (hr/yr):

$$EDLC = PLC \times 8760 \tag{1.13}$$

given there are 8760 hours in a year.

3. EDNS - Expected Demand Not Supplied (MW):

$$EDNS = \sum_{i \in S} C_i p_i \mathbb{1}_{\{l_i < L\}} \tag{1.14}$$

where C_i is the load curtailed in system i.

This list is not exhaustive. For a full list see [29].

1.5.2 System Security

A measurement of system security is typically to do $N - m$ security assessment [30], where N is the set of components in the system that we are examining. For example N may be the set of transmission circuits in the systems. This is a deterministic security constraint which tests the operation of a power system under fault scenarios by removing m components simultaneously, running an optimal power flow and repeating for every combination of m components in the system. The most common test is a single fault scenario $N - 1$. This involves rerunning an optimal power flow, with a different component removed in each run, and testing that a solution is still available in each run which satisfies the constraints. This method is called the security constrained optimal power flow.

The classical optimal power flow, (1.1), can be wrote in compact form as:

$$\begin{aligned} & \min_{\underline{u}_0} \underline{f}_0(\underline{u}_0) \\ \text{subject to} \quad & \\ & \underline{g}_0(\underline{x}_0, \underline{u}_0) = \underline{0} \\ & \underline{h}_0(\underline{x}_0, \underline{u}_0) \geq 0 \end{aligned} \tag{1.15}$$

with $\underline{f}_0$ as the vector of cost functions with element i corresponding to $f : \mathbb{R}^+ \to \mathbb{R}$ in (1.1). $\underline{u}_0$ are the control variables such that $u_{0,i}$ corresponds to $P_{gi} \in [P_{gi,min}, P_{gi,max}]$. $\underline{x}_0$ as the state variables corresponding to V_i, δ_i, Q_{gi} for all i as described for (1.1). $\underline{g}_0$ are the power flow equality constraints such that

$$g_{0,1} = P_i - \sum_{j=1}^{N} |V_i||V_j|(G_{ij}\cos(\delta_i - \delta_j) + B_{ij}\sin(\delta_i - \delta_j)) = 0$$

$$g_{0,2} = Q_i - \sum_{j=1}^{N} |V_i||V_j|(G_{ij}\sin(\delta_i - \delta_j) - B_{ij}\cos(\delta_i - \delta_j)) = .$$

$\underline{h}_0 \geq 0$ are the inequality constraints corresponding to

$$\begin{aligned} P_{gi,min} &\leq P_{gi} &&\leq P_{gi,max} \\ Q_{gi,min} &\leq Q_{gi} &&\leq Q_{gi,max} \\ V_{i,min} &\leq V_i &&\leq V_{i,max} \\ &|F_{ij}| &&\leq F_{ij,max} \end{aligned}$$

These are all in the pre-fault state, denoted by subscript 0. Security constrained optimal power flow (SCOPF) is denoted by:

$$\begin{aligned} &\min_{\underline{u}_k} f_0(\underline{u}_k) \\ \text{subject to} \quad & \\ &\underline{g}_k(\underline{x}_k, \underline{u}_k) = \underline{0} \quad k = 0, 1, \ldots, N_c \\ &\underline{h}_k(\underline{x}_k, \underline{u}_k) \geq 0 \quad k = 0, 1, \ldots, N_c \end{aligned} \tag{1.16}$$

where the variables are the same as described above for the classical OPF but, for subscript $k > 0$, are in the post-fault state meaning that the parameters and functions with subscript $i = k$ are omitted. N_c is the number of fault cases to be examined. If a system had N circuits, and we wanted to perform $N - 1$ security, then $N_c = N$, assuming a circuit is a single component.

One criticism of this method is that it is time consuming. Assume the running time, T, of (1.15) is proportional to the square of the number of circuits, N, in the system, with proportionality constant one, i.e. $T = N^2$. If running a SCOPF, we must deal with the original N constraints and another set of N constraints for every fault. The total number of constraints for the SCOPF problem is $N + N_c N = (N_c + 1)N$. Under our assumption for running time this translates to $(N_c+1)^2 T$. This means that the running time for SCOPF is $(N_c+1)^2$ times larger than the running time of a basic optimal power flow. Another criticism is that $N - 1$ security treats the probability of occurrence for all scenarios as equal.

Given the above criticisms, and the occurrence of severe power outages, such as that of Auckland, New Zealand which had an estimated cost of $600 million, or the blackout of North America which brought 50 million people to darkness and had an estimated cost of $6 billion, $N - 1$ security has been questioned. At the same time it is recognised that no utility can financially justify $N - 2$ or $N - 3$ security. For these reasons, research has turned towards developing probabilistic system security methods.

Probabilistic System Security

In [4] the authors discuss a method that use indices as a security measure, rather than using deterministic $N-1$ security. They argue that deterministic methods measure performance such as circuit ratings and voltage magnitudes but these reflect severity and not likelihood. Adequacy indices such as probability of load curtailment reflect likelihood, not severity. They argue indices should not only measure probability but also consequence. This consequence takes the form of a monetary value.

In [31] the authors created a security index for the thermal overload of independent conductors. They defined this index as:

$$Risk(I) = \int_{\theta_c > \theta_{max}} P(\theta_c|I) \times \big(\mathrm{Im}_{sag}(\theta_c|I) + \mathrm{Im}_{annealing}(\theta_c|I)\big) d\theta_c \tag{1.17}$$

calling it their "risk" index. $P(\theta_c|I)$ is the probability of the conductor having the temperature θ_c, given the current temperature is I. This probability is calculated using the ambient weather conditions and is defined as:

$$P(\theta_c|I) = \sum_{\underline{z}} P(\underline{z}) \quad \forall \underline{z} \in \{\underline{z} : \theta(\underline{z}, I) = \theta_c\}$$

where $\underline{z}$ are the weather conditions, $P(\underline{z})$ is the probability that the weather conditions $\underline{z}$ occur and $\theta(\underline{z}, I)$ is calculated using the steady state heat equation (1.3). $\mathrm{Im}(\cdot)$ is the impact, which can come from sag or annealing and is denoted by a subscript in each case. This holds a monetary value. θ_c is the conductor temperature and θ_{safe} is the maximum safe operating temperature. I is the current flow through the conductor. They use the equal risk criteria which is setting the risk level equal to the implicity acceptable static risk level. This insures that the overloaded ratings are as safe as the deterministic static ratings. Using the equal risk criteria, (1.7) and (1.17) they obtain ratings that are higher than those of static ratings while having the same level of reliability.

In [32] the authors test the security in stochastic optimal power flows, using the index developed in [31], and another voltage constraint security index developed in [33]. We only mention the voltage constraint and do not go into detail as in subsequent chapters we will be linearising the AC optimal power flow to a DC optimal power flow. One linearisation assumption we make is regarding the voltage. This assumption allows us to neglect the voltage constraint. This is focused more in chapter 2.

For the stochastic system they assumed all bus loads, branch flows and bus voltage magnitudes were normally distributed, as these assumptions were already shown to be reasonably accurate [34]. They calculated the expected value of (1.17) for each branch, ij, over the normally distributed branch flows, where ij is the branch connecting bus i to bus j. They did the same for the voltage constraint developed in [33] but finding the expectation over the normally distributed bus voltages. The two expectations were denoted $RiskC_{ij}(I_{ij})$ and $RiskV_k(V_k)$ respectively. $RiskC_{ij}(I_{ij})$ is calculated as:

$$RiskC_{ij}(I_{ij}) = \int_{-\infty}^{\infty} P(I_{ij}) \times Risk(I_{ij}). \tag{1.18}$$

The same method was used to calculate $RiskV_j(V_j)$. The authors developed an adapted optimal power flow using $RiskC_{ij}(I_{ij})$ and $RiskV_j(V_j)$ as either constraints, or as weighted parameters in the objective function.

Adding $RiskC_{ij}(I_{ij})$ and $RiskV_k(V_k)$ as constraints, (1.1) becomes:

$$\min_{\underline{P}_g} \sum_{i=1}^{N_B} f_i(P_{gi})$$

subject to

$$\begin{aligned}
P_k = &\quad \sum_{j=1}^{N} |V_k||V_j|(G_{kj}\cos(\delta_k - \delta_j) + B_{kj}\sin(\delta_k - \delta_j)) \\
Q_k = &\quad \sum_{j=1}^{N} |V_k||V_j|(G_{kj}\sin(\delta_k - \delta_j) - B_{kj}\cos(\delta_k - \delta_j)) \\
P_{gi,min} &\le P_{gi} \le P_{gi,max} \\
Q_{gi,min} &\le Q_{gi} \le Q_{gi,max} \\
&RiskC_{ij}(I_{ij}) \le RiskC_0 \\
&RiskV_k(V_k) \le RiskV_0
\end{aligned} \tag{1.19}$$

where $RiskC_0$ and $RiskV_0$ are the assumed maximum risk values tolerated by the system operator, $RiskC_{ij} : \mathbb{R}^+ \to \mathbb{R}$ is the current overload risk function and $RiskV_j : \mathbb{R}^+ \to \mathbb{R}$ is the voltage overload risk function. All other functions and arguments in (1.19) are the same as that defined in (1.1). Another method was to sum the last two constraints and make one maximum risk tolerance value:

$$RiskC_{ij}(I_{ij}) + RiskV_j(V_j) \le RiskCV_0.$$

When including in the objective function, the objective function becomes:

$$\min_{\underline{P}_g} \omega_1 \sum_{i=1}^{N_B} f_i(P_{gi}) + \omega_2\Big(\sum_{ij \in N_c} RiskC_{ij}(I_{ij}) + \sum_{k \in N_B} RiskV_k(V_k)\Big) \tag{1.20}$$

where ω_1 and ω_2 are weighting coefficients, N_c is the set of circuits and N_B is the set of buses. This is further developed in [35] by running a security constrained optimal power flow, (1.16) with (1.20) as the objective function. It is found that this method is cheaper than running the classical security constrained optimal power flow and risk based optimal power flow while more expensive than running the classical optimal power flow. However, the extra expense results in a more secure system.

Other methods of probabilistic system security involve using Monte Carlo methods to simulate random outages. A component is generally consider to have two states [29]. A random fault is generated from an exponential distribution with constant hazard rate η. If the fault is in a down state a repair time is generated using constant repair rate μ .

These methods have been developed in various forms when considering probabilistic security assessment. One such method is the development of a weather dependent hazard rate [36]. The authors suggest five weather conditions: 1) normal; 2) thunderstorm; 3) freezing rain/wet snow; 4) high winds; and 5) dry spell followed by fog. The average failure is then adjusted by a weighting factor to obtain a weather dependent hazard rate. In [37] the author introduces a time-varying hazard rate known as the "bathtub curve" which comprises of three stages: an early "infant mortality" stage, a "random" constant hazard rate and an increasing "aging" hazard rate.

The classical optimal power flow has been developed to account for stochasticity in the system. In [36] the authors examine the expected cost of unplanned outages, which they define as the value of security. This method is further developed in [38]. The authors develop an adaptation of the classical optimal power flow called the optimal probabilistic security problem. The objective function is to minimise the expected social cost which is defined as the sum of the expected operating costs, which is effectively the classical optimal power flow, and the expected interruption cost which is a calculated in the same way as the value of security. The constraints in this optimisation are the same as that in (1.1).

1.6 Summary

It has been shown in [8] that dynamical thermal ratings has the greatest potential for future power systems modelling as it can provide over a 120% gain in energy transfer capacity, in comparison to the static rating, at the cheapest installation cost over other alternatives. The benefit of using forecasted ratings to aid the reliability in system operations has been shown in [23]. The system operator can use the forecasted ratings to redispatch power or curtail power if needed in order to avoid a cascading fault. To aid with the expected increase in electricity demand, and the potential benefit that using dynamical thermal ratings has to the system operator, dynamical thermal ratings will be used throughout this thesis when modelling system resilience.

Previously power system reliability modelling used deterministic methods which modelled all scenarios equally and did not account for probability of the scenario occurring. This method has a high level of reliability but also incurs relatively high investment and operational costs [4]. As the power system has shifted from a regulated system to a competitive market environment, probabilistic methods are needed to account for the uncertainty that has become present in the system. Uncertain future climate scenarios, coupled with an expected increase in demand on the system and pressure to utilise more renewable energy, which itself is stochastic, makes the use of probabilistic methods in system reliability assessment appealing.

In chapter 2 we examine the effect of the proposed climate models on the resilience of a power system by performing quantitative risk assessment under various climate and fault scenarios. This is done through the use of adequacy indices as well as economically, through the optimal power flow solution and value of security index. Dynamical thermal ratings are utilised given their appeal in the industry. We shall examine the system security from a probabilistic measure by generating random faults using a time-dependent hazard rate, as in [37], coupled with a three state transition model, which is a development of the two state model by considering the probability of being in a derated state [5]. A method of reducing risk is then devised by implementing the method used in [16] to examine how using temporary overloading of components, which doesn't violate the temperature constraint, can benefit the operational resilience of the power system.

In chapter 3 stochastic optimisation is used as a decision making tool for uncertain future scenarios. The decision we want to make is for the dispatch of generation in a future time period. Given we know the probability of a future set of weather variables occurring, we can calculate the dynamical thermal ratings for discrete values of the weather variable and optimise over them. Choosing a set of ratings implies choosing a generation when running an optimal power flow. We use an adapted optimal power flow as defined in [39] which also considers the cost of interruptible load. Interruptible load is a contract, between a consumer and a utility, for the consumer to reduce their demand with advanced notice if requested and has an associated cost to the utility [40]. We quantify and control the resilience of the system by adding system adequacy and security constraints. This is developed for a one and two period model.

Chapter 2

Investigating the Effects of Climate Change in Power Systems

The objective of work package 4 is to "quantify the potential impacts of future climate upon the day to day resilience and resilience to extreme events of the overall GB electricity transmission system" [1]. We have defined resilience as the ability of the network to provide and maintain an acceptable level of service in the face of various faults and challenges to normal operation. As part of the objective we will first examine if climate change has an impact on the relevant components of the power system under normal operating conditions through the use of dynamical thermal ratings. We then examine how climate change affects the model under hazardous conditions. This is done by simulating random faults. Finally, we implement the temporary overload method to try reduce the effect of climate change on the resilience of the system. We examine resilience through the use of reliability indices and through cost functions, namely the cost of the optimal power flow and the value of security.

2.1 Predicted Climate Change

We can obtain climate change data and predictions from a number of sources but the most consistent information is provided by the Met Office. The Met Office is the United Kingdom's national weather service [41]. The Met Office has been working in the area of climate change for more than two decades. The standard climate change information from the Met Office comes in the form of the UKCP09 climate projections [42]. The

UKCP09 presents probabilities of different future climates. They have classified the future climate into three scenarios: low emissions scenario, medium emission scenario and high emission scenario. Probabilities were created by weighting future climate projections on how well they represent the past climate. They can be seen as the relative degree to which each climate outcome is supported by the evidence available. They provide probabilities of these scenarios for different time periods in the future, up to the year 2100.

There is a weather generator based on the UKCP09 projections [43]. From the weather generator we can simulate hourly or daily data in which we get current variables and future variables. In the case of daily data we are given the minimum and maximum daily temperature while the hourly generated data provides us with the average temperature for each hour. Current variables are the baseline climate conditions and the future variables represent a future climate based on the emission scenario chosen. Throughout this chapter we will examine the effect of all four climates on the power system. The future time period we use is the year 2080 as this was one of the decided time periods for the RESNET project.

Figure 2.1 shows the curves of the monthly cumulative distribution functions, of maximum daily temperature, for one year, taken from one simulation of the weather generator, for the current climate, low emissions scenario climate, medium emissions scenario climate and high emissions scenario climate for the year 2080. From these plots we can see that the UKCP09 anticipate a rise in temperature in the future, for each of the emission scenarios. This can the seen from the right shift of the curve corresponding to the current climate, once for the low emissions scenario, again for the medium emissions scenario and a third time for the high emissions scenario. This rise leads to the need for examination of how future temperature increase will affect the components of the model, and how it will affect the power system economically as a whole.

On a side note, if we were to plot the monthly cumulative distribution functions for the maximum daily temperature, for one year, for all simulations, we would see that there is a lot of uncertainty in the data outputted from the weather generator under the UKCP09 climate models. This would be seen from the slopes of the curves for the emissions scenarios, which would be much more gentle than those of figure 2.1,

Generator	**1**	**2**
Minimum Output (p.u.)	0	0
Maximum Output (p.u.)	12.5	12.5
Cost (£/p.u.)	400	800

Table 2.1: Specifications of the maximum and minimum output of the generators and the cost for generation.

and have a wider range of values which have positive probability.

Given these rises in temperature, we shall investigate the differences between the dynamical thermal ratings of the components using the current climate and future climate scenarios. We will then examine the economical difference these ratings have on an overall power system and the effect the climate models have on the system security.

2.2 Power Systems Model

To investigate the effects of climate change on the transmission components in a power system I have developed a three busbar model, as seen in figure 2.2. In this model, there are three buses, labelled Bus 1, Bus 2 and Bus 3. Buses are nodal points in a power system. All buses are set to 400kV or 1 p.u. Bus 1 and Bus 2 have generators (G) attached. Table 2.1 displays information about the generators. Bus 2 and Bus 3 have loads (L) attached. Load, also known as demand, is a point at which power is taken out of the system. Generators, on the other hand, put power into the system. There are three transmission circuits in the model, labelled circuit one, circuit two and circuit three. The components of each circuit are listed in table 2.2 and are real components as used in the National Grid System [15]. Three busbar system are often used in power system reliability analysis and model testing, as for example in [5] and [4], due to both their simplicity and sufficiency as a model without losing real world characteristics. Three busbar systems are relative simple to understand for a non power systems specialist in comparison to larger systems. Also, the multi directional power flow between buses makes the model a realistic model of a true power system, to the degree of realism that is necessary for this project.

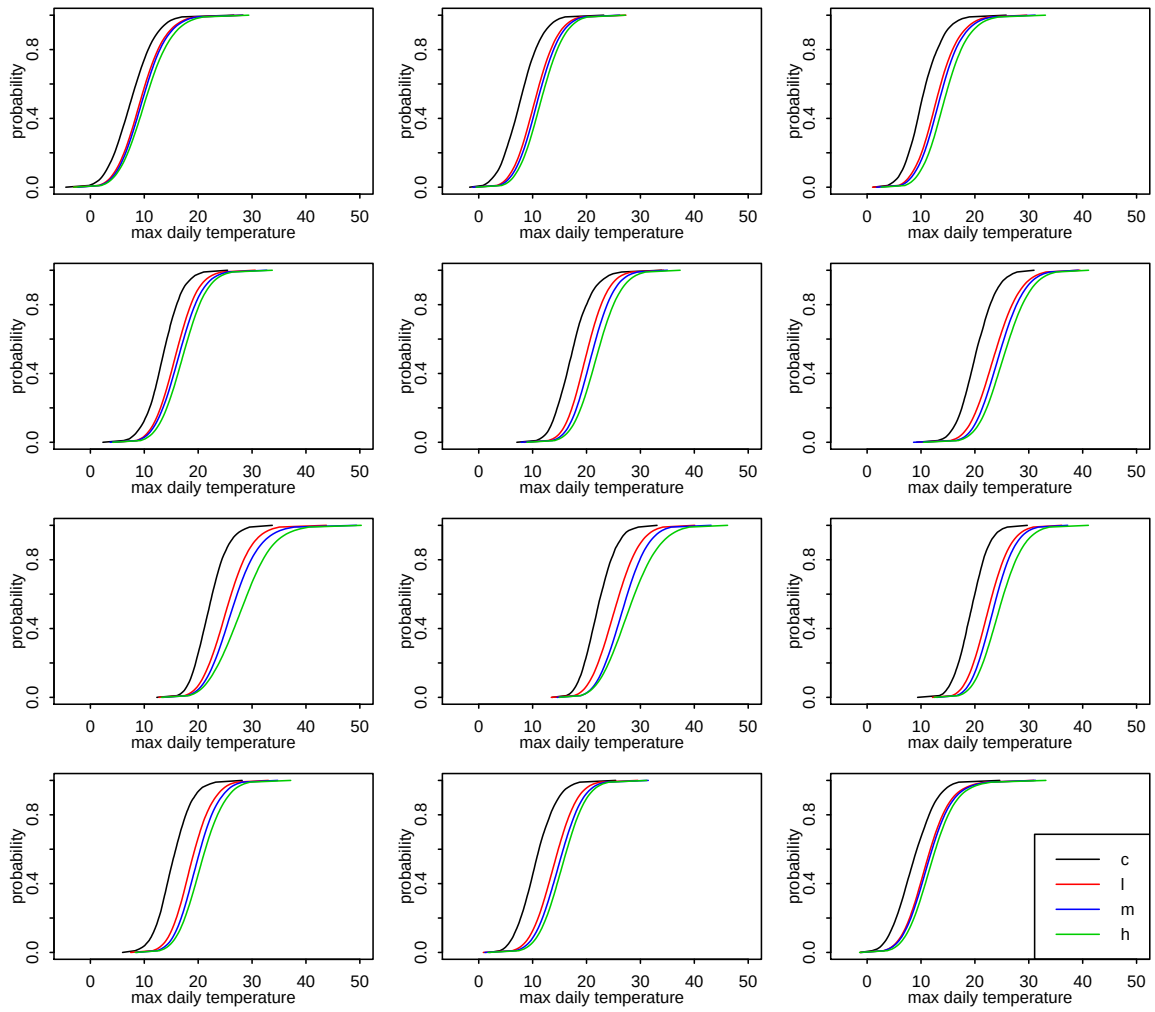

Figure 2.1: Cumulative distribution functions of maximum daily temperature for each month in the year 2080, taken from one simulation of the weather generator. It contains plots of the current ('c') climate, low ('l') emissions scenario, medium ('m') emissions scenario and high ('h') emissions scenario data. Combining one months maximum daily temperature data, and breaking it into 100 evenly spaced centiles, we can obtain a cumulative distribution function for that month for a given year (2080). .

Circuit One	
1	2×400 mm^2 Zebra ACSR OHL
Circuit Two	
2	2×570 mm^2 Sorbus AAAC 30.5n.m OHL
Circuit Three	
3	4×400 mm^2 Zebra ACSR OHL

Table 2.2: Specifications of components used in the model.

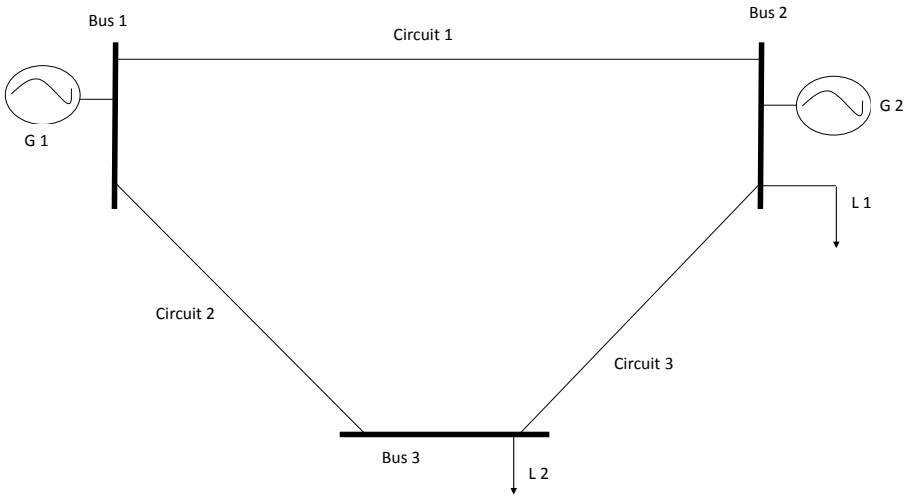

Figure 2.2: Three busbar power flow system. This comprises of three buses, three circuits, two generators ('G') and two load points ('L').

2.2.1 DC Optimal Power Flow

The optimal power flow described in (1.1) is for the full AC power flow which comprises of real and reactive power. This is an optimisation over a non-linear system of equations. To solve these is it necessary to use iterative methods such as the Newton-Raphson or Gauss-Seidel method. These methods can be computationally expensive when converging to accurate solutions, especially for large power systems which are often quite sparse. For these reason we linearise the AC power flow system to a Direct Current (DC) power flow system.

It is acceptable to use DC power flow as all of the reliability indices which we will be examining are associated with real power load curtailments and real power costs. Therefore, calculating these indices only requires real power related information. Power flow calculations in practical application indicate that in many systems there are relatively small (3%-10%) differences between AC and DC power flows. These are small compared to the possible errors due to uncertainties in basic reliability data such as hazard and repair rates [5].

DC load flow is based on the following three assumptions [44]:

- Branch resistances are much smaller than branch reactances, thus we neglect

branch resistances in our calculation. This means we are neglecting real power losses. To do this we set:

$$G_{ij} = 0.$$

in (1.1).

- The voltage angle difference between two buses connected by a line is small so we make the following two approximations:

$$\begin{aligned} \sin(\delta_i - \delta_j) &= \delta_i - \delta_j \\ \cos(\delta_i - \delta_j) &= 0 \end{aligned}$$

where δ_i is the voltage angle at bus i.

- All bus voltage magnitudes are assumed to be constant at 1.0 p.u.:

$$|V_i| = |V_j| = 1$$

Using these assumptions the AC optimal power flow (1.1) is now converted to the DC optimal power flow and takes the form:

$$\begin{aligned} &\min_{\underline{P}_g} \sum_{i=1}^{N_B} f_i(P_{gi}) \\ &\text{subject to} \\ &\qquad P_i = \sum_{j=1}^{N} (B_{ij}(\delta_i - \delta_j)) \\ P_{gi,min} \leq &\quad P_{gi} \leq P_{gi,max} \\ &\quad |F_{ij}| \leq F_{ij,max} \end{aligned} \tag{2.1}$$

$\underline{P}_g$ is the set of generators power outputs, f_i is the cost function for generator i which is linear with no start up cost. The values can be seen in table 2.1. P_{gi} is the power generated from generator i, N_B is the set of buses. P_i is the real power injection with $P_i = P_{gi} - P_{di} \, \forall i \in N_B$, where P_{di} is the demand at bus i. B_{ij} is the susceptance of the circuit between bus i and bus j. F_{ij} is the power flow between bus i and bus j. $F_{ij,max}$ is the rating of the circuit connecting bus i to j. $P_{gi,min}$ and $P_{gi,max}$ are the minimum and maximum generation from generator i. A derivation of the AC power flow equations (1.1), and a more detailed derivation of the DC approximation is included in appendix B. It has been shown in [45] that the DC optimal power flow has a unique solution.

2.3 Simulations

Simulations were performed on a timescale of one year with time intervals corresponding to one hour. These were sampled 100 times for the same year from the weather generator, the year 2080.[1] The weather data used was the baseline (current) climate and the future (low emissions, medium emission and high emission scenarios) climate for the year 2080. The demand data being used is a rescaled version of the 2011 National Grid load profile for the whole of Great Britain [46], adapted to per-unit figures.

A week snapshot of both the weather data and demand data is shown in figure 2.3, as to give some clarity for the reader. We can see that there is quite a difference between the current climate and future climates. Averaged over the simulated yearly data, the mean different between the current climate and low emissions scenario is 2.58°C, between the current climate and medium emissions scenario is 3.38°C, and between the current climate and high emissions scenario is 4.27°C. The average maximum differences between the current climate and the emissions scenarios are 16.61°C, 17.55°C and 18.73°C for the low, medium and high emission scenarios respectively. We can also see the periodicity of the demand data with daytime peaks and nighttime troughs.

We used (1.7) to calculate the dynamical thermal ratings for the simulated climate data, for all three circuits. In modelling all weather variables were kept constant except for temperature. The values used for the constants were those used by the National Grid in calculating their static conductor ratings [15]. This is done as the UKCP09 does not include wind forecasts in the weather generator as they believe the probabilistic projections of changes in wind have too large an uncertainty range. They also state that there is little agreement between different global climate models on the effect global warming will have on wind speeds. Therefore, using the wind parameter that is used by National Grid to calculate the static ratings seemed like the best and the most reasonable conclusion.

The ratings for each circuit for each of the various climates can be seen in figure 2.4.

[1]The 'simulations' correspond to future weather data that is being generated by the weather generated. For each piece of weather data we receive the optimisation computed in (2.1) is the unique solution corresponding to that weather value.

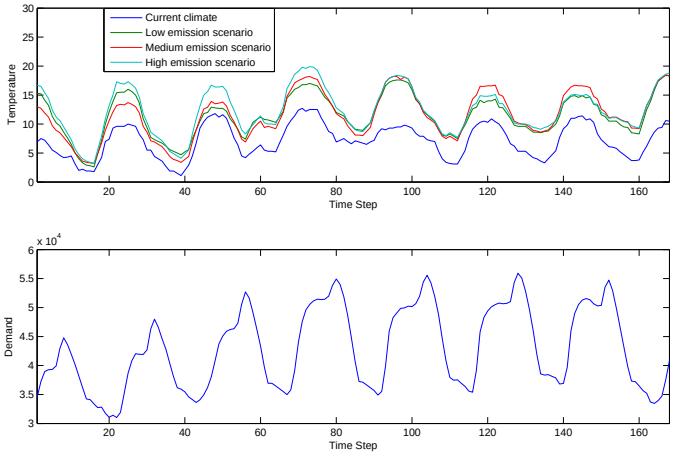

Figure 2.3: The top plot shows the curves of temperature. This is done for the current, low emissions scenario, medium emission scenario and high emission scenario. We can see there is an average rise between the current climate and future climate, with the rise increasing as the emission scenarios increase. The bottom plot shows the daily load profile used in this model. The load profile is a rescaled version of the load profile for 2011 in the National Grid. We can see the periodicity of the demand data with daytime peaks and nighttime troughs.

It can be seen that the current climate, which has lowest temperatures, corresponds to higher ratings. The emission scenarios, which have higher average temperatures, have lower ratings for each of the circuits.

2.3.1 Secure System Simulation

A secure system is defined as one where random component faults are not considered. For each climate: current, low emissions, medium emissions and future emissions, for the year 2080, 100 simulations of each weather data were generated from the weather generator. Each weather data simulation contained 8760 hourly data points so 8760 optimal power flows were calculated for each simulation, with the ratings and load of the optimal power flows varying. This consisted of 876000 optimal power flows, times by four as it was done for current climate, low emissions, medium emissions scenario and high emissions scenario. This simulation is represented by the flow chart as seen in figure 2.5.

Before discussing results we shall discuss the numerical simulation itself. The software used to create this model was Matlab [47]. The simulations were ran using

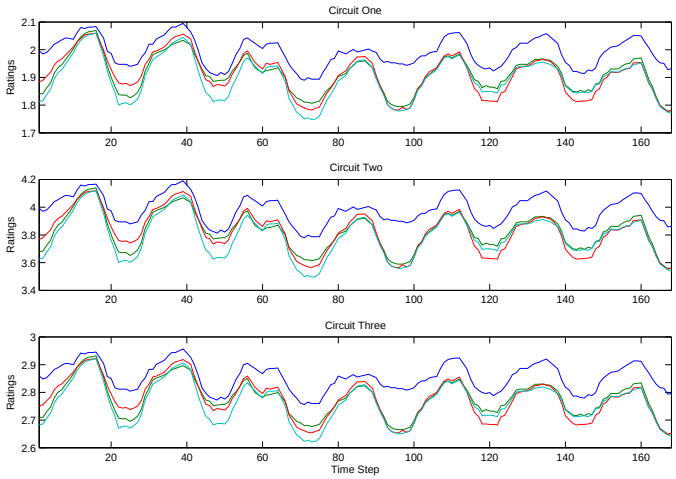

Figure 2.4: This is the plot of the ratings for circuit one, circuit two and circuit three respectively. The top plot shows the curves for circuit one, the middle plot shows the curves for circuit two and the bottom plot shows the curves for circuit three. The colours correspond to that of figure 2.3, with the current climate being represented by a blue curve, the low emissions scenario is represented by a red curve, the medium emissions scenario is represented by a green curve, and the high emissions scenario is represented by a cyan curve.

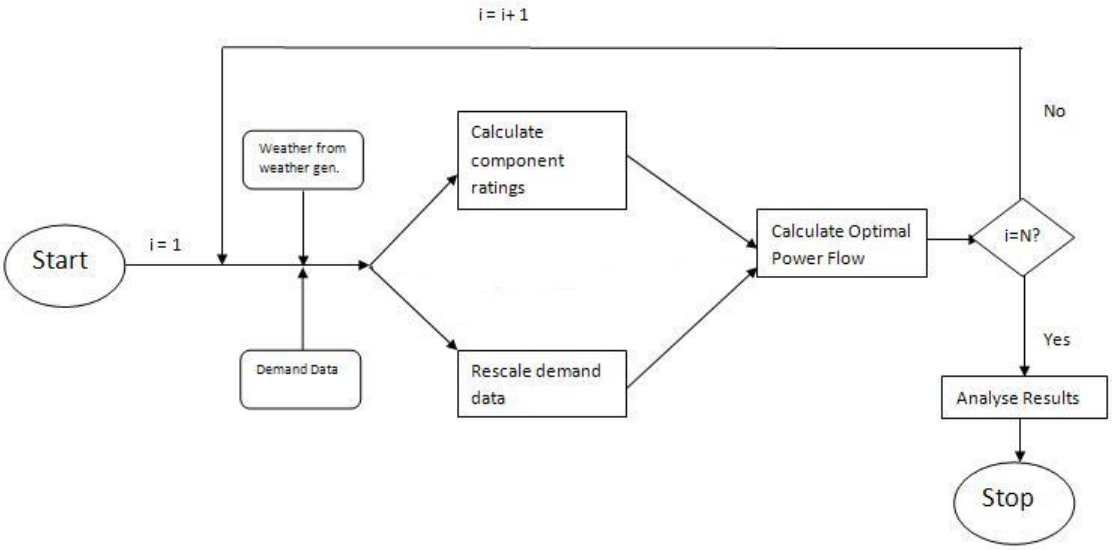

Figure 2.5: Flow chart for simulation as described in section 2.3.1. N is the number of simulations of weather data we want to run and in our case equals 100.

two different methods. The first method was using a package of Matlab M-files called Matpower [48]. The second method was using a built in linear programming function linprog [49].

Using MatPower

Using ratings calculated in (1.7), we call a software package called Matpower. Matpower is a package of Matlab M-files for solving power flow and optimal power flow problems. A formatted M-file is built which contains all the necessary power flow information. Using this file, and the package Matpower, simulations can be run. Matpower returns to the user the optimal power flow. This consists of a summary of how much power flowed through each line, what generation was dispatched from each generator, the voltage angle at each busbar and the cost of the power flow. In the case of load curtailment, using this information, we can calculate how much of the demand was not supplied to each load point.

Using linprog

Matlab requires the linprog function to take the form:

$$\begin{aligned} &\min_{\underline{x}} \underline{f}^T \underline{x} \\ &\text{such that} \\ &\mathbf{A} \cdot \underline{x} \leq \underline{b} \\ &\mathbf{Aeq} \cdot \underline{x} = \underline{beq} \\ &\underline{lb} \leq \underline{x} \leq \underline{ub} \end{aligned} \tag{2.2}$$

where $\underline{f}, \underline{x}, \underline{b}, \underline{beq}, \underline{lb}$ and $\underline{ub}$ are vectors, and $\mathbf{A}$ and $\mathbf{Aeq}$ are matrices. We thus need to transform (2.1) into the form of (2.2), which results in:

$$\begin{aligned} &\min_{\underline{P_g}} \sum_{i \in N_B} f_i(P_{gi}) \\ &\text{such that} \\ &\underline{P} = \mathbf{B}'\underline{\theta} \\ &\underline{P}_B = (\mathbf{D} \times \mathbf{A}) \times \underline{\theta} \\ &-\underline{P}_{B,max} \leq \underline{P}_B \leq \underline{P}_{B,max} \\ &P_{gi,min} \leq P_{gi} \leq P_{gi,max} \end{aligned} \tag{2.3}$$

$\underline{P_g}$ is the set of generators, f_i is the cost function for generator i, which is linear with no start up cost. The values can be seen in table 2.1. P_{gi} is the power generated from generator i, N_B is the set of buses, $\underline{P}$ is the vector of power injections with $P_i = P_{gi} - P_{di} \forall i \in N$, where P_{dk} is the demand at bus k. $\underline{P_B}$ is the vector of line flows. $\mathbf{B'}$ is the nodal admittance matrix. $\underline{\theta}$ is the vector of voltage angles. $\mathbf{D}$ is the adjacency (node-arc) matrix which is a diagonal matrix with element D_{ii} equal to the admittance of line i. $\mathbf{A}$ is the bus adjacency matrix which takes values:

$$A_{ij} = \begin{cases} 1 & \text{if circuit } j \text{ "begins" at bus } i \\ -1 & \text{if circuit } j \text{ "ends" at bus } i \\ 0 & \text{otherwise} \end{cases}$$

A circuit is said to "begin" at bus i if the power flowing across circuit j is defined positive for a direction from bus i flowing to the other nodal bus. A circuit is said to "end" at bus i if the power flowing across circuit j is defined positive for a direction to bus i flowing from the other nodal bus. θ is the vector of bus voltage angles. $\underline{P_{B,max}}$ is the vector of line ratings and is calculated from equations (1.7). $P_{gi,min}$ and $P_{gi,max}$ are the minimum and maximum generation outputted from generator i. All values are adapted to per-unit.

We can change (2.3) into the form of (2.2) by setting:

$$\underline{x} = \begin{bmatrix} \underline{P_g} \\ \underline{P_B} \\ \underline{\theta} \end{bmatrix} \tag{2.4}$$

The cost function $\underline{f}$ is a vector made up of the generator costs and zeros elsewhere. $\underline{b} = \underline{beq}$ and is made up of the demand values and zeros elsewhere, $\underline{lb}$ and $\underline{ub}$ take the same structure of $\underline{x}$ with the minimum and maximum values respectively.

$$\mathbf{Aeq} = \mathbf{A} = \begin{bmatrix} \mathbf{0}_{3\times4} & -\mathbf{I}_3 & (\mathbf{D} \times \mathbf{A}) \\ -\mathbf{C} & \mathbf{0}_{3\times3} & \mathbf{B'} \end{bmatrix}$$

where $\mathbf{D}, \mathbf{A}$ and $\mathbf{B'}$ have been defined previously. $\mathbf{I}_i$ is the identity matrix of square dimension i, $\mathbf{0}_{i\times j}$ is a matrix of zeros with i rows and j columns, and $\mathbf{C}$ is the connection matrix which comprises of zeros and ones, where $\mathbf{C}_{ik}$ is one if bus i has generation/demand point k attached to it, otherwise it is zero. Using this method the

ratings of the circuits can be altered by simply changing the corresponding values in $\underline{lb}$ and $\underline{ub}$ to match the corresponding $\underline{P_B}$ values in $\underline{x}$.

Method Differences

Both methods give relatively the same results with slight numerical errors, less than 3% error. These errors are assumed due to rounding. The computation time differs significantly. To run a simulation of 100 sets of data, with 8760 data points in each set, took over seven hours and thirty minutes using the MatPower approach on an Intel i7 quad four processor at 3.40GHz and 3.23 GB of RAM. This is compared to just under one hour and thirty minutes using linprog on the same machine. This is a massive reduction in computation time for a simulation which depicts similar results. From now on, due to the difference in computation time, we will only use the linprog method.

Indices

There are numerous indices which help us get a better understanding of how well our power system is working, under a variety of weather conditions and faults. We define load curtailment as any power which is demanded by the model but not supplied, i.e. when the full load capacity cannot be delivered. We will examine the following indices in our results:

- **Frequency of load curtailment (FofLC):** is the number of times the full load capacity could not be delivered per year:

$$\text{FofLC} = \sum_{i=1}^{8760} \mathbb{1}_{l_i<L_i} \tag{2.5}$$

  with $\mathbb{1}_{l_i<L_i}$ as the indicator function defined in (1.12), l_i is the load delivered in run i and L_i is the load demanded in run i. Load curtailment may occur due to a circuit having too low a rating or, if random faults are simulated, a component fault. This index is quite vague as it only indicates how often the total demand isn't satisfied. We do not get an idea of whether it was 1% or 100% that was curtailed. We therefore must also consider an index which measures severity, and not just likelihood.

- **Load curtailed (LC):** is the amount of power which could not be delivered in the system as a whole:

$$\text{LC} = \sum_{i=1}^{8760} (L_i - l_i). \tag{2.6}$$

  This index provides us with a better understanding of the overall severity of the load curtailments.

- **Cost of load curtailment (CofLC):** is the cost associated with the demand which is not satisfied.

$$\text{CofLC} = g(LC). \tag{2.7}$$

  where $g(\cdot)$ is a cost function. Load curtailed is approximately a thousand times the cost of production [2].

To examine the model economically we will also include the Yearly Cost (YC), which is the summed hourly cost of each optimal power flow plus the associated value of security. The value of security is equal to the cost of load curtailment [36].

Results

Table 2.3 highlights some of the relevant indices from the optimal power flow simulation, each containing data for current, future low emissions, future medium emissions and future high emissions scenarios for the year 2080. For each climate, a simulation for the 100 data sets were ran. The results not only show the predicted economical cost but also various reliability indices.

For each index, and each climate, there are two numbers. We have both the mean, with the standard deviation in brackets. We can see from these indices that there are substantial increases for the various climates.

Looking first at the frequency of load curtailment, we can see the mean increases over three fold between the current and low emissions scenario climate, almost four fold between the current and the medium emissions scenario climate, and almost five fold between the current and the high emissions scenario climate. Further to this, we can see that the standard deviation between scenarios increases in even larger steps in comparison to the mean. This implies there is more variability in the system concerning future scenarios, with the high emissions scenario having the greatest amount of variability.

Climate:	Current	Low Emissions	Medium Emissions	High Emissions
FofLC	15.14 (3.64)	50.79(15.73)	57.99 (18.19)	70.82 (24.16)
LC [per unit]	1.65 (0.45)	8.68(3.83)	10.38 (4.43)	13.25 (6.11)
CofLC [£M]	0.71 (0.02)	3.55 (.15)	4.81 (.18)	5.38 (.24)
YC [£M]	52.80 (0.02)	55.94(0.16)	56.78 (0.19)	57.97 (0.26)

Table 2.3: This table is a comparison of results between the current climate, the low emissions future climate scenario, the medium emissions future climate scenario and the high emissions future climate scenario. For each index, I have included the mean and standard deviation (as displayed in brackets).

Examining load curtailment we see that the mean amount curtailed between the emission scenarios and the current climate is of a higher multiple than the corresponding difference between frequency of load curtailment values. For example, the frequency of load curtailment between the current climate and high emissions scenario increases almost five fold, while the load curtailment difference between the current climate and high emissions scenario increases over eight fold. This means that in the emission scenarios, on average, load curtailments are more severe than in the current climate. Again, the variability of load curtailment between the future emission scenarios and the current climate increases.

The cost of load curtailment index indicated the same results as the load curtailment index but signifies the monetary value associated to it. The results being that as the emission scenario increase, so too does the mean cost of load curtailment as well as the variability in the index.

Finally we have the yearly cost. This includes the cost of the optimal power flow plus the cost of the load curtailment. There is almost a 6% average increase in the yearly cost between the low emissions and current climate. The medium emissions scenario is on average 7% more expensive than the current climate while there is almost a 10% increase between the high emissions scenario and current climate. Also, the standard deviation increases eight fold, almost ten fold and over ten fold respectively for the low emissions, medium emissions and high emissions scenario climate over the current climate. These results can also be seen in figure 2.6.

From these results we can see the impact the proposed future climate change will have on both the reliability and the economical cost of a power system. To study how climate change will affect the resilience of a power system we introduce random fault

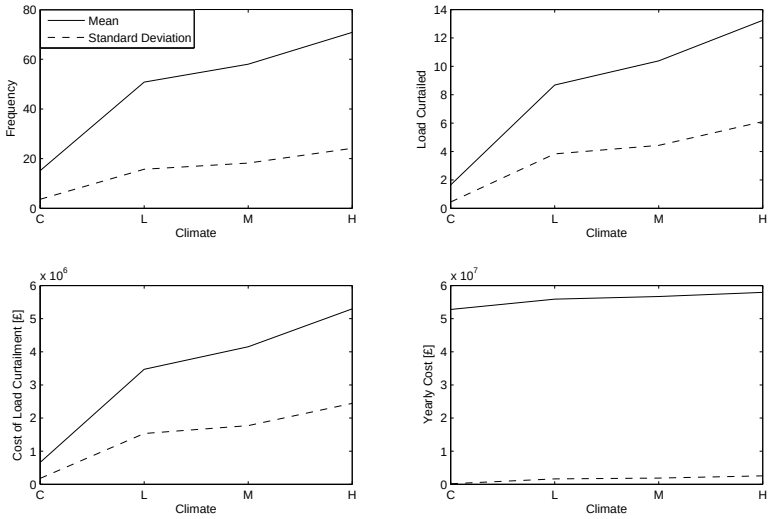

Figure 2.6: This is a plot of the results of table 2.3. The top left plot is the curves for the frequency of load curtailment, the top right plot is the curves for the amount of load curtailed, the bottom left plot is the curves for the cost of load curtailment and the bottom right plots is the curves of yearly cost. This is plotted for the current ('C') climate, the low ('L') emissions scenario, the medium ('M') emissions scenario and the high ('H') emissions scenario.

scenarios into our modelling and run them under various climate models.

2.3.2 Simulation with Random Faults

In 2.3.1 the simulations we performed were for a secure system meaning they did not exhibit random faults. We will now introduce random faults into the model. We will model all failures as independent. Given that we are trying to examine resilience in the transmission network, we will assume all generators and buses are secure components, meaning they are fully working and not liable to random faults. We only run fault simulations on the circuits. In a real power system, the network would be much more interconnected. For this reason, when modelling the transmission network, assuming the system has adequate buses and generators is reasonable and well used as if a generator was to fault, power would be dispatched from another source.

In modelling failures the most simplistic method is to have a constant hazard rate and constant repair rate. In this modelling we will use a constant repair rate but for failures the hazard rate will comprise of a time-dependent part and a constant part.

The term hazard rate and failure have identical implication and are interchanged throughout this section.

Time-Dependent Hazard Rate

Let us introduce the failure density function, $f(t)$, by first introducing a distribution function.

Definition *For a random variable ξ on a probability space $(\Omega, \mathcal{F}, \mathrm{P})$, let $F(x)$ denote the probability that ξ does not exceed x, that is*

$$F(x) = \mathrm{P}\left(\{\omega : \xi(\omega) \leq x\}\right), x \in \mathbb{R}.$$

The function F is called the distribution function of the random variable ξ [50].

Definition *If there exists a function $f : \mathbb{R} \to \mathbb{R}^+$ such that the distribution function F of the random variable ξ satisfies*

$$F(x) = \int_{-\infty}^{x} f(u)\, du$$

then we call f the density function of the random variable ξ [50].

We shall model the time-dependent hazard rate using the Weibull distribution, as it is frequently used in reliability analysis [37].

Definition *A Weibull distribution is a two parameter distribution with scale parameter, λ, and shape parameter, β, and takes the form:*

$$f(t;\lambda,\beta) = \begin{cases} \frac{\beta}{\lambda}\left(\frac{t}{\lambda}\right)^{(\beta-1)} e^{-(\frac{t}{\lambda})^{\beta}} & t \geq 0 \\ 0 & t < 0. \end{cases} \tag{2.8}$$

In the case of using the Weibull distribution, the cumulative distribution function is calculated as:

$$F(t) = \int_{-\infty}^{t} \frac{\beta}{\lambda}\left(\frac{u}{\lambda}\right)^{(\beta-1)} e^{-(\frac{u}{\lambda})^{\beta}} du = 1 - e^{-(\frac{t}{\lambda})^{\beta}} \tag{2.9}$$

Next we shall introduce the reliability function $R(t)$.

Definition *A reliability function, R(t), also known as a survival function, calculates the probability that no failure has occurred before time t.*

From its definition, the reliability function is calculated as:

$$R(t) = 1 - F(t) = 1 - \int_{-\infty}^{t} f(u)du. \tag{2.10}$$

Using (2.9) and (2.10), we can calculate the reliability function as:

$$R(t) = 1 - (1 - e^{-(\frac{t}{\lambda})^{\beta}}) = e^{-(\frac{t}{\lambda})^{\beta}}. \tag{2.11}$$

Knowing the failure density function and the reliability function we can calculate the hazard rate function.

Definition *The hazard rate function, $\eta(t)$, is defined as the ratio of the failure density function to the reliability function.*

$$\eta(t) = \frac{f(t)}{R(t)}. \tag{2.12}$$

We will denote the hazard rate at time t as η_t, i.e.:

$$\eta_t = \eta(t).$$

Under the assumption that time-dependent failures follow a Weibull distribution, the hazard function is calculated as:

$$\eta_t = \frac{\beta}{\lambda}\Big(\frac{t}{\lambda}\Big)^{(\beta-1)} \tag{2.13}$$

by substituting (2.8) and (2.11) into (2.12).

Constant Hazard Rate and Repair Rate

When the hazard rates and repair rates are constant the Weibull distribution is equivalent to an exponential distribution distribution.

Definition *The exponential distribution is a one parameter distribution which describes the time between independent consecutive events that occur at a constant rate η_c, i.e. those that follow a Poisson process (for information on Poisson processes see [51]).*

$$f(t) = \begin{cases} \eta_c e^{-\eta_c t} & t \geq 0 \\ 0 & t < 0 \end{cases} \tag{2.14}$$

This distribution has cumulative density function:

$$F(t) = 1 - e^{-\eta_c t} \tag{2.15}$$

and reliability function

$$R(t) = e^{-\eta_c t}. \tag{2.16}$$

Substituting (2.14) and (2.16) into (2.12) we see that the hazard rate function is constant for the exponential distribution.

$$\eta_t = \frac{f(t)}{R(t)} = \frac{\eta_c e^{-\eta_c t}}{e^{-\eta_c t}} = \eta_c. \tag{2.17}$$

The Weibull distribution takes the same form as the exponential distribution when the shape parameter takes value one. When $\beta = 1$, the constant rate parameter for the exponential distribution is equal to the inverse of the scale parameter for the Weibull:

$$\eta_c = \frac{1}{\lambda}.$$

Bathtub curve

The hazard rate we shall use in this modelling is more complex than having just a single hazard rate. It is familiar in reliability analysis and survival analysis and is called the 'Bathtub Curve' [37]. This can be seen in figure 2.7.

The bathtub curve comprises of three parts. Firstly, we have a decreasing function, known as the early stage or "infant mortality" stage. The second part is a constant hazard rate and corresponds to the random failures which occur through the life of the component. The final part of the curve is a wear out, or "aging", stage. This is an increasing function and corresponds to the higher rate at which faults normally occur as they get older. If we combine these three hazard rates we get the observed hazard rate.

For scale $\beta < 1$ in the Weibull distribution, η_t becomes a decreasing function of time and can be used as the "infant mortality" stage. For $\beta = 1$ the Weibull distribution takes the same form as the exponential distribution and gives a constant hazard rate. This is then used as the "random" hazard rate. For $\beta > 1$, η_t becomes an increasing function of time and can be used as the "aging" hazard rate. Define the observed hazard rate η_t^o as:

$$\eta_t^o = \eta_t^{\beta<1} + \eta^{\beta=1} + \eta_t^{\beta>1} \tag{2.18}$$

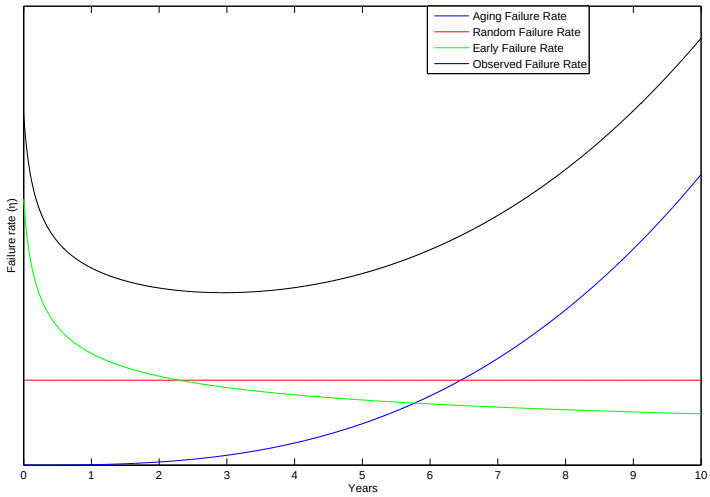

Figure 2.7: Bathtub curve hazard rate as used in reliability analysis.

where $\eta_t^{\beta<1}$ is the hazard rate corresponding to the hazard rate of the "infant mortality" stage, $\eta^{\beta=1}$ corresponds to the "random" hazard rate which is constant, and $\eta_t^{\beta>1}$ corresponds to the hazard rate of the wear out stage.

Failure data is not readily available nor is the age of components in the National Grid system. I have examined failure data from other sources [2], [5] and [37] and have devised an approximation based on these. In [37] the authors argue that due to technological advances, and pre-testing of the system using modelling and advanced computational simulations, the early stage hazard rate, as seen in figure 2.7, is non-existent in modern times. Following this I will model faults using only the constant random hazard rate, $\eta^{\beta=1}$, and increasing aging hazard rate, $\eta_t^{\beta>1}$, as seen in figure 2.8. The observed failure rate for this case is defined as:

$$\eta_t^o = \eta^{\beta=1} + \eta_t^{\beta>1}. \tag{2.19}$$

The aim of this thesis was not to examine failure rates of components as members of the project team in WP3 are examining them. For this reason the method used to approximate the curves in figure 2.8 to data in the literature was a simple trial and error approximation method in which parameters were guessed in order to find a suitable curve. Simulations were ran for a range of values corresponding to various hazard rate functions and it was found that increasing the hazard rate increases the values of the results. Likewise decreasing the hazard rates decreases the values in the

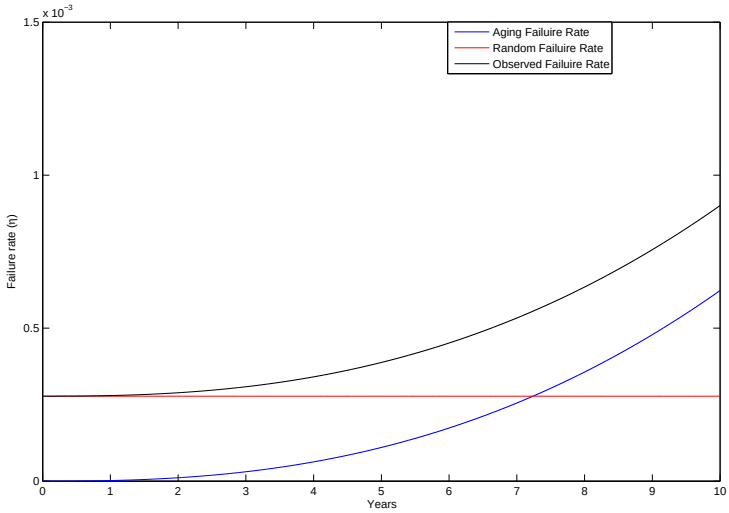

Figure 2.8: Bathtub curve for hazard rate with no early "infant mortality" stage. This hazard rate comprises of two parts, a constant hazard rate corresponding to the random failures which occur through the life of the component and an increasing function corresponding to the aging hazard rate.

Failure Rate	Random Failure Rate	2.8e-4
	Aging Failure Rate (at 30 years)	6.2e-4
	Observed Failure Rate (at 30 years)	9.0e-4
Weibull Parameters	Scale Parameter λ	87600
	Shape Parameter β	3.5

Table 2.4: Time-dependent hazard rate data and Weibull parameter data as used in section 2.3.2. Component age is assumed to average 30 years [ref maybe].

results. The results are comparable as the trend in the results between different climate scenarios remains the same. Below we discuss the results of a simulation for one hazard rate function. The values of the hazard rates being used, and the parameters of the distributions, can be seen in table 2.4.

Outage Model for System Components

When modelling forced outages in power system components the two models deemed acceptable are: the two state up-down model, and the three state up-derated-down model [5]. Forced outages are random outages which are not planned in advance and cannot be altered to a different time. The majority of forced outages occur due to component failure. We will assume all forced outages can be repaired.

Figure 2.9(a) is the transition diagram of the two state model. A component travels

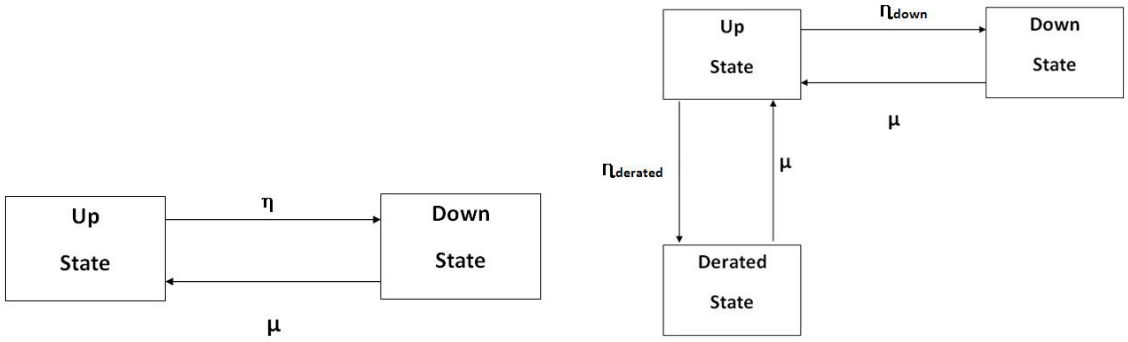

(a) Two state transition diagram.

(b) Three state transition diagram.

Figure 2.9: In figure 2.9(a) we have the two state transition diagram for a component. In figure 2.9(b) we have the three state transition diagram for a component.

from a working (up) state to an outage (down) state with failure rate η. It completes the cycle by travelling from an outage state to a working state with repair rate μ.

Figure 2.9(b) shows the transition diagram for a three state model. A component can travel from an up state to a down state with failure rate η_{down}, and from an up state to a derated state with failure rate $\eta_{derated}$. In a down state, a component can transverse to an up state with repair rate μ but cannot transverse to a derated state. In a derated state, a component can only travel to an up state with repair rate μ and cannot travel to a down state.

It is generally accepted in reliability analysis to ignore the transition between derated and down states. Reason being: if a component is in a down state it is highly unlikely to be repaired to a derated state. Almost always the component will be repaired to its full up state. Also, given that the repair rate is much higher than the failure rate, it is much more common for a component to be repaired before making a transition from a derated to a down state.

In non-severe failures, high-voltage direct current (HVDC) transmission circuits are known to work in a derated state. HVDC transmission lines are overhead lines or cables that work at high voltages to transport large amounts of power. They are normally used over long distances. Direct current is used to minimise losses. Given our components are 400kV overhead lines we can classify them as high voltage components. For this reason we shall model our components using a three state model. We will assume circuits work at 50% of their full capacity in a derated state. Theoretically

this value could be set to any percentage or indeed be stochastic itself which would represent the severity of the fault.

To make the capacity of the derated state stochastic we could introduce a uniform random variable in the interval [0, 1]. Each time a random fault is generated, as discussed next, a uniform random variable in the interval [0, 1] would be generated too. The value of this random variable would be the ratio of the capacity of the derated state to the full capacity of the conductor.

For the three state method, we shall let $\eta_{down} = \eta_{derated} = \eta_t^o$ where η_t^o is the observed time-dependent hazard rate at time t, which is calculated as the sum of the constant hazard rate and aging hazard rate. This assumes the rate at which a component traverses to a down state is the same as the rate at which it traverses to a derated state. These functions could be set differently. However, there is a lack of derated failure data available given most components utilies record faults using the two state, up-down, model.

Generating Random Faults

Random faults are generated using the state duration sampling approach [5]. This involves sampling the probability distribution of the component state duration. The component state duration is the same as the time to failure distribution, $f(t)$, used in (2.12). In the event of failure we sample from the time to repair distribution, which is an exponential distribution. Repeating this we generate the chronological component state transition process for each component, as seen in figure 2.10.

We begin by specifying the initial component state, normally as the up state. Next, given the component was initialised to the up state, we want to sample the failure distribution. For this we need to sample from two distributions as we have two failure rates. We cannot simply add the failure rates and sample from a given distribution as the failure rate distributions have different parameters for each of the stages of the bathtub curve.

We generate two random times to failure: t_c and t_a. t_c corresponds to the time to failure using the constant "random" failure rate and is sampled from an exponential distribution. t_a is the time to failure corresponding to the "aging" failure rate and is sampled from a Weibull distribution with shape parameter, β, greater than one.

The time to failure, t_{down}, we use for the chronological state transition process is the minimum of the two randomly generated times to failure t_c and t_a.

The above method of generating two random times to failure and choosing the smallest is repeated twice. This is because we are using the three state transition method. The first run of the method corresponds to generated a time to failure which transitions the state from up to down, denoted t_{down}. We must also do a run which generates a time of transition from up to derated, denoted $t_{derated}$. Having run the above method twice to calculate t_{down} and $t_{derated}$ we choose the smallest and that decides whether it is transitioned to the down state or the derated state, in time t_f, where $t_f = \min(t_{down}, t_{derated})$ is the failure time.

Having generated a time to failure, we must now generated a time to repair, t_r. This is generated using an exponential distribution with fixed repair rate μ.

The method used to generate random Weibull and exponential values is the inverse transform method and a description of this method is included in appendix A.

We repeat the above sampling method of chronological state transition for the duration of each simulation, T. We repeat this for each component in the system and for each set of simulated weather variables.

Results

A simulation similar to that in section 2.3.1 was ran but included random faults. Random faults are generated using the state duration sampling approach as described above. For each of the four climates: current, future low emissions scenario, future medium emissions scenario and future high emissions scenario for the year 2080, a simulation was run for the 100 data sets, each with its own randomly generated chronological state transition process for each component. To begin we assume all components are fully working. Each simulation has one year worth of data points.

Figure 2.10 is a plot of the chronological state transition process for one simulation for one of the circuits. It can be seen how the component transverses between the up, down and derated states. A flow chart of the simulation can be seen in figure 2.11.

Table 2.5 shows the results using the same indices as used in table 2.3 for the secure system simulation. The results in table 2.5 have a similar trend to that of table 2.3 but are more severe. We can see in table 2.3 that the mean load curtailment

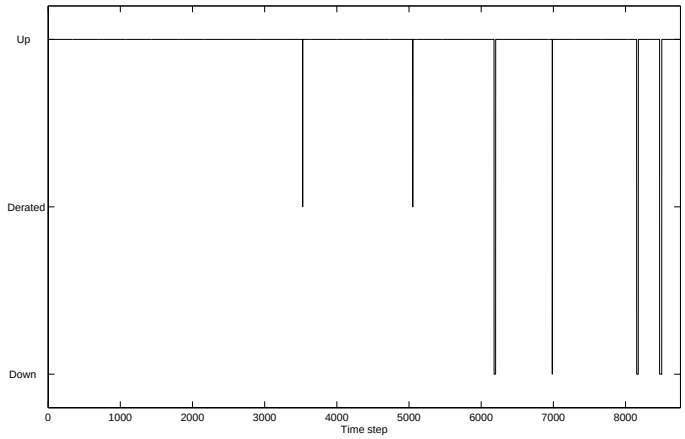

Figure 2.10: This is the chronological state transition process for one simulation for one of the circuits. It can be seen how the component transverses between the up, down and derated states.

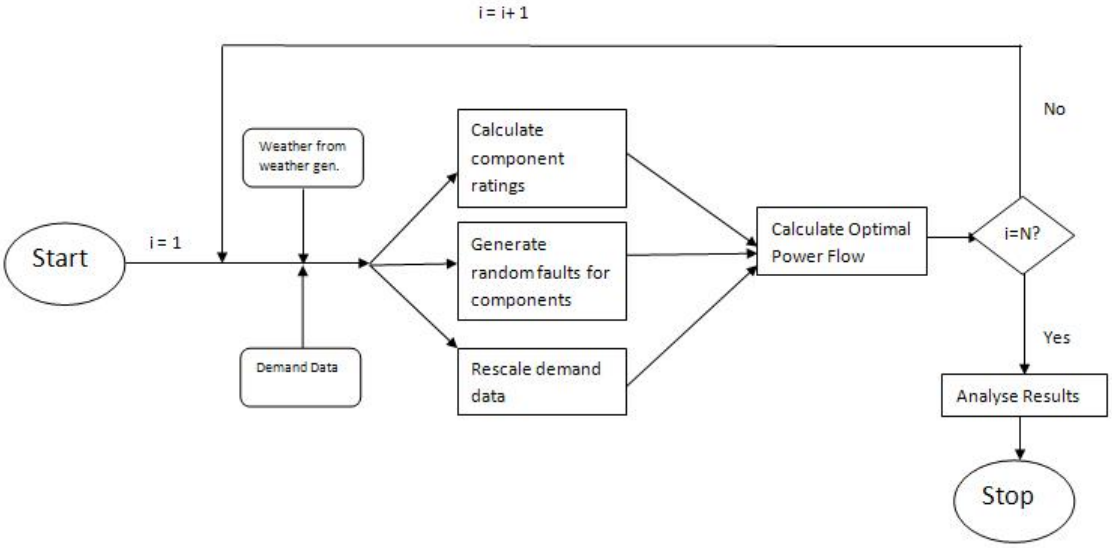

Figure 2.11: Flow chart for simulation as described in section 2.3.2

Climate:	Current	Low Emissions	Medium Emissions	High Emissions
FofLC	78.4 (43.9)	116.3 (48.9)	124.17 (49.3)	138.7 (53.4)
LC [per unit]	78.0 (64.5)	90.1 (67.4)	93.6 (68.7)	98.7 (69.4)
CofLC [£M]	31.2 (25.8)	36.0 (27.0)	37.4 (27.5)	39.5 (27.8)
YCofOPF [£M]	83.3 (25.8)	88.5 (26.9)	90.0 (27.5)	92.1 (27.8)

Table 2.5: This table is a comparison of results between the current climate, the low emission scenario climate, the medium emissions scenario climate and the high emissions scenario climate with random faults generated for each component. For each index, I have included the mean and standard deviation (as displayed in brackets).

difference between the current and low emissions scenario is 11.6 units, the current and medium emission scenario is 8.73 units, and the current and high emissions scenario is 15.45 units, for the basic model. This is in contrast to the fault model which has a mean load curtailment difference of 12.01 units for the current and low emissions scenario, a difference of 15.55 units for the current and medium emissions scenario and a difference of 20.68 units for the current and high emissions scenario. Also, the yearly cost increases by 6.2%, 8% and 11% for the low, medium and high emissions scenario respectively in comparison to the current climate. These three values are greater than the respective values for the basic model. This suggests that when random faults are introduced, the system will become less resilient and more expensive to operate for each of the given future climate scenario.

When testing the resilience of the system it can be seen that climate change will impact the system both operationally and economically. To combat this we introduce a method that should help reduce this impact.

2.3.3 Temporary Overload Method

In power systems operations one of the constraints that needs to be fulfilled for each component is:

$$\theta_t \leq \theta_{max} \tag{2.20}$$

where θ_t is the temperature of the component at time t and θ_{max} is the maximum safe operating temperature at normal operation. A straight forward way to satisfy this constraint is to ensure

$$|I_t| \leq I_{max} \tag{2.21}$$

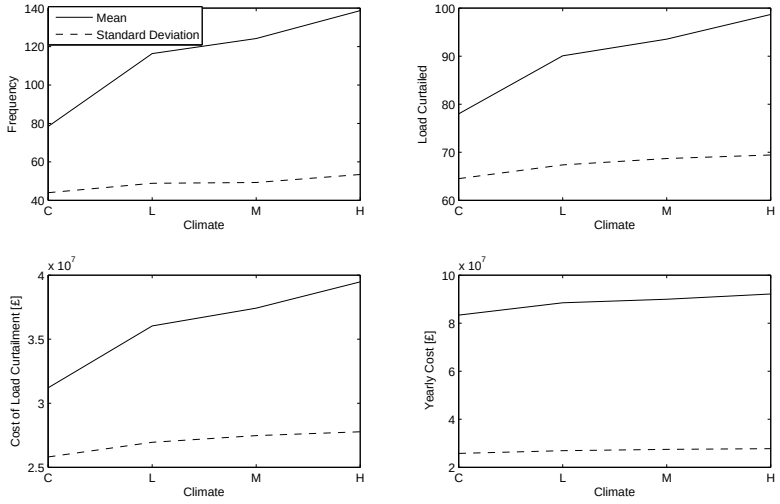

Figure 2.12: This is a plot of the results of table 2.5. The top left plot shows the mean frequency of load curtailment, the top right plots the mean amount of load curtailed, the bottom left plots the cost of load curtailment and the bottom right shows the mean yearly cost. This is plotted for the current ('C') climate, the low ('L') emissions scenario, the medium ('M') emissions scenario and the high ('H') emissions scenario.

where, I_t is the current at time t and as before I_{max} is the maximum safe operating current, known as the rating, as calculated in (1.7). The steady state heat equation, (1.3), assumes that I_{max} correspond to θ_{max}. This is true in the sense that if $I_t = I_{max}$ for all times t then:

$$\lim_{t\to\infty} \theta_t = \theta_{max}. \tag{2.22}$$

These maxima vary from conductor to conductor depending on its physical properties. Therefore, various conductors take different lengths of time to reach their steady state maximum temperature, θ_{max}, when the maximum current, I_{max}, is applied.

In reality, the transient temperature adjustment incurs some lag time. As a result of this lag time, a violation in (2.21) may not lead to a violation in (2.20). It is for this reason that we will apply the method developed in [16] to the power system.

In [16] the authors examine the short term overloading of components. They examine how the conductor temperature responds to current violations for various values of the thermal time constant. The thermal time constant is the length of time it takes the conductor to reach its steady state temperature. They find that fewest violations occur for higher values of the thermal time constant. In the paper the authors concentrate on how the component could be better utilised from an engineering

perspective but do not examine the economic benefit that using this method could have. They also examine the method under static ratings and do not consider using dynamical thermal ratings. As a further development I will apply this method to a power system in order to examine how a power system could benefit both operationally and economically. I will do this while implementing dynamical thermal ratings.

Methodology

The transient temperature of a conductor at time t, θ_t, is described by the first-order ordinary differential equation:

$$\tau \frac{d\Theta_t}{dt} + \Theta_t = \frac{|I_t|^2}{I_{max}^2} \tag{2.23}$$

in which we have used the change of variables

$$\Theta_t = \frac{\theta_t - \theta_a}{\theta_{max} - \theta_a} \tag{2.24}$$

which Θ_t is the relative temperature, θ_t is the absolute temperature, θ_a is the ambient temperature and τ is the thermal time constant. It is for various values of τ that we want to examine the model. Tables displaying values for τ for various components can be found in [52].

We can discretise (2.23) into hourly time steps:

$$\tau(\Theta_t - \Theta_{t-1}) + \Theta_{t-1} = \frac{|I_t^2|}{I_{max}^2}. \tag{2.25}$$

Rearranging (2.25) for I_t we obtain:

$$I_t = I_{max}\Big(\tau(\Theta_t - \Theta_{t-1}) + \Theta_{t-1}\Big)^{1/2} \tag{2.26}$$

If we were to set $\tau = 1$, (2.26) would become:

$$I_t = I_{max}\sqrt{\Theta_t}. \tag{2.27}$$

To satisfy constraint (2.20) we need:

$$\Theta_t \leq 1.$$

In (2.27), if $\tau = 1$, I_t must be less than or equal to I_{max}, the normal conductor rating, which is the constraint in (2.21). However, if we allow $\tau > 1$, we will see that we can use ratings higher than I_N for short durations, without violating constraint (2.20), as we can set $\Theta_t \leq 1$ which implies $\theta_t \leq \theta_{max}$ from (2.24). We can then examine, for various values of τ, how well the system operates using this method.

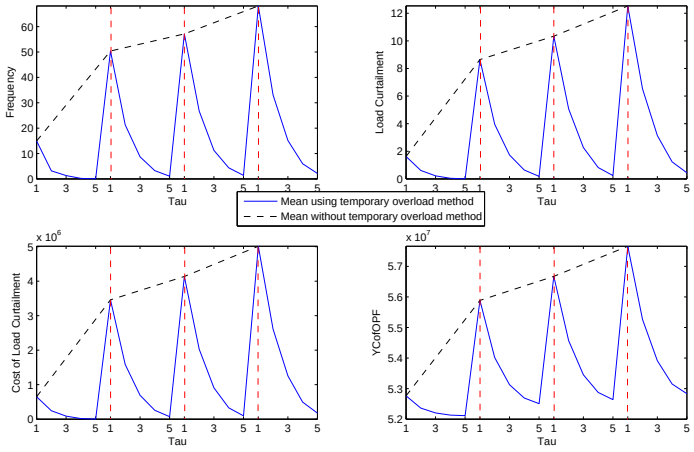

Figure 2.13: This is a plot of the results of the secure system model using temporary overloading, as discussed in section 2.3.3. The top left plot shows the mean frequency of load curtailment, the top right plots the mean amount of load curtailed, the bottom left plots the cost of load curtailment and the bottom right shows the mean yearly cost. The red dashed line divides the curve into the respective climates in the order of current, low emissions scenario, medium emissions scenario, and finally high emissions scenario. The blue line corresponds to the mean using the temporary overload method. The dashed black curve in each plot corresponds to the mean curve shown in the respective plot in figure 2.6, i.e. when $\tau = 1$.

Secure System Model

First we apply the above method to a secure model, as described in section 2.3.1. We run the simulation for $\tau = 1, 2, 3, 4, 5$ for the four climates: current, low emissions scenario, medium emissions scenario and high emissions scenario. The results of this simulation are shown in figure 2.13. We can see when $\tau = 1$, the temporary overload method produces the same results as the basic method used in section 2.3.1. However, for higher values of τ we can see that all curves decrease for each climate. This is because the temporary overloads result in less curtailments and thus less load curtailment costs as more power flows through the lines. For higher values of τ we obtain even less load curtailments and thus even lower load curtailment costs than lower values of τ.

Fault Generating Model

Next we look at applying the temporary overload model to a simulation which exhibits component outages through simulated faults as discussed in section 2.3.2. Again we

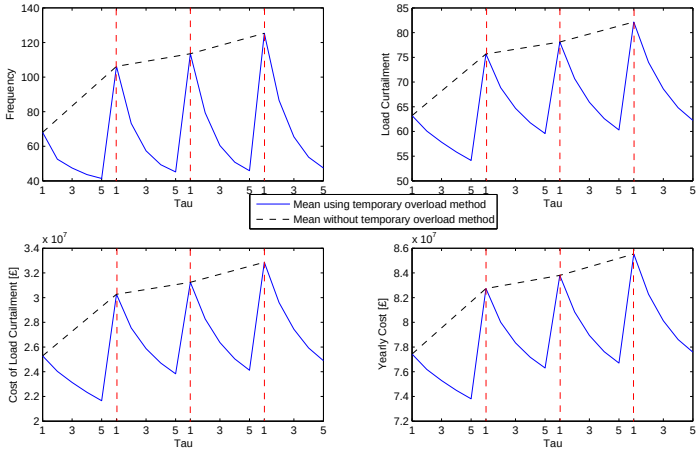

Figure 2.14: This is a plot of the results of the model using temporary overloading when random faults are considered. The top left plot shows the mean frequency of load curtailment, the top right plots the mean amount of load curtailed, the bottom left plots the cost of load curtailment and the bottom right shows the mean yearly cost. The red dashed line divides the curve into the respective climates in the order of current, low emissions scenario, medium emissions scenario, and finally high emissions scenario. The blue line corresponds to the mean using the temporary overload method. The dashed black curve in each plot corresponds to the mean curve shown in the respective plot in figure 2.12, i.e. when $\tau = 1$.

apply the temporary overload for $\tau = 1, 2, 3, 4, 5$ for the four climates. The results of this simulation are shown in figure 2.14. The resultant curves are similar to that described in figure 2.13. However, it is observable that the method is much more effective when random faults are considered. This is because load curtailment occurs more often and more severely. The temporarily overloaded circuits can work to a higher capacity when more energy is needed to be transported. In the case of the basic model, temporary overload may occur but not to its fullest capacity. When faults occur, power has to be redispatched and this puts more pressure on the available lines. Thus the lines that are available work to a higher capacity and when overloaded, the overload is more utilised than in a basic model. For higher values of τ we obtain even less load curtailments and thus even lower load curtailment costs than lower values of τ.

2.4 Summary

In this chapter we have examined how future climate, predicted by the UKCP09, will affect the resilience and cost associated with a power system, when using dynamical thermal ratings. We have seen from section 2.3.1 that future climate change, under any of the proposed emission scenarios, will both increase the cost and decrease the operational resilience of the power system.

Next, in section 2.3.2, we examined how the resilience of the system would cope under simulated faults using dynamical thermal ratings. We used the bathtub curve model, see figure 2.7, to simulate random faults. This involved sampling from time-dependent hazard rates. Under this method we saw that the resilience of the power system would decrease for future climate scenarios, with the lowest resilience associated to the highest emission scenario. The difference between the load curtailment of the emission scenarios and the current climate was greater for the fault model than for the no fault model, even though each climate was subject to the same faults. This indicated that the current climate could withstand some faults while the emission scenarios could not. These differences increased with respect to the emission scenario.

In section 2.3.3, given the conclusion on the effect of climate change on a power system in section 2.3.1 and 2.3.2, we examined looking at a method which allows the conductor to temporarily go above its rating provided it does not break its maximum temperature constraint. We saw that this method produces results which are beneficial in terms of system resilience and economical cost.

Chapter 3

Application of Stochastic Optimisation in Power Systems

In this chapter we examine the application of stochastic optimisation in power systems. Stochastic optimisation methods are optimisation methods that involve random variables [53]. In a power system, that uses dynamical thermal ratings, a lot of uncertainty is present when trying to plan for the future. The problem we are examining is associated with finding the optimal dispatch of generation for some future time, under uncertain conditions, in a power system that incorporates interruptible load. The optimal dispatch is determined by minimising the combined cost of all generators that are available to us, while satisfying stochastic constraints. Interruptible load occurs when consumers are given advanced notice that they may have their power switched off or reduced. Interruptible load is pre-arranged with consumers and as such the penalty to the utilty company is less than the value of load curtailment as discussed in section 2.3 [39]. The uncertainty that we will examine is found in the weather variables used to calculate the ratings of the circuits. The ratings are calculated using the steady state heat equation (1.3).

We first examine a one period model which optimises over a future weather variable for one time step ahead in the future and chooses which generation to dispatch. This is first done for a single random variable, wind speed, and then for two independent random variables, wind speed and temperature. Constraints are then added to the single random variable model in the form of system adequacy and system security constraints. We then examine adding a ramp rate constraint. A ramp rate is defined

as the maximum change in generation output per time step. This involves looking back at the dispatch planned in the previous time step and finding a planning value for the next time step which implies a generation that in range of the previous, as set by ramp rate.

We next examine a two period model. This involves optimising over two future time periods ahead in the future, and planning the generation for each time period accordingly. The second time period is liable to be changed when we perform an optimisation in the next time step. The optimisations are coupled by ramp rates constraints and thus cannot be treated as independent. We add the same constraints to the two period model as in the one period. We conclude with a comparison of the two methods.

3.1 One Period Model

Imagine the scenario in which we are given a finite set of values from the Met office, each corresponding to a weather variable for some future time. From this we can calculate the corresponding rating for each circuit and then, by running an optimal power flow, set our generation accordingly for the future time period to which the set of values corresponds to. This is the trivial case as if we know for certain what future weather values are going to occur we can calculate the thermal ratings and, given we know the load, run the optimal power flow.

Instead consider the scenario in which a forecast is provided to us from the Met office. A forecast is defined as a probability distribution over a future weather variable for some specific time in the future. Now we get a set of probability distributions for the set of circuits rather than a single value for each circuit as before. Each set of ratings, set as we have three circuits, from the probability distributions will have a corresponding optimal power flow. The generation from this power flow is the generation we would want to set our generators to if we knew that set of ratings was to occur, i.e. the trivial case. This would only happen if we knew that set of weather values was to occur. However, since we know the probability of each value occurring, we can optimise over the forecast by first taking the expectation and from that choosing which generation is optimal to use. This will then be our optimal dispatch.

In this model we assume that the components are fully working and not subject to random faults and the demand in the system is constant. This is done throughout the literature when modelling dynamical thermal ratings, as discussed in section 1.4.2. It is regularly assumed in power systems that no randomness is present other than that we are trying to model, and as such we shall adapt this assumption.

3.1.1 Methodology

The method we use is described below and can be seen as a flowchart in figure 3.1 as follows:

1. At time t we assume we are given a forecast from the Met office, f_{X_t}. All random variables, X_t, take real values. If we concentrate on one variable, say wind speed, then we will receive one probability distribution for each time step. But say we concentrate on two (or more) variables, then we will receive a distribution for each variable at each time step (or a joint distribution). We will revisit this again later. Assume for now that we are dealing with only one weather variable, wind speed. We also assume that the forecast we get at time t, will be a probability distribution for some weather variable for one time step ahead, $t + 1$.

2. Let us define a planning weather value as the weather value we choose at time t to calculate the ratings used in the optimal power flow which decides the generation for time $t + 1$. We denote a planning weather value, at time t, as a_t. We can choose to use planning weather values as the weather calculates the ratings which in turn decides what generation is dispatched so setting a planning weather value implies setting a planned generation.

3. Every value x_k has a corresponding set of dynamical thermal ratings. This set comprises of a rating for each circuit in the system, calculated using (1.7). With each set of ratings we can calculate an adapted optimal power flow (AOPF), given we have preset our dispatch using planning value a_t. An Adapted Optimal Power Flow is an optimal power flow that incorporates the interruptible load cost [39].

4. We want to choose a planning value which minimises our expected adapted

optimal power flow cost over the random weather variable X_t, and use this weather value to calculate the ratings which in turn sets our optimal generation. Define the optimal planning value, a_t^*, as the weather value which minimises the expected cost over the forecast.

Now let's put this in mathematical terms. We have previously defined the random weather variable, X_t, and the planning value, a_t, with optimal planning value denoted a_t^*. Our cost function is defined as:

$$c(x_k, a_t) = \min_{\underline{P}_g} \sum_{i=1}^{N_B} f_i(P_{gi}) + ILC(IL)$$

such that

$$\begin{aligned} P_i &= \sum_{j=1}^{N} (B_{ij}(\delta_i - \delta_j)) \\ |F_{ij}| &\leq F_{ij,max}(x_k) \\ P_{gi} &= P_{gi}(a_t) \end{aligned} \tag{3.1}$$

with cost function $c : \mathbb{R} \times \mathbb{R} \to \mathbb{R}^+$. N_B is the number of buses in the system, $\underline{P}_g$ is the set of generator power outputs with $P_{gi} : \mathbb{R} \to \mathbb{R}^+$ is the power generated from generator $i \in \{1, \ldots, N_B\}$. The function $f_i : \mathbb{R}^+ \to \mathbb{R}$ is the cost function for generator i which is linear with no start up cost. The coefficients are listed in table 3.2. $ILC : \mathbb{R}^+ \to \mathbb{R}^+$ is the interruptible load function, which is linear. The coefficients are listed in table 3.2. $IL \in \mathbb{R}^+$ is the amount of interruptible load. $P_i \in \mathbb{R}$ is the real power injection with $P_i = P_{gi} - P_{di} \, \forall i \in \{1, \ldots, N_B\}$, where $P_{di} \in \mathbb{R}^+$ is the demand at bus i. $B_{ij} \in \mathbb{R}^+$ is the susceptance of the circuit between bus i and bus j. $\delta_i \in [0, \pi]$ is the voltage angle at bus i. $F_{ij} \in \mathbb{R}$ is the power flow between bus i and bus j. $F_{ij,max} : \mathbb{R} \to \mathbb{R}^+$ is the maximum safe amount of power that can flow through the circuit connecting bus i to bus j and is calculate using the value x_k and equation (1.7). This is an adapted optimal power flow using generation from the result of the optimal power flow using planning value a_t, with ratings calculated using the value x_k from the random variable X_t. $P_{gi} : \mathbb{R} \to \mathbb{R}^+$ is the generation from generator i associated to planning value a_t and is set by first running an optimal power flow with ratings $\underline{F}_{max}(a_t)$ and maximum generation $P_{gi,max}$, which is the maximum generation as set by the manufacturer, and then setting $P_{gi}(a_t) = P_{gi}^{a_t}$, where $P_{gi}^{a_t}$ is the power generated from generator i when ratings $\underline{F}_{max}(a_t)$ are used.

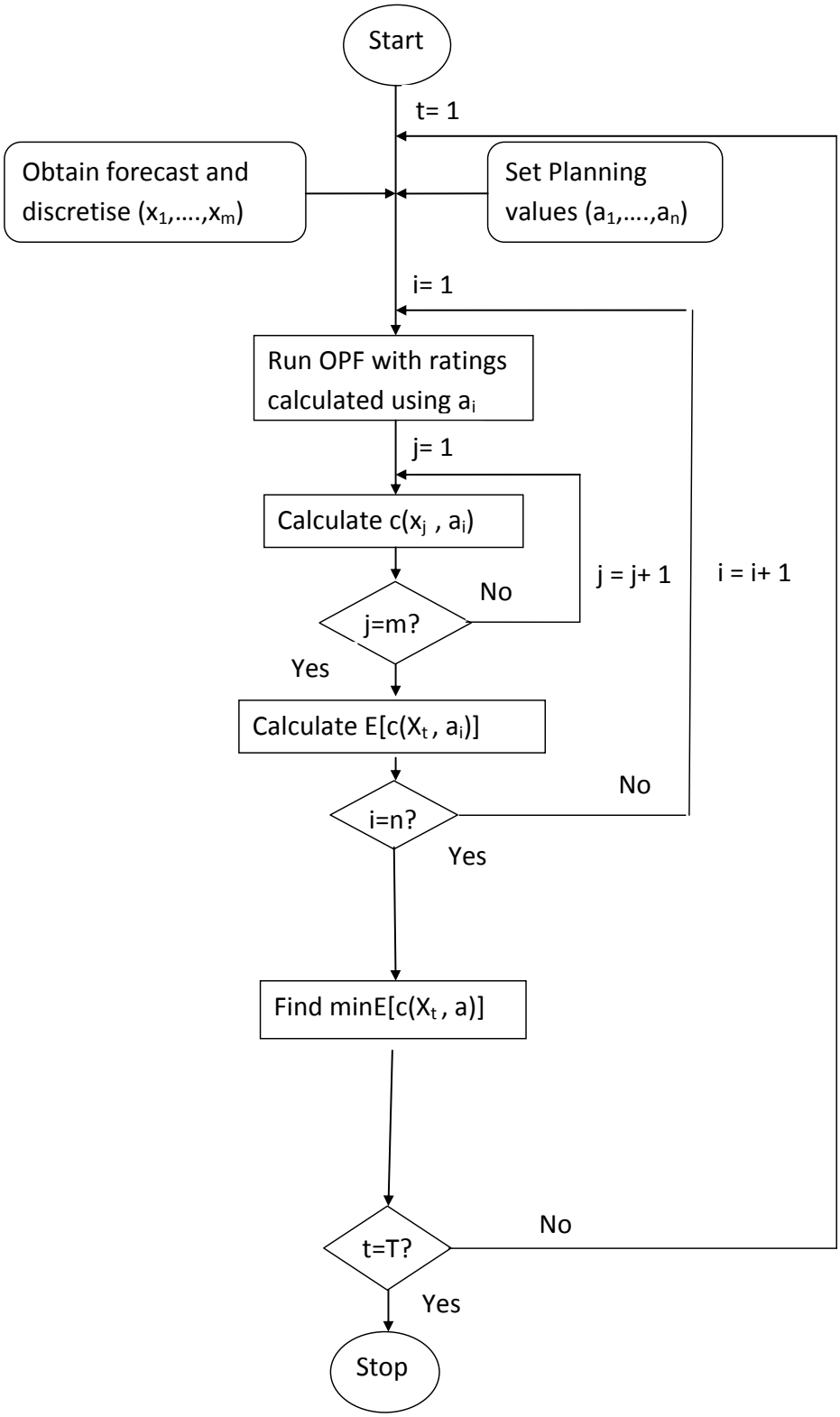

Figure 3.1: Flow chart for method used in section 3.1.1.

Generator	**1**	**2**
Minimum Output (p.u.)	0	0
Maximum Output (p.u.)	10	15
Cost (£/p.u.)	400	800

Table 3.1: Specifications of the maximum and minimum output of the generators and the cost for generation.

Demand at bus 2 (p.u.)	12.5
Demand at bus 3 (p.u.)	4.875
Interruptible Load Cost (£/p.u.)	1600

Table 3.2: Specifications of the demand and the cost for interruptible load.

The expected cost function using planning value a_t, and the t^{th} forecast X_t is defined as:

$$V_t(a_t) = \mathbb{E}[c(X_t, a_t)] \tag{3.2}$$

We want to minimise our expected costs so we the take the minimum over all planning values:

$$V_t = \min_{a_t} \mathbb{E}[c(X_t, a_t)] \tag{3.3}$$

Every scale value λ_t from the Weibull distribution, governing a wind speed forecast with random variable X_t, has a corresponding optimal planning value a_t^*.

Since an adapted optimal power flow is an optimisation we cannot find the expectation by doing an integral as an analytical solution does not exist. We thus do the expectation numerically by discretising the random variable X_t. This involves choosing a finite number of discrete values for the random variable, running an adapted optimal power flow for each value and multiplying each value by its associated probability of occurring:

$$\mathbb{E}[c(X_t, a_t)] = \sum_{i=1}^{M} P(X_t = x_i) \times c(x_i, a_t) \tag{3.4}$$

where $P(X_t = x_i)$ is the probability that the random variable X_t takes value x_i. M is the amount of samples we take and x_i is the i^{th} sample of the random variable X_t. This approximates to the continuous case as $M \to \infty$, i.e.:

$$\sum_{i=1}^{M} P(X_t = x_i) \times c(x_i, a_t) \approx \int_{-\infty}^{\infty} f_{X_t}(x) \times c(x, a_t) dx. \tag{3.5}$$

for large values of M. The expectation in (3.2) exists as the expected value of the random variable X_t, which is Weibull distributed, exists and the left hand side of (3.4)

has absolute convergence as $M \to \infty$ (this is equivalent to $\int_{-\infty}^{\infty} f_{X_t}(x) \times |c(x, a_t)| dx < \infty$ for the continuous case).

3.1.2 Single Stochastic Variable Model

For the single stochastic variable model we are considering that the only random variable is wind speed. Therefore, all other parameters in the calculation of ratings using (1.7), are constant. The distribution we assume for the forecast is a Weibull distribution, as defined in (2.8), but with parameter t replaced by x. The Weibull distribution was chosen as previous research on empirical wind speed data has shown that using the Weibull distributions when modelling wind speed results in the best fitting model [54]. The Weibull distribution we use will itself be random. This is done by using a random variable Λ_t for the scale, which is calculated as:

$$\Lambda_t = \lambda_0 + \epsilon_t \tag{3.6}$$

where λ_0 is a fixed constant and ϵ_t follows a standard normal distribution.

Definition *A normal distribution is a two parameter distribution and takes the form:*

$$f(x; \mu, \sigma^2) = \frac{1}{\sigma\sqrt{2\pi}} e^{-\frac{1}{2}(\frac{x-\mu}{\sigma})^2} \tag{3.7}$$

where μ is the mean and σ^2 is the variance.

A standard normal has mean $\mu = 0$ and variance $\sigma^2 = 1$, which is denoted as $\mathcal{N}(0, 1)$.

We will keep the shape parameter for the Weibull distribution, β, constant as to examine one source of randomness. Having the scale follow a random walk is similar to having the mean follow a random walk as the scale value and mean value are directly proportional, and given as:

$$\text{mean} = \lambda\Gamma(1 + \frac{1}{\beta})$$

where $\Gamma(\cdot)$ is the gamma function.

λ_0 and β have both been calculated using empirical data. The data used was wind speed data measured from 1973 to 1993 at Heathrow, London and was obtained from the British Atmospheric Data Centre (BADC) [55]. Using this data we can calculate the maximum likelihood estimates of the scale and shape parameter for each year and use the mean of each as λ_0 and β respectively. The method of calculating the

maximum likelihood estimates for the Weibull distribution is included in appendix C.1. We could have used other methods to calculate λ_0 and β such as the method of moments or least squares method. A comparison between the three methods is given in [56]. The author concluded that the order of methods based on computational time are:

1. Least Squares Method.
2. Maximum Likelihood Estimator
3. Method of Moments.

while the order based on accuracy are:

1. Method of Moments.
2. Maximum Likelihood Estimator
3. Least Squares Method.

Choosing the maximum likelihood method seemed like a good choice as it has an average ranking in both computational time and accuracy.

The random variable X_t is defined as:

$$X_t \sim \text{Weibull}(\Lambda_t, \beta) \tag{3.8}$$

Figure 3.2 shows the probability density functions of a Weibull distribution, with varying scale value, λ, and fixed shape parameter, β.

In this model we use the same three busbar model as before, as seen in figure 2.2. Information about the generation output in the model can be seen in table 3.1 and information about the demand in the model can be seen in 3.2.

Figure 3.3 shows the expected adapted optimal power flow cost against the wind speed chosen as the planning value with a_t^*, the optimal planning value which corresponds to the minimum expected cost, outlined by a circle. The simulation was run for the scale values corresponding to that of figure 3.2. The optimal planning value and corresponding expected adapted optimal flow cost of each simulation can be seen in table 3.3. We observe the variability in a_t^* as well as the variability in V_t due to the variability of the random scale Λ_t.

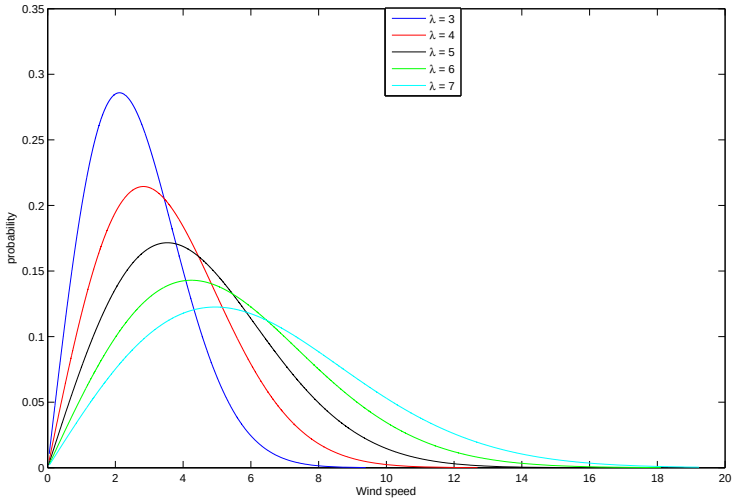

Figure 3.2: Plot of Weibull distribution probability density functions with varying scale parameter, λ, and fixed shape parameter, β. The scale parameter λ is plotted for values 3, 4, 5, 6 and 7 with β fixed equal to 1.5. We can observe that as λ increases, the range of values for which the probability of occurrence is greater than zero becomes larger.

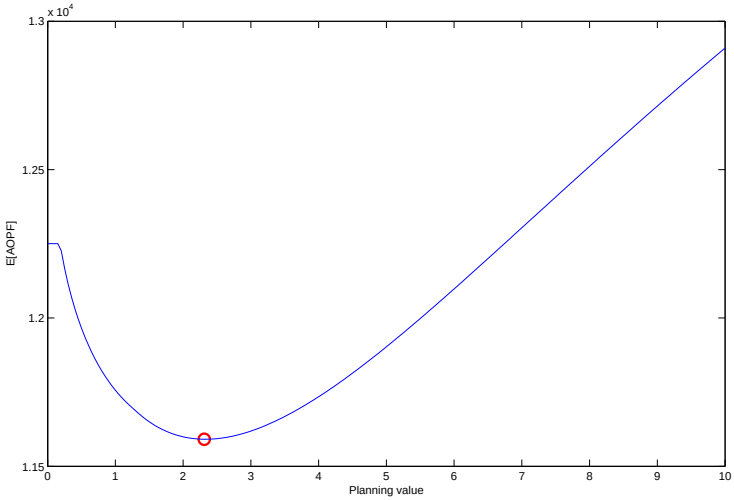

Figure 3.3: Expected adapted optimal power flow cost against the planning wind speed value, for $\lambda = 4.5$. The circle corresponds to the minimum expected adapted optimal power flow cost. If we draw a vertical line from the circle to the x-axis, this corresponds to the optimal planning wind speed one should choose. A horizontal line from the circle corresponds to the expected adapted optimal power flow cost given you choose the corresponding wind speed. Initially, as the planning wind speed increases, the expected adapted optimal power flow decreases. This occurs up to a certain point, which is the optimal planning value, a^*, to choose. After that, the expected cost of interruptible load comes into account when calculating (3.1) and this is why the curve begins to increase.

λ_t	a_t^*	V_t
3.00	1.63	11366
4.00	2.25	11458
5.00	2.65	11528
6.00	3.06	11619
7.00	3.27	11736

Table 3.3: Optimal planning values and corresponding expected adapted optimal power flow cost for various values of the scale, λ, corresponding to those of figure 3.2.

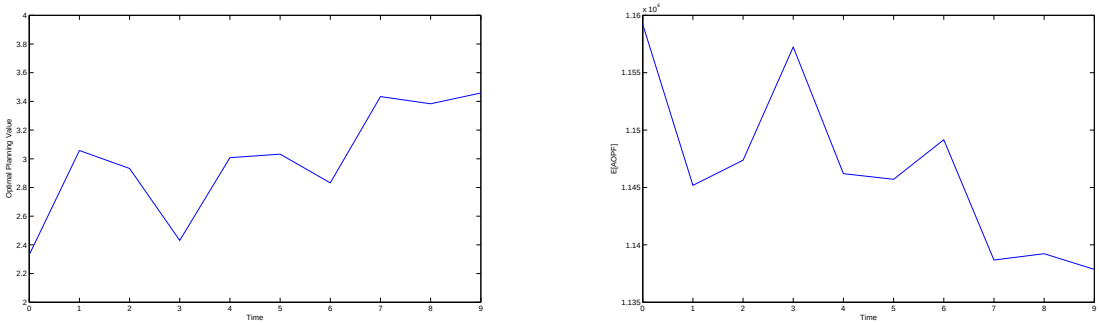

(a) Variation of optimal planning value.

(b) Variation of expected adapted optimal power flow cost.

Figure 3.4: Figure 3.4(a) shows the optimal planning value (wind speed) to choose for the 10 time steps we have run in our simulation. This shows how the optimal planning value can vary under varying forecast $f_{X_t}(\Lambda_t, \beta)$. Figure 3.4(b) shows the expected adapted optimal power flow cost associated with the optimal planning value (wind speed) chosen for the 10 time steps, corresponding to figure 3.4(a).

Figure 3.4(a) shows the optimal planning wind speed value corresponding to a_t^* for 10 time steps generated using (3.6). The scale values used can be seen in table 3.4. The variability in a_t^* is due to the variability in the Weibull distribution we are using in our forecast as a result of the randomness of the scale value Λ_t. Figure 3.4(b) shows the expected adapted optimal power flow cost corresponding to each a_t^* shown in figure 3.3. Again the variability in the expected adapted optimal power flow cost is due to the same randomness that causes the variability of a_t^*. It can be seen how the curves in figures 3.4(a) and 3.4(b) follow a random walk corresponding to that of Λ_t.

Time Step:	1	2	3	4	5	6	7	8	9	10
Scale:	4.36	6.25	5.88	4.57	6.07	6.15	5.60	7.64	7.50	7.85

Table 3.4: Scale values for one period simulation.

3.1.3 Two Stochastic Variables model

We can adapt the previous method for a two stochastic variables model which contains two sources of randomness: wind speed and ambient temperature. Consider if the Met office was to provide us with a forecast for both wind and temperature in the form of two independent probability distributions, a Weibull and a normal distribution respectively.

Denote the forecast for temperature at time t as the random variable $Y_t \sim \mathcal{N}(\mu_t, \sigma^2)$ with:

$$\mu_t \quad = \quad \mu_0 + \zeta_t \tag{3.9}$$

where μ_0 and σ^2 are given constants calculated from empirical data and $\zeta_t \sim \mathcal{N}(0, 1)$. The data used to calculate μ_0 and σ^2 was sampled from the weather generator [43]. With this data we can apply the maximum likelihood estimation method. The maximum likelihood method for a normal distribution is described in appendix C.2.

As before, the Weibull has scale Λ_t, calculated using (3.6), constant shape β and has random variable denoted, for time t, as $X_t \sim Weibull(\Lambda_t, \beta)$.

For this method we must take the expectation over all X_t and Y_t and find the optimal planning value, $\mathbf{a}_t^* = [a_{X_t}^*, a_{Y_t}^*]$, where $a_{X_t}^*$ is the optimal planning value corresponding to X_t and $a_{Y_t}^*$ is the optimal planning value corresponding to Y_t. The methodology is the same as that in section 3.1.1, but now we optimise over two random variables and then obtain a set of planning values $\mathbf{a}_t = [a_{X_t}, a_{Y_t}]$, with a_{X_t} corresponding to the planning value for random variable X_t and a_{Y_t} corresponding to the planning value for Y_t. The cost function is the same as that in (3.1) but when calculating the ratings using (1.7) we don't use a constant temperature anymore. The expected total cost function for planning value $\mathbf{a}_t = [a_{X_t}, a_{Y_t}]$, given we start with $\mathbf{X}_t = [X_t, Y_t]$ is:

$$V_t(\mathbf{a}_t) = \mathbb{E}[c(\mathbf{X}_t, \mathbf{a}_t)] \tag{3.10}$$

We want to minimise our expected costs so we need to find the minimum set of planning values:

$$V_t = \min_{\mathbf{a}_t} \mathbb{E}[c(\mathbf{X}_t, \mathbf{a}_t)] \tag{3.11}$$

A graphical interpretation of this can be seen in figure 3.5. It can be seen that wind speed has a much greater affect on the expected adapted optimal power flow cost

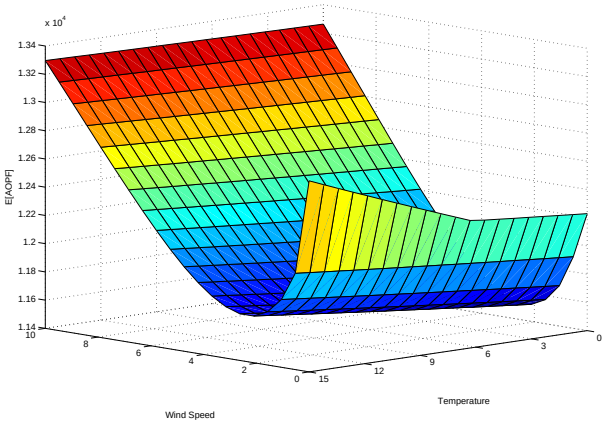

Figure 3.5: This plot shows the expected adapted optimal power flow cost against the combination of the planning wind speeds and planning temperatures, i.e. the planning values.

than temperature. This can be seen as the expected adapted optimal power flow cost decreases relatively gently, as the planning temperature decrease. On the other hand, the expected adapted optimal power flow decreases significantly as the planning wind speed is increased. This occurs up to a certain point, which is the optimal plan. After that it begins to increase quite rapidly before steadying. This rapid increase is due to the cost of the expected load curtailment being included in the adapted optimal power flow cost. For the rest of the modelling we will concentrate on the single stochastic variable model, using wind speed as the random variable.

3.1.4 Adding Constraints to model

So far we have minimised a function over a random variable. When we find the optimal planning value to use, by finding the corresponding minimum expected adapted optimal power flow value, we do not consider how secure or unsecure the system will be when using this value. A system operator would like to know what level of security he has in his system and be able to control that level if possible. Rather than telling consumers that they may lose load it would be better to tell them with what probability a load curtailment may occur.

As discussed in section 1.5, in [5] the authors have a set of indices for which they can use to evaluate the adequacy in there system. Using one, or a combination of two or more, we can constrain the adequacy in our system. Also we have discussed

using probabilistic security assessment. In [35] the authors add a constraint to the optimal power flow as to control their liability to risk, which in essence is controlling the security in the system.

We can examine, and control, both adequacy and security in our system by adding constraints to the stochastic optimisation approach. To examine and control adequacy, we can calculate individual, or sets of, adequacy indices using (1.11), (1.13) and (1.14). When running the stochastic optimisation method we then bound these values to a value we are satisfied with by adding a constraint. To manage risk, we take a similar approach by putting a constraint on the model. This constraint should contain some monetary value as to take the form of a risk index, as defined in section 1.5.2.

Adding System Adequacy Constraint

As described in section 1.5.1, there are many indices which measure system adequacy in the transmission system. In this approach we choose one of the indices and use it as a constraint in our optimisation model. The index we will use is the probability of load curtailment (PLC), which was defined in section 1.5.1 as (1.11) as:

$$PLC = \sum_{x_t} p_i \mathbb{1}_{\{l_i < L\}}$$

where p_i is the probability of being in system state i, l_i is the load delivered in state i, L is load demanded and $\mathbb{1}_{\{l_i<L\}}$ is the indicator function as defined in (1.12). The system states depend on the thermal ratings, which depend on the the forecast X_t. Thus, we can rewrite the probability of load curtailment as:

$$PLC = \sum_{x_i} P(X_t = x_i) \mathbb{1}_{\{l_{x_i,a_t} < L\}} \tag{3.12}$$

where $P(X_t = x_i)$ is the probability that the random variable X_t has value x_i, where x_i is one of the discrete values taken from X_t. l_{x_i,a_t} is the load delivered when the random variable X_t takes value x_i using planning value a_t.

We could have chosen any of the indices listed, or any combination of them, but for the purpose of this example we will focus on only one. If we over constrain the model it would lead to extensive computation time, particularly for large systems. Adding extra adequacy constraints doesn't alter the complexity of the methodology. Therefore, using one index is sufficient to use in an example.

We want to ensure that the probability of load curtailment in our power system is bounded by some value, $p_{max} \in [0, 1]$, which is the maximum probability of load curtailment we are willing to accept in our system. In section 3.1.2 we found the optimal planning value but we did not consider the probability of load curtailment associated with it. Given we choose the optimal planning value a^*, we can calculate the probability of load curtailment for that value. If it is greater than p_{max} we reject the planning value and find the next minimum. We repeat this until we find the lowest expected adapted optimal power flow cost who's associated planning value gives a probability of load curtailment less than p_{max}. To put mathematically:

$$\begin{aligned} V_t &= \min_{a_t} \mathbb{E}[c(X_t, a_t)] \\ \text{such that:} & \\ PLC &= \sum_{x_i} P(X_t = x_i) \mathbb{1}_{\{l_{x_i,a_t} < L\}} \leq p_{max} \end{aligned} \tag{3.13}$$

The method used in this optimisation is a trial and error method. If the optimal planning value doesn't satisfy the constraint in (3.13) then we reject the associated expected adapted optimal power flow and find the next minimum. This is repeated until we find a minimum that satisfies the constraint. This in portrayed in the flow chart in figure 3.6.

It has been shown that the optimisation problem (3.1) is convex and has a unique solution [57]. Given the expectation (3.2) exists, we can conclude that a solution of (3.13) must also exist. We can see the solution of the problem in figure 3.7. The same argument holds for (3.14) and (3.15) which are introduced in the following sections.

A graphical interpretation of (3.13) can be seen in figure 3.7 and figure 3.8. For this simulation the scale values in table 3.4 were used. In figure 3.7 we see that as the constraint it implemented, the optimal planning value changes to a value which corresponds to a higher expected adapted optimal power flow cost. The lower the constraint the higher the expected adapted optimal power flow cost. Figure 3.8 is the expected adapted optimal power flow cost using the optimal planning value against various values of p_{max}. We can see that as p_{max} becomes smaller, the expected adapted optimal power flow cost increases. Using this we can compare various expected adapted optimal power flow costs against the associated probability of load curtailment and try find one which happily balances reliability and economy. A system controller and

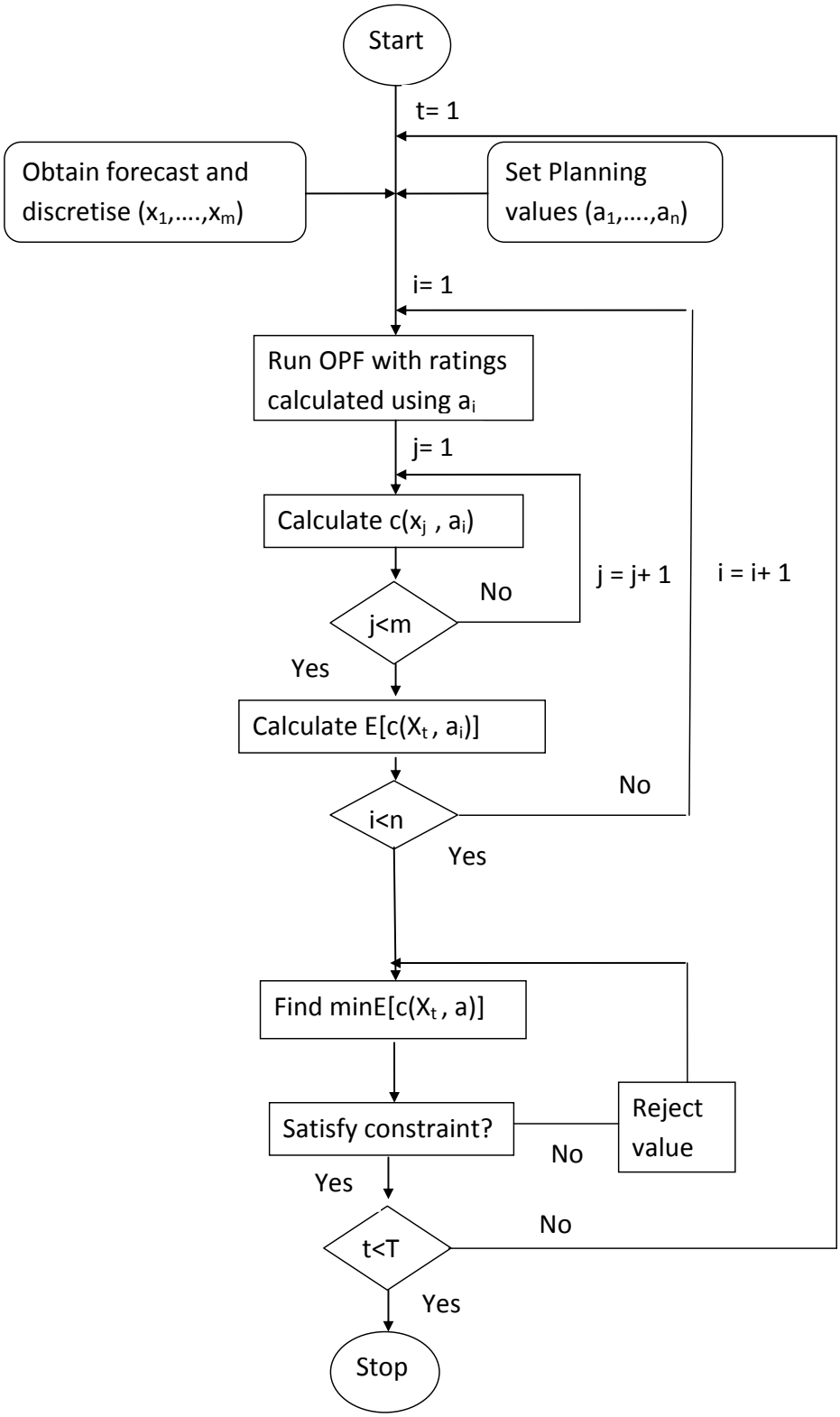

Figure 3.6: Flow chart for method used in section 3.1.4.

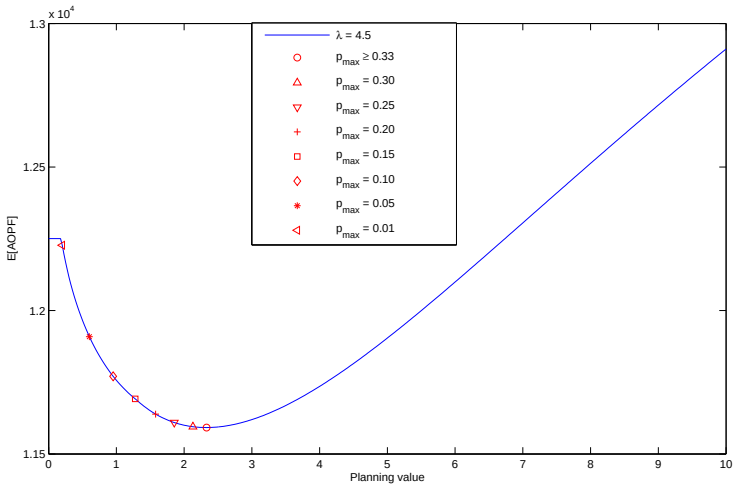

Figure 3.7: Expected adapted optimal power flow cost against the wind speed chosen as the planning value, examining both the constrained and non-constrained models. The constraint on the model is that the probability of load curtailment has to be below a set limit, p_{max}. The circle corresponds to the optimal planning value to set in the non-constrained model while the other symbols correspond to the constrained model for various values of p_{max}.

designer must decide on what level of trade off is acceptable between the expected adapted optimal power flow cost and the probability of load curtailment.

Adding System Security Constraint

Previously we examined adding a constraint to the model which can help us to understand the adequacy of the system. We will now examine adding a constraint which examines the security of the system. Investigating system security involves investigating the risk that the system is liable to. As stated, risk is defined as the product of the event's probability by its impact. When investigating the adequacy of the system we used an index which did not take into account the severity of the occurrence. Probability of load curtailment counts losing 1MWh (Mega-Watt hour) as the same as counting the loss of 10GWh (Giga-Watt hour). They are both counted as one occurrence. Therefore to measure system security, we use a constraint which takes into account the severity of each event occurring, and not just the likelihood. One area of power systems under current research is examining the cost of security in a power system, and whether people would pay extra costs for a higher level of security or whether they would rather have themselves liable to be the first cut off in the event

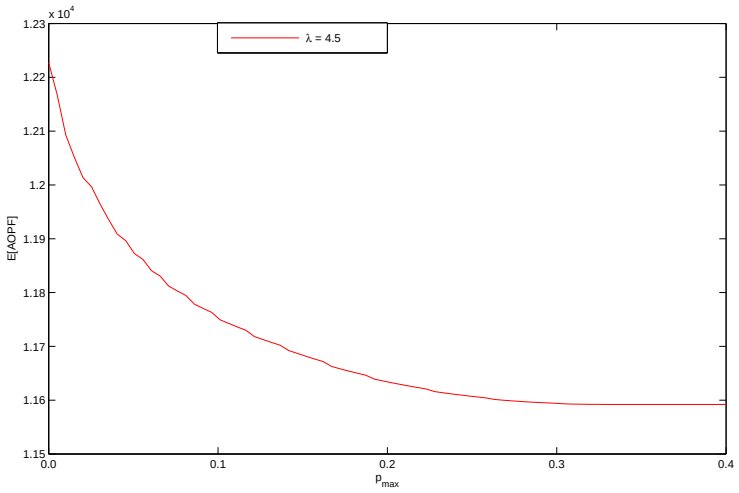

Figure 3.8: Expected adapted optimal power flow cost using the optimal planning value against various values of the p_{max}, the maximum probability of load curtailment we accept.

of a power shortage. At time of writing, this was currently under investigation by WP5. This idea was the motivation behind [38], as discussed previously, trying to find a balance between security and economy. We use an index which can allocate a monetary value to impact so we can calculate the risk in the system. The index we shall use is the expected cost of load curtailment over the total cost of the adapted optimal power flow. This will let the system operator define an acceptable percentage level he is willing to pay for security. For the security constraint the optimisation function is defined as:

$$V_t = \min_{a_t} \mathbb{E}[c(X_t, a_t)]$$

such that:

$$\begin{aligned} \mathbb{E}[CLC] &= \sum_{x_i} \frac{P(X_t = x_i) \times (L - l_{x_i,a_t}) \times CLC}{P_g C_g} \mathbb{1}_{\{l_{x_i,a_t} < L\}} \\ &\leq CLC_{max} \end{aligned} \tag{3.14}$$

where $\mathbb{E}[CLC]$ is the expected cost of load curtailment over the total cost, $P(X_t = x_i)$ is the probability that the random variable X_t has value x_i. $(L - l_{x_i,a_t})$ is the amount of load that is curtailed when value x_i occurs using planning value a_t, CLC is the cost of load curtailment, P_g is the power generator output vector and C_g is the generator output cost vector. CLC_{max} is the maximum cost of load curtailment over the total cost that the system operator accepts. The flow chart for this method is the same as

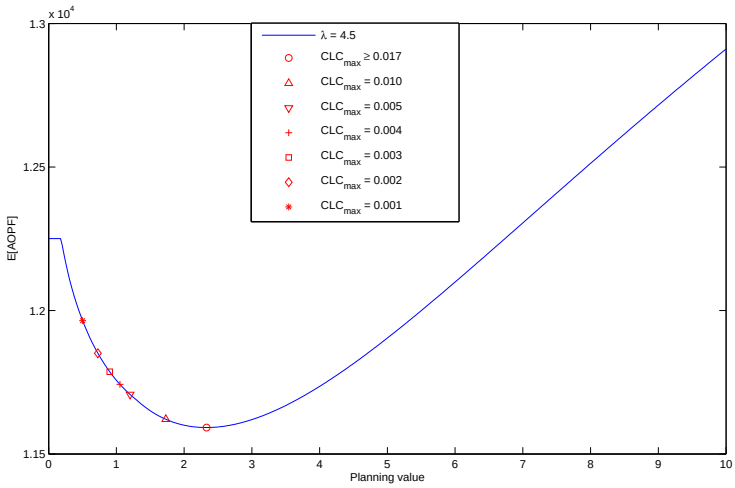

Figure 3.9: Expected adapted optimal power flow cost against the wind speed chosen as the planning value, examining both the constrained and non-constrained models. The constraint on the model is that the expected cost of load curtailment over total cost had to be below a set limit, CLC_{max}. The circle corresponds to the optimal planning value for the non-constrained model while the other symbols correspond to the constrained model for various values of CLC_{max}.

that found in figure 3.6.

(3.14) is expressed graphically in figure 3.9 and figure 3.10. For this simulation the scale values in table 3.4 were used. In figure 3.9 we see that as the constraint is implemented, the optimal planning value changes to a value which corresponds to a higher expected adapted optimal power flow cost. Figure 3.10 is a similar graph to figure 3.8, but with the expected cost of load over total cost as the constraint. We can see it portrays similar results. As CLC_{max} increases, the expected cost decreases. That is to say that as the security decreases, so too does the expected cost. Using this we can compare various expected costs against the associated expected cost of load curtailment over total cost and try find a value which happily balances security and economy. If we want sufficient security which is economically viable a balance between how secure the system is and how much the consumer is willing to pay must be found. Examining finding a balance is outside the scope of this thesis but, at time of writing, was being examined by WP5.

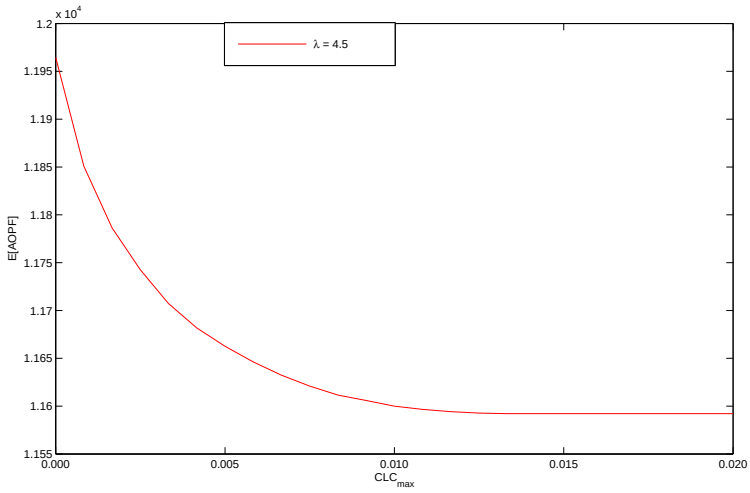

Figure 3.10: Expected adapted optimal power flow cost using the optimal planning value against various values of the CLC_{max}.

Adding Ramp Rate Constraint

We will now introduce a different type of constraint in the model. Previously, when choosing the optimal planning value, each time step was independent. We did not consider previous time steps and thus previous planning values. Some generators cannot instantaneously change from a small output to a large output or vice verse. Therefore, to consider this factor, we constrain the change in generation by introducing a ramp rate. A ramp rate, $\Delta g_{\max}$, is defined as the maximum change in output power in a generator, between time steps. Adding the ramp constraint to (3.3) gives:

$$\begin{aligned} V_t &= \min_{a_t} \mathbb{E}[c(X_t, a_t)] \\ \text{such that:} & \\ 0 \leq & \ |\Delta g(a^*_{t-1}, a_t)| \leq \Delta g_{max} \end{aligned} \tag{3.15}$$

where $\Delta g(a^*_{t-1}, a_t)$ is the change in generation between the optimisation at time $t-1$ and time t using optimal planning value a^*_{t-1} and planning value a_t for time $t-1$ and t respectively. For this constraint we must constantly look back to the previous time step. This is true except for the first time step. When we begin running the model we make the assumption that all generators are originally off. Therefore, on first run of the model we can imagine that we are turning the generators on and setting them to the desired output. Therefore the ramp rate will be zero.

As mentioned previously for the non-constrained model, every scale value λ_t from

the Weibull distribution, governing a wind speed forecast, has a corresponding optimal planning value a_t^*. This is calculated using (3.3). Let a_t' denote the planning value which minimises the objective function in (3.15), prior to checking the constraint, for forecast random variable X_t with scale value λ_t which is a realisation of Λ_t, i.e. a_t' is the unconstrained optimal planning value. For time t_0:

$$a_{t_0}^* = a_{t_0}'$$

as we assume the generators are initially off and thus there is no ramp rate constraint. For time $t > t_0$, having obtained a_t' we check the ramp rate constraint

$$\Delta g(a_{t-1}^*, a_t') \leq \Delta g_{max}.$$

If the constraint is satisfied then we set

$$a_t^* = a_t'.$$

If the constraint is not satisfied for the value a_t' we can observe the following:

- If $\lambda_t > \lambda_{t-1}$ then $a_t^* < a_t'$.
- Likewise, if $\lambda_t < \lambda_{t-1}$ then $a_t^* > a_t'$

If

$$a_t^* \neq a_t'$$

the constrained expected adapted optimal power flow will be more expensive then the unconstrained. The above is shown graphically for time t_0 and t_1 in figure 3.11. For this example $\lambda_{t_1} > \lambda_{t_0}$. We can see for various values of the ramp rate that $a_t^* < a_t'$ and this leads to a more expensive expected adapted optimal power flow. The values a_t' are labelled by a 'o'. Values of a_t^* constrained by the ramp rate are labelled with various symbols. Observing how λ_t and λ_{t-1} affect the value a_t^* will help us to understand the two period model when we examine it in section 3.2.

The ramp rate constraint was applied to the optimisation run in section 3.1.2, see figure 3.4. The results produced curves as seen in figure 3.12 and figure 3.13. For this simulation the scale values in table 3.4 were used. In figure 3.12, we see that as the ramp rate decreases, the values of the optimal planning value are less varied and at $\Delta g_{max} = 0$ the curve is a straight horizontal line meaning that the optimal planning

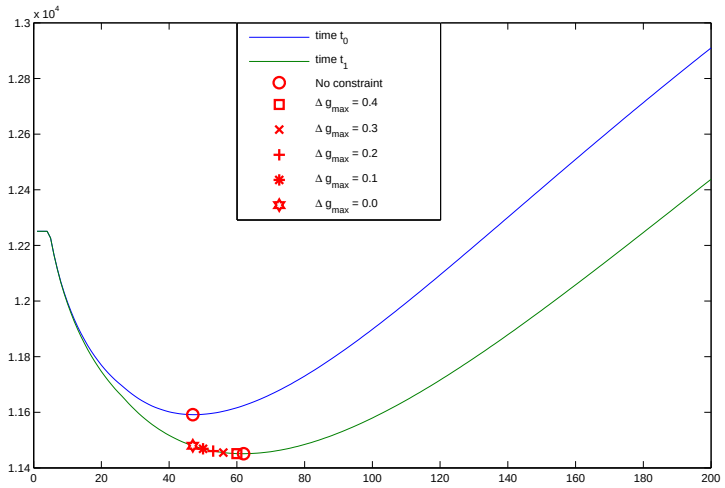

Figure 3.11: Variation of expected adapted optimal power flow cost for various ramp rates for two time steps. This figure investigates how the ramp rate constraint affects the solution in comparison to the unconstrained model.

value is stationary in time. However, this does not result in a constant expected cost. In figure 3.13 we can see that as the ramp rate increases from zero, the curves converge towards the original simulation which didn't have any constraint.

Combining Adequacy and Ramp Rate Constraint

We will now examine the combination of using two constraints, an adequacy constraint as well as a ramp rate constraint. Using an adequacy or security constraint comprises of the same methodology. For this example we will use an adequacy constraint. The adequacy constraint we will impose is on the probability of load curtailment as defined in (3.12). For two constraints the optimisation problem becomes:

$$\begin{aligned} V_t &= \min_{a_t} \mathbb{E}[c(X_t, a_t)] \\ \text{such that:} & \\ PLC = & \sum_{x_t} P(X_t = x_i) \mathbb{1}_{\{l_{x_i,a_t} < L\}} \leq p_{max} \\ 0 \leq & \ |\Delta g(a^*_{t-1}, a_t)| \leq \Delta g_{max} \end{aligned} \tag{3.16}$$

What this is effectively doing is taking every curve in figure 3.13 and applying the probability of load curtailment constraint. This simulation was under the same forecasts as we used in the optimisation we originally ran, with scale values as in table 3.4, which is discussed in section 3.1.2 and can be seen in figure 3.4. The best means of

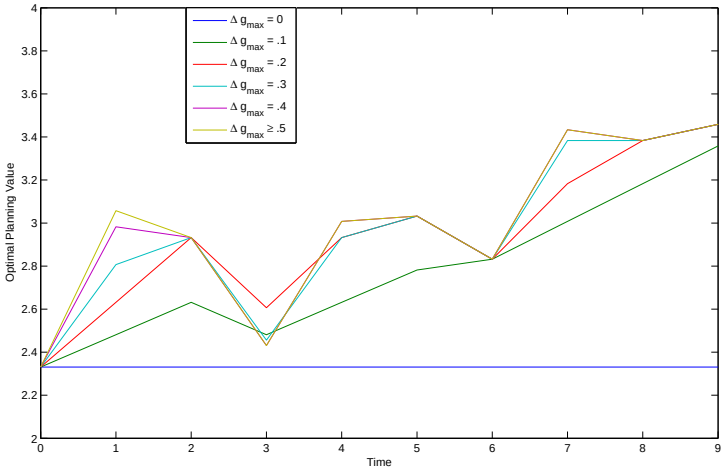

Figure 3.12: In this figure we see how adding the ramp rate constraint affects the optimal planning value in time. This is done for various values of the ramp rate. The curve with the highest ramp rate has the most variation in values, and is identical to the non-constraint curve as seen in figure 3.4(a). As the maximum allowable ramp rate decreases, the variation in the curve decreases until we have a straight line corresponding to $\Delta g_{max} = 0$. This line is straight as the planning value cannot change in subsequent steps after being decided in step 1.

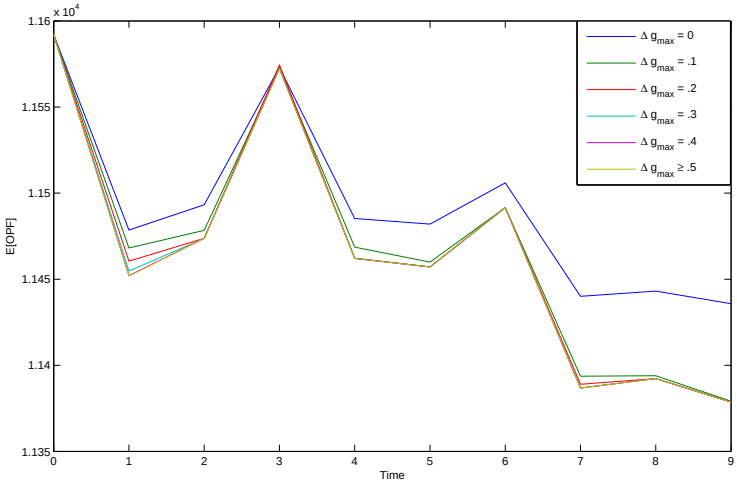

Figure 3.13: In this figure we see how adding the ramp rate constraint affects the expected adapted optimal power flow cost in time. The curves of the expected adapted optimal power flow cost for various ramp rates. If the ramp rate constraint was not imposed in this model then all curves would be identical to that of the curve in figure 3.4(b). We can see however that all curves do follow the same trend and for large values of the ramp rate the curves are identical to that of figure 3.4(b). As the ramp rate increases from zero we can see that the curves converge towards the curve identical to that with no ramp rate constraint. It is evident from this plot that lower ramp rates result in higher expected adapted optimal power flow costs.

examining this graphically is to examine each time step individually as a 3-dimensional plot of expected adapted optimal power flow cost against ramp rate and probability of load curtailment. The plots of the second and fourth time step can be seen in figure 3.14(a) and figure 3.14(b) respectively. I have plotted the second time step as the first time step isn't constrained by the ramp rate constraint and is flat across the axis corresponding to Δg_{max}. The third time step is similar to the second time step with all solutions available. The fourth time step is the first time step in which solutions are unavailable. As you more forward in time more solutions become unavailable.

Figure 3.14(a) corresponds to the second time step of the simulation with p_{max} on the x-axis, Δg_{max} on the y-axis and the expected adapted optimal power flow cost on the z-axis. It can be seen that the expected adapted optimal power flow cost decreases as p_{max} and Δg_{max} increase. Again this brings about the need of a system operator deciding how secure he wants his system and at what economical cost.

Figure 3.14(b) corresponds to the fourth time step of the simulation. We can see that for some values of Δg_{max} and p_{max} no corresponding expected adapted optimal power flow costs are present. We saw in figure 3.13 how solutions were always available for various ramp rate values. However, these solutions may not always satisfy the reliability constraints.

The lower the ramp rate, the more constrained the model is. This leads to higher expected adapted optimal power flow values. It also decreases the range of the solution set for the next time step. The solution set is the range of planning values which satisfies the ramp rate constraint. In the case where no planning value in the solution set satisfies the adequacy constraint we say that the solution is unavailable. This usually occurs for lower values of Δg_{max} when there is a decrease in the random scale variable Λ_t. For higher values of Λ_t, the mean wind speed is higher and thus the probability of the wind speed being above a set planning value is less than it is for lower values of Λ_t. Therefore higher values of Λ_t will have a lower probability of load curtailment than lower values of Λ_t for a set planning value. If the solution set is tightly constrained due to the ramp rate, and the scale value moves from a higher to a lower value, it may be the case where all solutions in the solution set may not be able to satisfy the probability of load curtailment constraint.

For example, in the case of $\Delta g_{max} = 0$, the optimal planning value is constant for

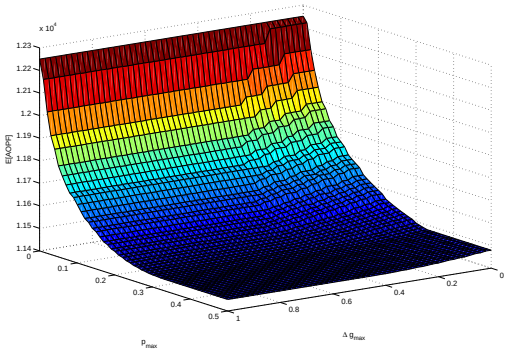

(a) Expected adapted optimal power flow cost against ramp rate and adequacy constraint, p_{max}, for second time step $t = t_1$.

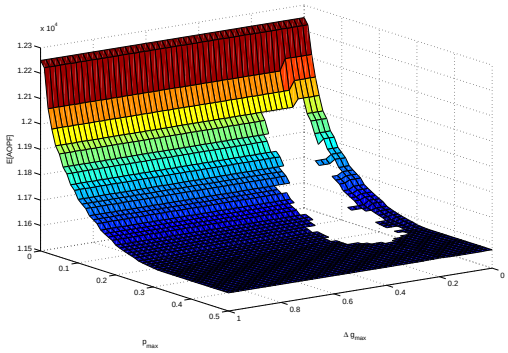

(b) Expected adapted optimal power flow cost against ramp rate and adequacy constraint, p_{max}, for fourth time step $t = t_3$.

Figure 3.14: In these plots we see the expected adapted optimal power flow cost plotted against various ramp rate values and values of the adequacy constraint, p_{max}. This can be seen for the second and fourth time step in figure 3.14(a) and figure 3.14(b) respectively. I have plotted the second time step as this is constrained by both constraints. Was I to plot the first time step, then the second constraint in (3.16) would not affect the model. Also, the fourth time step shows how the constraints affect the solution as time passes, in which sometimes solutions aren't available due to the constraints.

the duration of the simulation for each value of p_{max} tested and are the values chosen in the first time step. If $\Lambda_t < \Lambda_{t_0}$ for some $t > t_0$, the values chosen as the optimal planning values will not satisfy the probability of load curtailment constraints for time t. If a solution is not available in one time step for a combination of Δg_{max} and p_{max} then we assume it is not available for subsequent time steps as the ramp rate would become invalid due to no solution being available in the previous time step and thus no generation being dispatched.

3.2 Two Period Model

In the previous section, section 3.1, we assumed at each time t we are given a forecast in the form of a probability distribution for one time step ahead in the future. This is the one period model as we are optimising over only one time period at each time step.

Assume now that at time t we are given two forecasts, in the form of two probability distributions, for the same weather variable, wind speed, but for two different time

periods. One probability distribution is a forecast for one period ahead and the other is a forecast for two periods ahead. We define a period as a future time step as to distinguish between the current time step we are in and the future time step (time period) we are optimising over. The two forecasts have random variables denoted $X_t^{(1)}$ and $X_t^{(2)}$ for one period and two periods in the future, with planning values denoted $a_t^{(1)}$ and $a_t^{(2)}$ respectively and $\mathbf{a_t} = \{a_t^{(1)}, a_t^{(2)}\}$.

For the two period optimisation we want to minimise the sum of the expected adapted optimal power flows for the two periods. The objective function for the two period optimisation is defined as:

$$\min_{\mathbf{a}_t=\{a_t^{(1)},a_t^{(2)}\}} \sum_{i=1}^{2} \mathbb{E}[c(X_t^{(i)}, a_t^{(i)})]. \tag{3.17}$$

When we do the optimisation we want to find two planning weather values, $\mathbf{a_t} = \{a_t^{(1)}, a_t^{(2)}\}$, one for time $t+1$ and one for time $t+2$, which minimises the expected cost of the two adapted optimal power flows. These will be the optimal planning values denoted $a_t^{(1)*}$ and $a_t^{(2)*}$ respectively

After running the optimisation, the optimal planning value $a_t^{(1)*}$ implies a dispatched generation for time $t+1$ and we assume this generation is dispatched at time $t+1$, as in the one period model. However, the dispatch which corresponds to the two period optimal planning value, $a_t^{(2)*}$, may not be dispatched at time $t+2$. This is because we receive an updated forecast at time $t+1$.

When we move forward to time $t+1$, we are provided with two new forecasts with random variables denoted $X_{t+1}^{(1)}$ and $X_{t+1}^{(2)}$ for one and two periods ahead, i.e. time $t+2$ and $t+3$. $X_{t+1}^{(1)}$ is an update of $X_t^{(2)}$, as we receive $X_t^{(2)}$ at time t and $X_{t+1}^{(1)}$ at time $t+1$. Both forecasts correspond to time $t+2$. When we run the optimisation for random variables $X_{t+1}^{(1)}$ and $X_{t+1}^{(2)}$, we calculate two optimal planning values denoted $a_{t+1}^{(1)*}$ and $a_{t+1}^{(2)*}$. The optimal planning value $a_{t+1}^{(1)*}$ is an update of $a_t^{(2)*}$ and the generation implied by the optimal planning value $a_{t+1}^{(1)*}$ is the generation that is dispatched.

3.2.1 Calculating Scale value

We assume the one period forecast will be more accurate than the two period forecast. This is an appropriate assumption as in weather forecasting uncertainty increases the further into the future one is trying to predict [23]. The two forecasts, at time t, for

time $t+1$ and $t+2$ will have random variables denoted $X_t^{(1)}$ and $X_t^{(2)}$ respectively. As the forecasts are for wind speed, both forecasts are Weibull distributions:

$$\begin{aligned} X_t^{(1)} &\sim \text{Weibull}(\Lambda_t^{(1)}, \beta) \\ X_t^{(2)} &\sim \text{Weibull}(\Lambda_t^{(2)}, \beta) \end{aligned} \tag{3.18}$$

where $\Lambda_t^{(1)}$ and $\Lambda_t^{(2)}$, the scale parameters, are random variables, and β, the shape parameter, is constant.

Since the forecasts we are given at time t are for times $t+1$ and $t+2$, we want some dependency between the climate conditions now, i.e. when the forecasts are being calculated, the one period forecast and the two period forecast. It would not be sensible if the current climate was not taken into consideration when calculating the one period forecast. Considering what we think is going to happen in the one step ahead forecast, this information should also be taken into account when calculating the two period forecast. This is the case for the first time step. When we move into the next time step, we want to calculate an update of the previous second period forecast. The updated forecast is based on the new information gained and is now for one period ahead. We then calculate a two period forecast based on the one period forecast. A mathematical description is provided below and a graphical interpretation is provided in figure 3.15.

We calculate the random scales as follows:

- Assume we start at time t_0 with fixed scale value, λ_0, calculated using the maximum likelihood estimator on empirical data, as discussed in section 3.1.2.

- For the one period scale value we add a random increment $\epsilon_{t_0}^{(1)} \sim \mathcal{N}(0,1)$ to λ_0. This is now the scale value for the one period forecast.

- The scale value for the two period forecast is chosen as the one period scale value plus a random increment $\epsilon_{t_0}^{(2)} \sim \mathcal{N}(0,1)$, where $\epsilon_{t_0}^{(1)}$ and $\epsilon_{t_0}^{(2)}$ are independent and identically distributed.

- Moving to subsequent time steps $t > t_0$, we calculate a scale value for the one period forecast, which is an update of the previous time step's two period scale value. We denote the new information obtained between time $t-1$ and t as $u_t \sim \mathcal{N}(0, \frac{1}{2})$. We add this u_t to the previous time step's two period scale value.

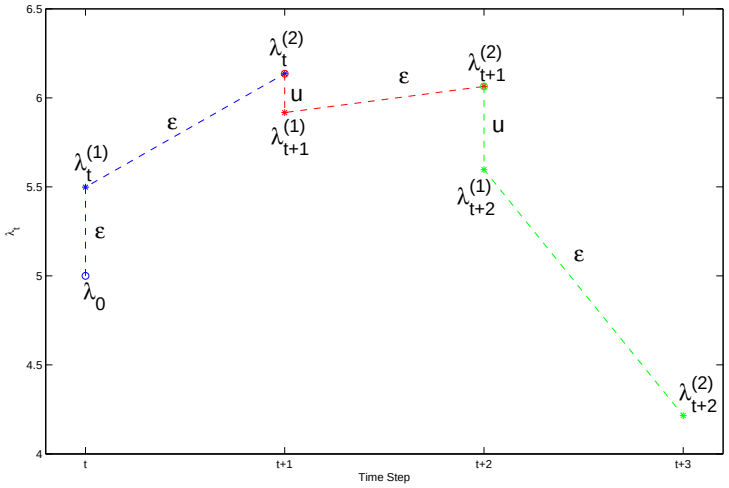

Figure 3.15: This figure shows the randomness of the scale value used in the Weibull Distributions for which we use as forecasts. Each colour segment corresponds to a time step, in which the scale value for the two future periods is generated. Since the shape parameter is constant, having the scale value as a random walk is effectively the same as having the first moment as a random walk since they are directly proportional.

- For time t's two period scale value we add a random increment $\epsilon_t^{(2)} \sim \mathcal{N}(0,1)$ to the one period scale.

Mathematically we define as:

$$\begin{aligned}
&\text{for } t = t_0 \\
&\qquad \Lambda_{t_0}^{(1)} = \lambda_0 + \epsilon_{t_0}^{(1)} \\
&\qquad \Lambda_{t_0}^{(2)} = \Lambda_{t_0}^{(1)} + \epsilon_{t_0}^{(2)} \\
&\text{for } t > t_0 \\
&\qquad \Lambda_{t}^{(1)} = \Lambda_{t-1}^{(2)} + u_t \\
&\qquad \Lambda_{t}^{(2)} = \Lambda_{t}^{(1)} + \epsilon_{t}^{(2)}
\end{aligned} \tag{3.19}$$

We can write these as conditional and unconditional random variables.

As conditional random variables:

$$\begin{aligned}
&\text{for } t = t_0 \\
&\qquad \Lambda_{t_0}^{(1)} \sim \mathcal{N}(\lambda_0, 1) \\
&\qquad \Lambda_{t_0}^{(2)} | \Lambda_{t_0}^{(1)} \sim \mathcal{N}(\Lambda_{t_0}^{(1)}, 1) \\
&\text{for } t > t_0 \\
&\qquad \Lambda_{t}^{(1)} | \Lambda_{t-1}^{(2)} \sim \mathcal{N}(\Lambda_{t-1}^{(2)}, \tfrac{1}{2}) \\
&\qquad \Lambda_{t}^{(2)} | \Lambda_{t}^{(1)} \sim \mathcal{N}(\Lambda_{t}^{(1)}, 1)
\end{aligned} \tag{3.20}$$

As unconditional random variables:

$$\begin{aligned} \text{for } t = t_0, \ldots, T & \\ \Lambda_t^{(1)} &\sim \mathcal{N}(\lambda_0, 1 + (1 + \tfrac{1}{2})(t - t_0)) \\ \Lambda_t^{(2)} &\sim \mathcal{N}(\lambda_0, 2 + (1 + \tfrac{1}{2})(t - t_0) \end{aligned} \tag{3.21}$$

When we do the optimisation we want to find two planning weather values, $\mathbf{a_t} = \{a_t^{(1)}, a_t^{(2)}\}$, one for time $t+1$ and one for time $t+2$, which minimises the sum of the expected cost of the two adapted optimal power flows. If we were only to do this, it would essentially be the same as running the unconstrained single stochastic variable model in section 3.1 for two time steps. To make the model both more interesting, complex and realistic we are going to add a constraint to the optimisation which will couple the optimsation between the two periods.

3.2.2 Adding Ramp Rate Constraint

We have previously examined adding a ramp rate constraint to a one period model. Now we will examine adding the constraint to a two period model, and the differences between this constraint for the one and two period model. For the one period, the ramp rate constraint was added in section 3.1.4 and was defined by (3.15) as:

$$\min_{a_t} \mathbb{E}[c(X_t, a_t)]$$

such that:

$$0 \leq \quad |\Delta g(a_{t-1}^*, a_t)| \leq \Delta g_{max}$$

In order to couple the two periods in the two period model we add two constraints to the objective function as defined in (3.17):

$$\min_{\mathbf{a}_t = \{a_t^{(1)}, a_t^{(2)}\}} \sum_{i=1}^{2} \mathbb{E}[c(X_t^{(i)}, a_t^{(i)})]$$

such that:

$$\begin{aligned} 0 \leq \quad & |\Delta g(a_t^{(1)}, a_t^{(2)})| && \leq \Delta g_{max} \\ 0 \leq \quad & |\Delta g(a_{t-1}^{(1)*}, a_t^{(1)})| && \leq \Delta g_{max} \end{aligned} \tag{3.22}$$

where $\Delta g(a_t^{(1)}, a_t^{(2)})$ is the change in the generation output implied by the two planning values $a_t^{(1)}$ and $a_t^{(2)}$, thus coupling the two periods. $\Delta g(a_{t-1}^{(1)*}, a_t^{(1)})$ is the change in the generation output between the one period optimal planning value at time $t-1$, denoted

Time Step:	1	2	3	4	5	6	7	8	9	10
First Period Scale:	4.36	6.25	5.88	4.57	6.07	6.15	5.60	7.64	7.50	7.85
First Period Scale:	6.33	5.93	4.54	6.25	6.36	5.72	7.53	7.86	7.74	7.59

Table 3.5: Scale values for two period simulation.

$a_{t-1}^{(1)*}$, and the one period planning value at time t, denoted $a_t^{(1)}$. This constraint was previously examined in section 3.1.4. We do not need to constrain $a_t^{(2)}$ with $a_{t-1}^{(2)*}$ as these planning values are liable to change. For time $t = t_0$ the second constraint doesn't apply as we assume the generators are in an off state and as such can be switched to whatever generation we choose upon start up.

We will first examine this method for a single time step, t_0. At time t_0 we are provided with two forecasts. One is for one period in the future and the other is for two periods ahead in the future. This is effectively only considering the first ramp rate constraint, $\Delta g(a_t^{(1)}, a_t^{(2)})$ in (3.22), as in the first time step, the second ramp rate constraint isn't considered.

Figure 3.16 shows the expected adapted optimal power flow cost against the planning wind speed values for both periods. The optimal planning values are marked on the curves and this is done for a range of values of Δg_{max}, as portrayed by various symbols. We can see as the ramp rate increases, the minimum expected adapted optimal power flow, for each period, that satisfies the constraints, decreases. For $\Delta g_{max} = 0$ the optimal planning values are the same value. This can be seen as one lies vertically above the other. The sum of these values is the most expensive pair. This will be more evident in figure 3.17.

Figure 3.17 shows the curves of the minimum expected adapted optimal power flow cost for both periods, for a range of ramp rates. We can see that as the ramp rate increases the minimum expected adapted optimal power flow cost for both periods decreases. The most expensive case is when $\Delta g_{max} = 0$.

We will now examine the case of subsequent time steps. This includes using both constraints in (3.22). The results of this simulation can be seen in figure 3.18 and figure 3.19. Table 3.5 contains the scale values used for the simulation. The scale values for the first period are the same as that used in the one period model simulations performed in section 3.1, as so we can make some comparisons between results. See table 3.4 for one period model scale values.

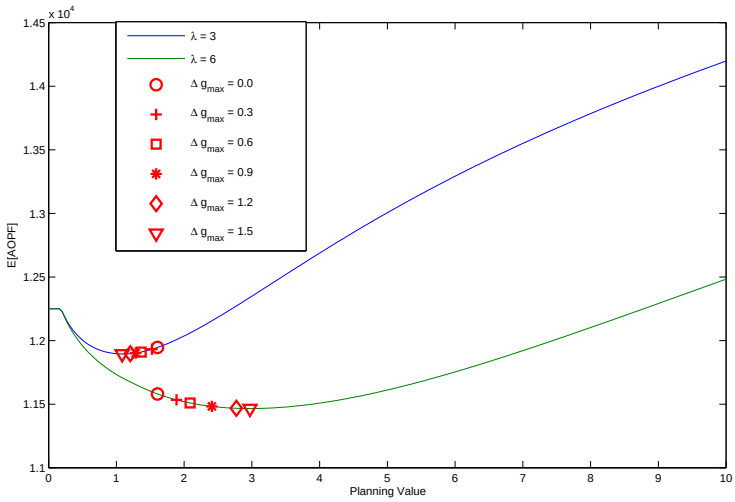

Figure 3.16: Expected adapted optimal power flow costs for two period model for single time step with varying ramp rate. This is done for various values of the ramp rate denoted by the various symbols. We can see as the ramp rate increases, the minimum expected adapted optimal power flow, for each period, that satisfies the constraints, decreases. When $\Delta g_{max} = 0$ the optimal planning values are the same value for each period and can be seen as they are vertically above each other.

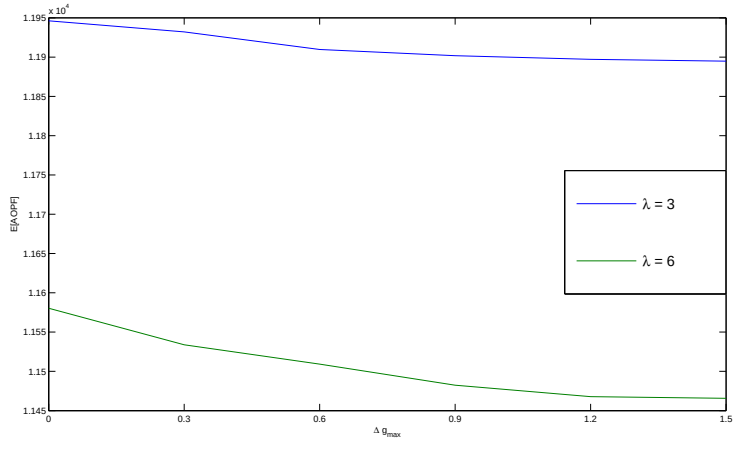

Figure 3.17: Minimum expected adapted optimal power flow costs for various ramp rates. We can see as the ramp rate increases, the expected adapted optimal power flow cost decreases for each time period.

Figure 3.18 shows the variation of the optimal planning value for various ramp rates in the two period model for ten time steps. This is similar to the one period model graph as shown in figure 3.12 but with some different values. When $\Delta g_{max} = 0$ we can see this produces a straight line as the optimal planning value chosen at time t_0 cannot be changed. We can see this line is different from that in figure 3.12. In this simulation it takes a higher value. However in others it can take a lower value. This is due to the influence of $\Lambda_{t_0}^{(2)}$, which is discussed in more detail further in the section. In the one period model the planning value corresponding to $\Delta g_{max} = 0$ is decided by simply choosing the optimal planning value that corresponds to the minimum expected adapted optimal power flow cost as the constraint in (3.15) isn't considered in the first time step. Thus it is influenced by the value of scale variable Λ_{t_0} corresponding to the forecast X_{t_0} in the one period model. In the two period model, at time t_0 the second constraint in (3.22) isn't considered. However the first constraint is and thus choosing the optimal planning value for $\Delta g_{max} = 0$ is influenced by the value of $\Lambda_{t_0}^{(1)}$ and $\Lambda_{t_0}^{(2)}$. If $\Lambda_{t_0}^{(2)}$ takes a value lower than the value of $\Lambda_{t_0}^{(1)}$ than the optimal planning value corresponding to $\Delta g_{max} = 0$ will be lower for the two period model than in the one period model. The opposite is true if the value of $\Lambda_{t_0}^{(2)}$ is higher than the value of $\Lambda_{t_0}^{(1)}$.

Figure 3.19 shows the variation of the expected adapted optimal power flow cost for various ramp rates in the two period model for ten time steps, corresponding to the curves in figure 3.18. These curves are similar to that of figure 3.13 but do have some variation due to the second period. At some times the one period model is more expensive than the two period model while at other times the two period model is more expensive than the one period model. We discuss this in more detail next.

Effect of Second Period Using Ramp Rate Constraint

We shall now examine how the constraint between the first and second period in the two period model affects the solution in relation to the one period model. We can do this comparison as the results we examine for both models are the first period optimal planning values and expected adapted optimal power flow costs, as seen in figures 3.12, 3.13, 3.18 and 3.19. For the two period model we only plot the first period as the second period is liable to change in the following time step.

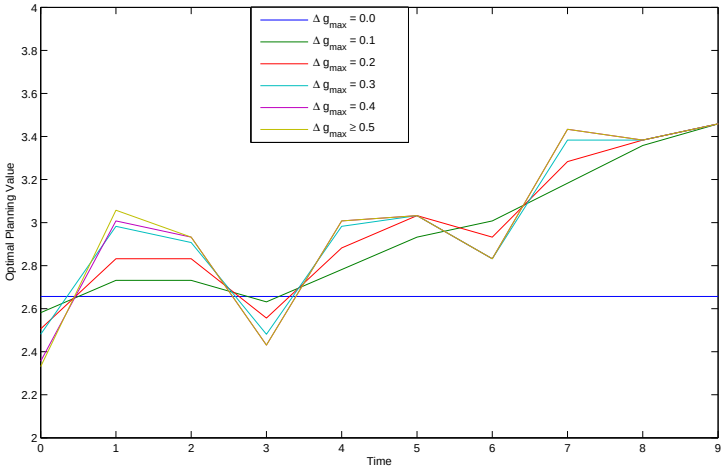

Figure 3.18: Variation of the optimal planning value for various ramp rates in the two period model. This is similar to that of figure 3.12 but for the two period model. Only the first period is plotted as the second period is liable to change in the next time step. The curve with the highest ramp rate has the most variation in values, and is identical to the none constraint curve as seen in figure 3.4(a). As the maximum allowable ramp rate decreases, the variation in the value of the curve decreases until we have a straight line corresponding to $\Delta g_{max} = 0$. This line is straight as the planning value cannot change in subsequent steps after being decided in at time t_0.

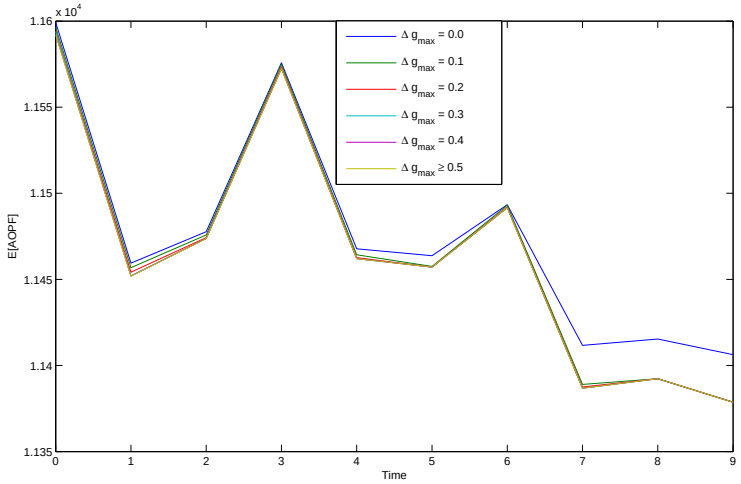

Figure 3.19: Variation of the expected adapted optimal power flow cost for various ramp rates in the two period model. If the second period ramp rate was not constraint then all curves would be identical to that of figure 3.13. We can see that as the ramp rate increases, all curves converge towards the curve $\Delta g_{max} \geq 0.5$.

An observation we can make is that if the planning values $a_t^{(1)'}$ and $a_{t-1}^{(1)*}$, where $a_t^{(1)'}$ is the first period unconstrained optimal planning value at time t, i.e. the optimal planning value that satisfies (3.17), and $a_{t-1}^{(1)*}$ is the first period constrained optimal planning value at time $t-1$, i.e. the optimal planning value that satisfies (3.22) at time $t-1$, do not satisfy the ramp rate constraint:

$$\Delta g(a_t^{(1)'}, a_{t-1}^{(1)*}) \leq \Delta g_{max} \tag{3.23}$$

or satisfy the constraint but the constraint is binding, then the second period does not affect the solution. This is because the value $a_{t-1}^{(1)*}$ cannot be changed at time t and thus $a_t^{(1)'}$ must be set within a range of $a_{t-1}^{(1)*}$, or be stationary in the case of a binding constraint, such that the ramp rate constraint is satisfied by the generation implied by the planning values. Let $a_t^{(1)''}$ be the planning value which satisfies constraint (3.23) meaning $a_t^{(1)''}$ takes the value of $a_t^{(1)'}$ when $a_t^{(1)'}$ satisfies constraint (3.23). When satisfying the constraint:

$$\Delta g(a_t^{(1)''}, a_t^{(2)'}) \leq \Delta g_{max} \tag{3.24}$$

$a_t^{(2)'}$ will be brought within range of $a_t^{(1)''}$. Therefore $a_t^{(1)''}$ is not changed or affected. The value that $a_t^{(2)'}$ is set to, to satisfy (3.24), will be the value set to $a_t^{(2)*}$. We also set

$$a_t^{(1)*} = a_t^{(1)''}$$

where $a_t^{(1)*}$ and $a_t^{(2)*}$ are the solutions to the constrained optimisation as in (3.22).

When the planning values $a_t^{(1)'}$ and $a_{t-1}^{(1)*}$ satisfy constraint (3.23), and the constraint is non-binding, then the second period does affect the first period solution. This only occurs when the unconstrained planning values $a_t^{(1)'}$ and $a_t^{(2)'}$ do not satisfy the constraint:

$$\Delta g(a_t^{(1)'}, a_t^{(2)'}) \leq \Delta g_{max}. \tag{3.25}$$

If $a_t^{(1)'}$ and $a_t^{(2)'}$ satisfy (3.23) and (3.25) then we set:

$$\begin{aligned} a_t^{(1)*} &= a_t^{(1)'} \\ a_t^{(2)*} &= a_t^{(2)'} \end{aligned}$$

However, if it is the case where $a_t^{(1)'}$ satisfies (3.23) we set:

$$a_t^{(1)''} = a_t^{(1)'}$$

and investigate how the second period affects the solution.

This investigation involves examining the scale values $\lambda_{t-1}^{(1)}$, $\lambda_t^{(1)}$ and $\lambda_t^{(2)}$ which correspond to the forecasts denoted by random variables $X_{t-1}^{(1)}$, $X_t^{(1)}$ and $X_t^{(2)}$ respectively. If:

- $\lambda_t^{(2)} > \lambda_t^{(1)} > \lambda_{t-1}^{(1)}$ then $a_t^{(1)*} \geq a_t^{(1)''}$ and $a_t^{(2)*} \leq a_t^{(2)'}$.
- $\lambda_t^{(2)} > \lambda_{t-1}^{(1)} > \lambda_t^{(1)}$ then $a_t^{(1)*} \geq a_t^{(1)''}$ and $a_t^{(2)*} \leq a_t^{(2)'}$.
- $\lambda_t^{(1)} > \lambda_{t-1}^{(1)} > \lambda_t^{(2)}$ then $a_t^{(1)*} \leq a_t^{(1)''}$ and $a_t^{(2)*} \geq a_t^{(2)'}$.
- $\lambda_{t-1}^{(1)} > \lambda_t^{(1)} > \lambda_t^{(2)}$ then $a_t^{(1)*} \leq a_t^{(1)''}$ and $a_t^{(2)*} \geq a_t^{(2)'}$.

For each of the λ scenarios, one or both of the inequalities involving the planning values are strict inequalities, depending on the difference between the planning values. For the scenarios:

$$\lambda_{t-1}^{(1)} > \lambda_t^{(2)} > \lambda_t^{(1)}$$

and

$$\lambda_t^{(1)} > \lambda_t^{(2)} > \lambda_{t-1}^{(1)}$$

if constraint (3.23) is satisfied then so too will (3.25) and thus the one period and two period will have the same values.

We will examine this graphically for the scenario of $\lambda_{t-1}^{(1)} > \lambda_t^{(1)} > \lambda_t^{(2)}$. This is seen in figure 3.20. In this example $a_t^{(1)'}$ and $a_{t-1}^{(1)*}$ satisfy constraint (3.23) and the constraint is unbinding. It can be seen how the value $a_t^{(1)*}$ decreases below the value $a_t^{(1)''}$, as outlined by the green star and circle respectively. It can also be seen how the value $a_t^{(2)*}$ increases above the value $a_t^{(2)''}$, as outlined by the red star and circle respectively.

Economically, if the constraint (3.23) isn't satisfied or is binding then the method gives the same results as in the one period model. If it is non-binding then we must examine the λ scenarios listed above. For:

- $\lambda_t^{(2)} > \lambda_t^{(1)} > \lambda_{t-1}^{(1)}$, the two period is cheaper than the one period if $a_t^{(1)*} > a_t^{(1)''}$. Otherwise it is the same.
- $\lambda_t^{(2)} > \lambda_{t-1}^{(1)} > \lambda_t^{(1)}$, the two period is more expensive than the one period if $a_t^{(1)*} > a_t^{(1)''}$. Otherwise it is the same.

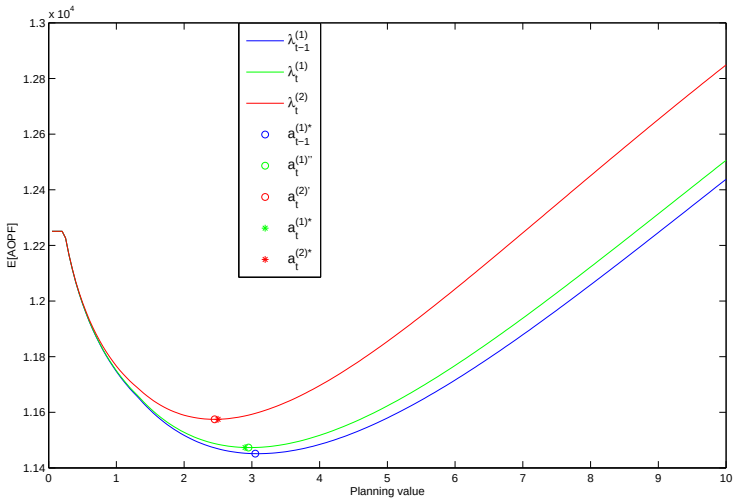

Figure 3.20: Observing how the second period ramp rate constraint affects the solution of the one period for $\lambda_{t-1}^{(1)} > \lambda_t^{(1)} > \lambda_t^{(2)}$.

- $\lambda_t^{(1)} > \lambda_{t-1}^{(1)} > \lambda_t^{(2)}$, the two period is more expensive than the one period if $a_t^{(1)*} < a_t^{(1)''}$. Otherwise it is the same.
- $\lambda_{t-1}^{(1)} > \lambda_t^{(1)} > \lambda_t^{(2)}$, the two period is cheaper than the one period if $a_t^{(1)*} < a_t^{(1)''}$. Otherwise it is the same.

This can also be seen in figure 3.20 for the case $\lambda_{t-1}^{(1)} > \lambda_t^{(1)} > \lambda_t^{(2)}$. When we say more expensive or cheaper, we mean in the comparative sense, i.e. if:

$$a_{t-1}^* = a_{t-1}^{(1)*}$$

where a_{t-1}^* is the optimal planning value using the one period model for time $t-1$. This would be the case if the second period forecast didn't affect the solution for all times up to $t-1$. However, this isn't always the case as the second period affects some solutions, for low ramp rates, for time t_0. The first time the second period affects the solution, it will keep the planning value at a higher or lower value until the next time the second period affects the solution. This is seen graphically in figure 3.21. This figure is the expected adapted optimal power flow cost for the one period model minus the first period's expected adapted optimal power flow costs for the two period model. This is affectively the curves in figure 3.13 minus the curves in figure 3.19.

In figure 3.21 we can see for the first time step t_0 the two period is more expensive or the same depending on the ramp rate. For the next time step, t_1, from table 3.5,

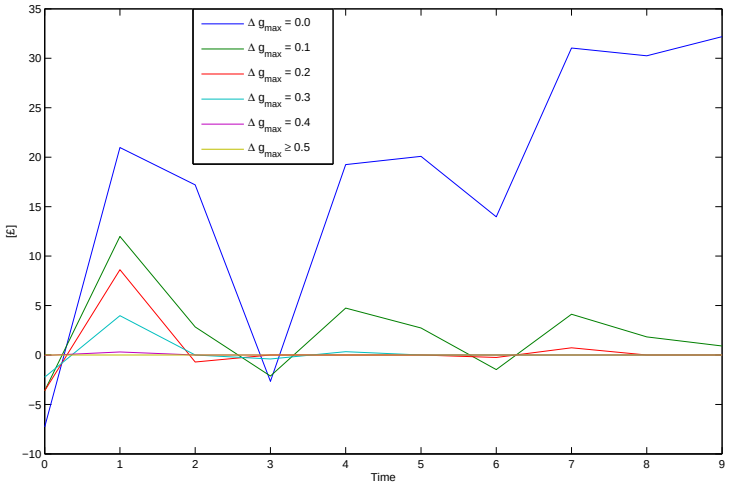

Figure 3.21: Difference in one period and two period expected adapted optimal power flow cost. This is the curves for the one period model, as seen in figure 3.17, minus the curves in the two period model, as seen in figure 3.19

we can see that $\lambda_{t_1}^{(1)} > \lambda_{t_1}^{(2)} > \lambda_{t_0}^{(1)}$. According to the list above this should make the two period model the same as the one period. This is the case for some ramp rates however for lower rates the two period model is cheaper due the constrain between the previous time step's optimal planning value, which isn't the same as the one period model due to the presence of $\lambda_{t_0}^{(2)}$. For time t_2, we can see that: $\lambda_{t_1}^{(1)} > \lambda_{t_2}^{(1)} > \lambda_{t_2}^{(2)}$. This should make the two period model cheaper or equal also. We can see for low values of Δg_{max} the difference between the model is positive, although lower than the difference in time t_1. Subsequent time steps follow the scenarios as listed previously. Forwarding to time t_5 we see $\lambda_{t_5}^{(1)} > \lambda_{t_4}^{(1)} > \lambda_{t_5}^{(2)}$. This corresponds to the more expensive solution for the two period than the one period, for low ramp rates. However, we can see that the model doesn't become more expensive for these ramp rates. The difference between the one and two period does decrease but does not become negative due to the positive difference at time t_4. The planning value cannot shift by an amount that would change the two period from cheaper to more expensive in a single time step due to the ramp rate constraint and as such still stays cheaper than the one period model.

3.2.3 Adding Reliability Constraint

The above method constrains the ramp rate but does not take into consideration other probabilistic scenarios such as load curtailment due to the overload of lines. In section 3.1.4 I discuss adequacy and security indices which can be added to the model as constraints. The same method can be applied to the two period optimisation. All the same indices as in section 3.1.4 could be used but for this example I have chosen probability of load curtailment, as defined in (3.12), as to compare with section 3.1.4.

To incorporate this adequacy index into the model we must add another constraint to (3.22). For the two period model, we check this for the first period only. We do this because the second period forecast are subject to recalculation in the next time step so will be checked then. If we wanted to check the second period reliability index constraint could be added to this method with ease. Implementing (3.12) into (3.22) the optimisation becomes:

$$\min_{\mathbf{a}_t=\{a_t^{(1)},a_t^{(2)}\}} \sum_{i=1}^{2} \mathbb{E}[c(X_t^{(i)}, a_t^{(i)})]$$

subject to:

$$\begin{aligned} 0 \leq \quad & |\Delta g(a_t^{(1)}, a_t^{(2)})| && \leq \Delta g_{max} \\ 0 \leq \quad & |\Delta g(a_{t-1}^{(1)*}, a_t^{(1)})| && \leq \Delta g_{max} \\ & \sum_{x_i} P(X_t^{(1)} = x_i) \mathbb{1}_{\{l_{x_i, a_t^{(1)}} < L\}} && \leq p_{max} \end{aligned} \tag{3.26}$$

3.2.4 Method

The method I used to compute the optimisation in (3.26) is described below and can be seen as a flow chart in figure 3.22:
Start at time $t = t_0$ and $p = 1$ (p denoting the time step ahead forecast):

1. Generate $\Lambda_t^{(p)}$.
2. Generate $x_1^{(p)}, \ldots, x_m^{(ip)} \sim Weibull(\Lambda_t^{(p)}, \beta)$.
3. For each planning wind speed, $a_t^{(p)} \in \mathbf{a}$, where $\mathbf{a}$ is the set of possible planning values, calculate:
$$\sum_{j=1}^{m} c(x_j^{(p)}, a_t^{(p)}) \times \Pr(X_t^{(p)} = x_j^{(p)})$$
then find $a_t^{(p)*}$, the optimal planning value.

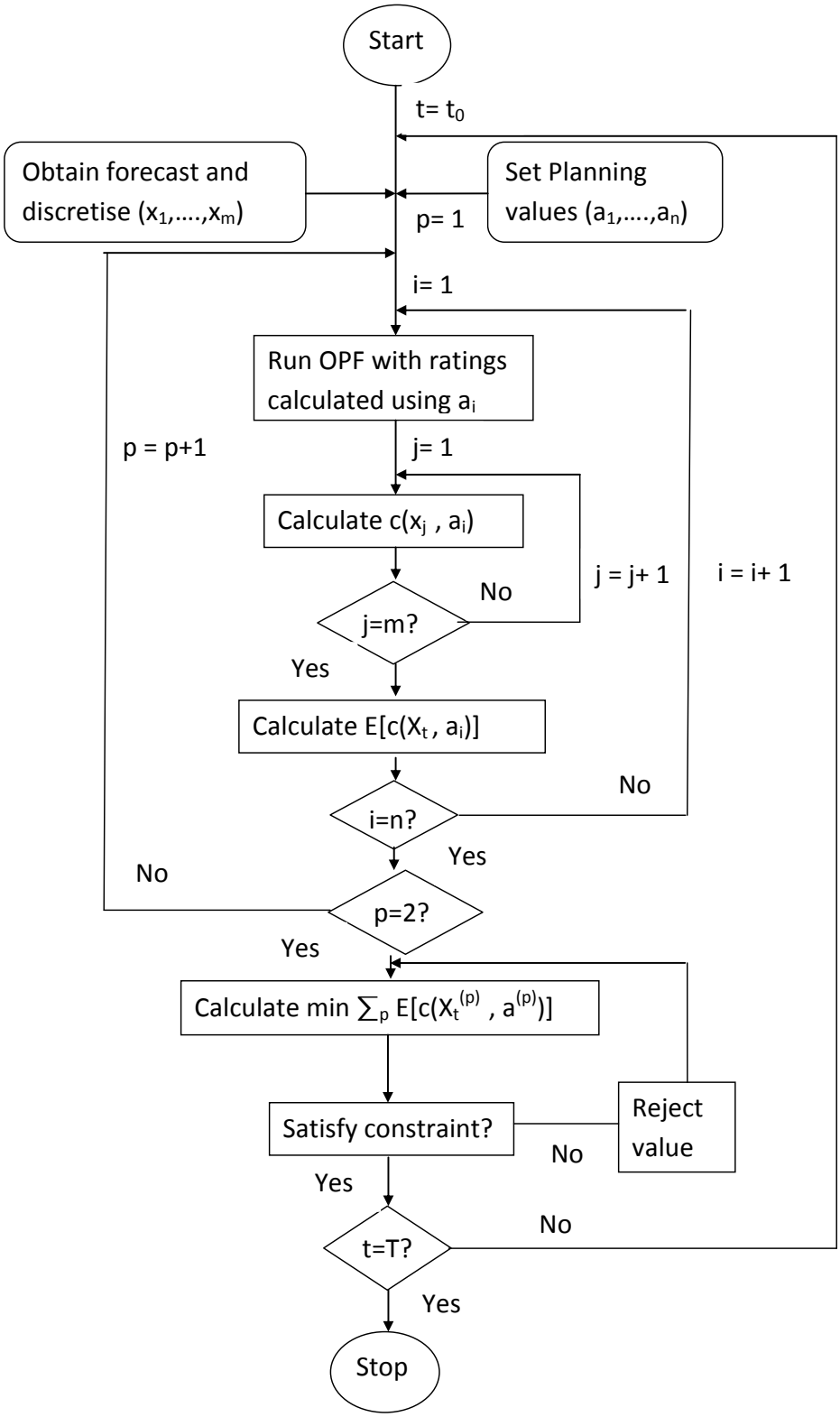

Figure 3.22: Flow chart for method used in section 3.2.3.

4. If $p = 1$, set $p = 2$ and go to step 1. Otherwise go to step 5.

5. Check constraints in (3.26). If unsatisfied, reject set, set p = 1 and return to step 3. If unsatisfied for all possible sets $\mathbf{a}_t = [a_t^{(1)}, a_t^{(2)}]$ then model is unable to run for the given ramp rate, Δg_{max}, and maximum probability of load curtailment, p_{max}, based on the scale value. End run. If satisfied go to step 6.

6. If $t < T$: increment t, set $p = 1$ and go to step 1. Else finish.

When we find the set $\mathbf{a}_t^*$ that satisfies constraints (3.26) for each time step from t_0 to T, we can then find the corresponding expected adapted optimal power flow costs associated with these planning weather values. We can do this for a range of ramp rate values, some of which will have solutions and some of which will not depending on the value of the constraint p_{max}, the value of the ramp rate Δg_{max} and the values of the scale values used in the forecasts.

3.2.5 Results

We ran a simulation of the method described in section 3.2.3 with scale values as in table 3.5. Firstly we will examine how the expected adapted optimal power flow cost changes with varying values of Δg_{max} and p_{max} for fixed time steps. I have shown this for two different time steps, the second and fourth, t_1 and t_3, in figure 3.23. It can be seen in both plots how the expected adapted optimal power flow cost decreases as the value of p_{max}, the maximum probability of load curtailment we allow in the system, increases. In figure 3.23(a) it is evident that there is also a decrease in the expected adapted optimal power flow cost as the ramp rate increases. In figure 3.23(b) we see that some of the plot is missing. This is because as t moves forward in time, some solutions aren't available. This was previously examined for the one period model in section 3.1.4. The one period and the two period model have similar results however not exactly identical. Depending on the scale values at each time step, the two period may have more or less missing solutions than the one period and may be more or less expensive for the solutions that are obtained.

Take for example the case when $\Delta g_{max} = 0$. As discussed in section 3.2.2, the optimal planning value for the two period model is influenced by $\Lambda_{t_0}^{(1)}$ and $\Lambda_{t_0}^{(2)}$, while the one period model's optimal planning value is influenced by Λ_{t_0} only. If $\Lambda_{t_0}^{(2)} > \Lambda_{t_0}^{(1)}$

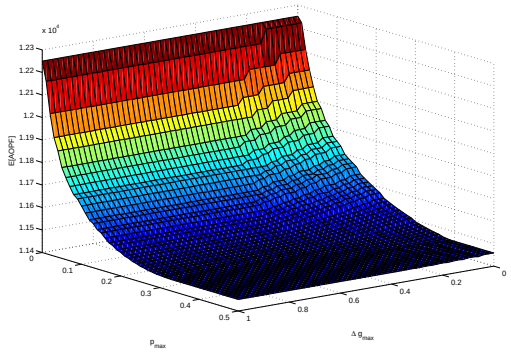

(a) Expected adapted optimal power flow cost against ramp rate and adequacy constraint, p_{max}, for second time step $t = t_1$.

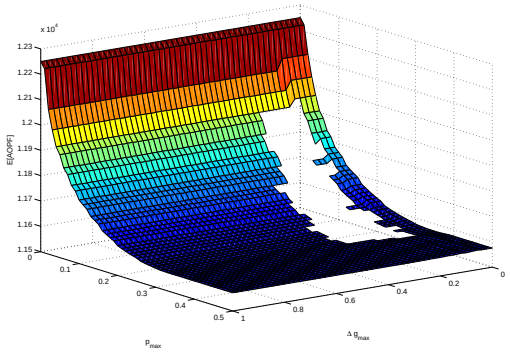

(b) Expected adapted optimal power flow cost against ramp rate and adequacy constraint, p_{max}, for fourth time step $t = t_3$.

Figure 3.23: In these plots we see the expected adapted optimal power flow cost for the first period plotted against various ramp rate values and adequacy constraint, p_{max}, values for the two period model. This can be seen for the second, figure 3.23(a), and fourth, figure 3.23(b), time step. I have plotted the second time step as this gives evidence to both constraints. Was I plot to the first time step, then the second constraint in (3.16) would not affect the model. The fourth time step shows how the constraints affects the solution as time passes.

the optimal planning value is higher for $\Delta g_{max} = 0$. This makes the model less conservative as there is a higher probability of wind speeds occurring that are below the optimal planning value and thus the model is more liable to the risk of having no solution in further time steps. This is due to the probability of load curtailment constraint. However, for solutions that do exist they are generally cheaper as the planned ratings are higher, due to higher planned wind speed values, so more cheaper generation can be utilised. The opposite is true for $\Lambda_{t_0}^{(2)} < \Lambda_{t_0}^{(1)}$. This model is more conservative then the one period model and will generally have more solutions for various values of p_{max} and will generally be more expensive than the one period model as the ratings will be lower and thus more power from the expensive generators will be dispatched.

We can generalise this for any time step. We saw in section 3.2.2 the effects that the second period has on the planning values in the two period model. This is turn affects the solutions that are available to us. We listed scenarios in section 3.2.2 for the various scale values, and the results of planning values when there was a difference in the scale values. These results carry forward to when adding an adequacy constraint. In the case when $\lambda_t^{(2)} > \lambda_t^{(1)} > \lambda_{t-1}^{(1)}$, the two period is cheaper than the one period

if $a_t^{(1)*} > a_t^{(1)''}$. Otherwise it is the same. If $a_t^{(1)*} > a_t^{(1)''}$ then the probability of load curtailment for the random variable $X_t^{(1)}$ will be greater than it would be in the one period model for the same time step. In this case the solution set will have higher probability of load curtailment and less solutions may be available to which meet the adequacy constraint in comparison to the one period model. The same is true for when $\lambda_{t-1}^{(1)} > \lambda_t^{(1)} > \lambda_t^{(2)}$.

The opposite is true for when $\lambda_t^{(2)} > \lambda_{t-1}^{(1)} > \lambda_t^{(1)}$ and $\lambda_t^{(1)} > \lambda_{t-1}^{(1)} > \lambda_t^{(2)}$. In these cases, $a_t^{(1)*} < a_t^{(1)''}$ and the solution set will be more expensive. However, the probability of load curtailment for the random variable $X_t^{(1)}$ will be lower than the corresponding one period model and the solution set will have lower probability of load curtailment values. In these cases, more solutions should be available than in the one period model.

Next we will examine how the expected adapted optimal power flow cost changes with time and maximum ramp rate, for various value of p_{max}. This is shown in figure 3.24 which shows three different curves, each ran under the same simulation, each with a different value of p_{max}. The top curve represents $p_{max} = 0.0$. This is flat for all values of t and Δg_{max}. This is the case as for very low values of p_{max}, the planning values are zero, and whether it is a still or windy day doesn't come into consideration. This will be the solution regardless of the ramp rate. This is approximately the static ratings method as using static ratings has a very low probability of overheating. Of course, true probability of load curtailment can never be zero due to random faults. The second curve represents $p_{max} = 0.1$. We can see that all costs are lower than then the curve representing $p_{max} = 0.0$. In this curve there are pieces missing meaning solutions weren't available. These correspond to the missing pieces of the curve in figure 3.23(b) as well as missing pieces that occur in subsequent time steps. The bottom curve corresponds to $p_{max} = 0.4$. As we can see no pieces are missing in this curve and solutions are much cheaper. However we pay for that by having a potentially unreliable power system. This amplifies the fact that a balance between security and economy must be established.

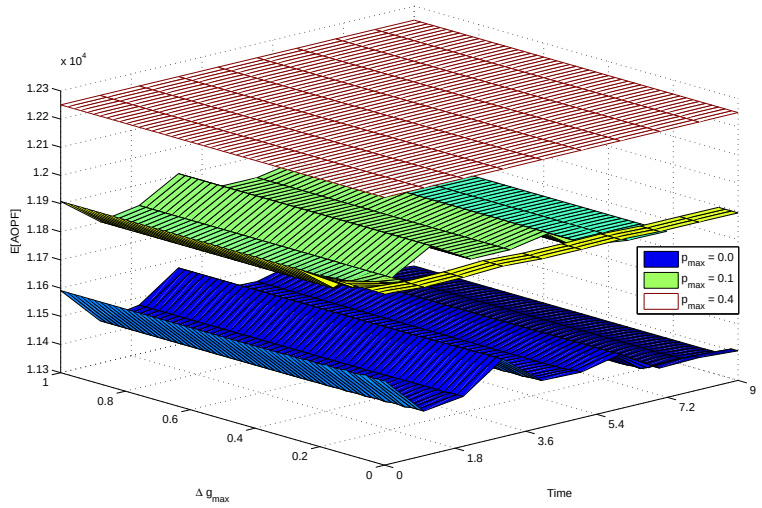

Figure 3.24: This figure shows three different curves, each ran under the same simulation, each with a different value of of p_{max}. The top curve represents $p_{max} = 0$. The second curve represents $p_{max} = 0.1$. The third curve represents $p_{max} = 0.4$.

3.3 Summary

In this chapter we examined the application of stochastic optimisation methods in power systems. Being able to plan for future time periods is of great benefit to system operators. We help the system operator to make uncertain decisions by running a stochastic optimisation over a random variable and choosing the minimum expected value. We then find the planning weather value corresponding to the minimum expected cost as a weather planning value implies generation by calculating dynamical thermal ratings and running an optimal power flow.

When we found the optimal planning value we did not consider the reliability in the system when dispatching future generation. To consider reliability we examined the model under a system adequacy constraint and system security constraint in which the adequacy or security index is bound by some maximum value that the system operator is willing to accept. We also examined the scenario of a ramp rate constraint. For bulk generators a lag time is normally involved for large shifts in the output power. For each time unit the output can change by a maximum amount known as the ramp rate. We added this constraint as so the model would have to look back at previous times steps.

A two period model was developed in which we were given two forecasts to plan for

the next two time steps, with the second decision liable to change in the subsequent time step. We introduced a ramp rate which coupled the two periods so we could not treat them as independent. Finally, an adequacy constraint was introduced as so the decision made by the system operator would have an adequacy index bound by some value as so keep the reliability in the system within a safe acceptable level.

The two period model was examined against the one period model. It was found under some weather forecast scenarios, the two period model can provide more expensive results while under other scenarios it can provide cheaper results. This was discussed in section 3.2.2. However, when cheaper results are available the model is generally less reliable and for some combinations of Δg_{max} and p_{max}, solutions may not be available that were available for the one period model. The opposite is true for more expensive solutions. The system is generally more reliable and for some combinations of Δg_{max} and p_{max}, solutions may be available that previously were not available for the one period model.

Chapter 4

Conclusions and further work

4.1 Conclusions

The aim of this thesis was to examine and improve the future of the resilience of a power system through the use of probabilistic methods. This is done by first using probabilistic risk assessment and comparing the quantitative results for current and future climate scenarios. Methods were then introduced which were shown to improve the resilience of the power system under stochastic conditions.

In chapter 2 we examined the resilience of a power system under the future probabilistic climate conditions devised by the Met Office, in the form of the UKCP09 climate projections. Dynamical thermal ratings coupled with random fault simulations were used and ran under various climate conditions. We first examined the adequacy of the system under secure conditions. We found that the future climate scenarios predicted by the UKCP09 will have a negative effect on a power system resulting in a higher costing and less reliable system. Next we examined the system from a probabilistic security perspective. This was done by generating random, time-dependent faults and then running power flows under these conditions. This was done while using dynamical thermal ratings. It was found that under random fault conditions, the model performs worse for the future climate scenarios, with load curtailments being more severe than in the current climate. A method was then implemented to increase the reliability of the power system. This was the temporary overload method. It was found the method reduces the effects of climate change on the system and performs better under more severe conditions.

In chapter 3 we examined using stochastic optimisation in which we optimised over the randomness encapsulated in future weather variables as to find the optimal future generation the system operator should dispatch. By adding constraints the system operator can choose to plan the dispatch which minimises costs and keeps the reliability of the system within a predefined set limit. We examine this for a one and two period model. To make the model more realistic we add ramp rate constraints. In the one period model it causes the optimisation to look back to the previous time step. This also occurs for the two period model. Another constraint is added which couples the first and second period in the two period model so the optimisations cannot be treated as independent.

Through the use of quantitative methods we have shown the impact that future climate change will have on a power system that incorporates dynamical thermal ratings. The temporary overload method was introduced which showed that introducing methods is necessary in order to keep the same level of resilience in a future power system that is present currently. This was just one method which was examined and the development of more would help make a future power system resilient. Being able to plan for future time periods is beneficial to the system operator and it was shown that using stochastic optimisation methods can help the system operator make decisions, while keeping the reliability of the power system within an acceptable bound. It is believed the development of these methods would further help the system operator. The code used in this thesis, along with any data used, is available from the author upon request.

4.2 Further work

A development of this thesis could be taking in various directions. Firstly, a move towards using a larger power system would increase the complexity of the methods used. In chapter 3 a simple trial and error method is used when the constraints are introduced. In this method minimum values are chosen and if they do not satisfy the constraints they are rejected and the next minimum is chosen. This is then repeated until the constraints are satisfied, or until no solution becomes available. If a larger

power system was introduced this method would not be feasible due to the large computation time involved. Therefore, development of stochastic optimisation methods would be one area of further work. This could be further developed if we were to introduce the full non-linear AC power flow equations. Only 50% of the National Grid's circuits are thermally constrained, the rest are voltage constrained. A move from DC to AC would not only increase the complexity but also the computation time involved.

Another method to examine would be to develop the two stochastic variable optimisation optimisation by involving constraints and subsequent time steps. We could also examine a two period model which has two random variables in each period. In the modelling the distribution for wind speed and temperature were independent. An investigation to correlating these distributions by means of examining joint density functions could lead to interesting work. Developing the two stochastic variable model to involve constraints and coupling between periods would result in the need for better optimisation techniques due to the computational burden involved when discretising the distributions.

A shift towards renewable energy is expected in the future as non-renewable resources become depleted. One problem associated with renewable energy is that there is a lot of uncertainty regarding the magnitude of its production, given some forms rely on stochastic weather conditions such as solar and wind production. Another development of the work in this thesis would be to make the model more realistic and introduce more stochasticity in the system. An example would be to introduce renewable energy in replacement of the generators, or working along side them. A particularly interesting case would be to have renewable wind energy that would be generated using the same wind that is used to calculate the ratings.

Appendix A

Generating Random Numbers Using Inverse Transform Method.

A.1 Inverse Transform Method

If a random variate U follows a uniform distribution in the interval [0, 1] the random variate $X = F^{-1}(U)$ has a cumulative probability distribution function F.
From this:

$$P(X \leq x) = P(F^{-1}(U) \leq x)$$

with $X = F^{-1}(U)$. Given F is a cumulative distribution function we know it is a monotonic increasing function. Therefore:

$$P(F^{-1}(U) \leq x) = P(U \leq F(x)).$$

As U is uniformly distributed in [0, 1]:

$$P(U \leq F(x)) = F(x)$$

and therefore:

$$P(X \leq x) = F(x).$$

Using this we can generate exponential and Weibull distributed random numbers from uniformly distributed random numbers.

A.2 Generating Exponentially Distributed Random Variables

An exponentially distributed random variate has a probability density function:

$$f(x) = \eta e^{-\eta x}$$

and a cumulative distribution function:

$$F(x) = 1 - e^{-\eta x}.$$

We can use the inverse transform method such that:

$$U = F(x) = 1 - e^{-\eta x}$$

so that:

$$X = F^{-1}(U) = -\frac{1}{\eta}\ln(1-U) = -\frac{1}{\eta}\ln(U)$$

where U is uniformly distributed random number on interval [0, 1] and X is an exponentially distributed random number with rate parameter η. If U is in a uniformly distributed random number between [0, 1] then so too is $1 - U$ and as such are interchangeable.

A.3 Generating Weibull Distributed Random Variables

The probability density function of the Weibull distribution takes the form:

$$f(x) = \frac{\beta}{\lambda}\Big(\frac{x}{\lambda}\Big)^{(\beta-1)} e^{-(\frac{x}{\lambda})^{\beta}}.$$

The cumulative distribution function takes the form:

$$F(x) = 1 - e^{-(\frac{x}{\lambda})^{\beta}}.$$

We can use the inverse transform method such that:

$$U = F(x) = 1 - e^{-(\frac{x}{\lambda})^{\beta}}$$

so that:

$$X = F^{-1}(U) = \lambda[-\ln(1-U)]^{\frac{1}{\beta}} = \lambda[-\ln(U)]^{\frac{1}{\beta}}$$

where U is uniformly distributed random number on interval [0, 1] and X is a Weibull distributed random number with scale parameter λ. and shape parameter β

Appendix B

Derivation of AC and DC Optimal Power Flow

B.1 Derivation of Alternating Current (AC) Optimal Power Flow

Kirchoff's current law states that the sum of currents meeting at a nodal point is zero. For a power system, the nodal equations, nodes being buses, are defined from Kirchoff's current law as:

$$\underline{I} = \mathbf{Y}\underline{V} \tag{B.1}$$

where I_i is the sum of injected currents at bus i, V_i is the bus voltage magnitude of bus i and $\mathbf{Y}$ is the admittance matrix which has values:

$$\begin{aligned} Y_{ii} &= \sum_{\substack{k=1 \\ k\neq i}}^{N} Y_{ik} \\ Y_{ik} = \ Y_{ki} &= \ -y_{ik} \end{aligned} \tag{B.2}$$

with:

$$y_{ik} = \frac{1}{r_{ik} + jx_{ik}} \tag{B.3}$$

where r_{ik} is the branch resistance between bus i and bus k and x_{ik} is the branch reactance. N is the number of buses in the system. j denotes the imaginary unit:

$$j = \sqrt{-1}$$

.

AC power, S_i, is complex and for bus i takes the form

$$S_i = P_i + jQ_i \tag{B.4}$$

where P_i and Q_i are the sum of the real power and reactive power injected at bus i respectively with:

$$\begin{aligned} P_i &= P_{gi} - P_{di} \\ Q_i &= Q_{gi} - Q_{di} \end{aligned} \tag{B.5}$$

where P_{gi} and Q_{gi} is the real and reactive power generated from bus i and P_{di} and Q_{di} is the real and reactive power demand at bus i.

Real and reactive power at bus i is calculated as:

$$\begin{aligned} P_i + jQ_i &= V_i \bar{I}_i \\ &= V_i \sum_{k=1}^{N} \bar{Y}_{ik} \bar{V}_k \\ &= \sum_{k=1}^{N} \bar{Y}_{ik} V_i \bar{V}_k \end{aligned} \tag{B.6}$$

where $\bar{I}_i$ denotes the complex conjugate of I_i. V_i is the voltage magnitude at bus i and can be wrote as:

$$V_i = |V_i| \angle \delta_i \tag{B.7}$$

where δ_i is the voltage angle at bus i.

Y_{ik} is the complex admittance and takes the form:

$$Y_{ik} = G_{ik} + jB_{ik} \tag{B.8}$$

where G_{ik} and B_{ik} are the conductance and susceptance respectively for branch connecting bus i and k. From (B.2) and (B.3):

$$\begin{aligned} G_{ik} &= \frac{r_{ik}}{r_{ik}^2 + x_{ik}^2} \\ B_{ik} &= \frac{-x_{ik}}{r_{ik}^2 + x_{ik}^2}. \end{aligned} \tag{B.9}$$

Substituting (B.7) and (B.9) into (B.6) we obtain:

$$\begin{aligned} P_i + jQ_i &= \sum_{k=1}^{N} (G_{ik} - jB_{ik}) |V_i| \angle \delta_i |V_k| \angle -\delta_k \\ &= \sum_{k=1}^{N} (G_{ik} - jB_{ik}) |V_i| |V_k| \angle (\delta_i - \delta_k) \\ &= \sum_{k=1}^{N} |V_i| |V_k| (G_{ik} - jB_{ik}) [\cos(\delta_i - \delta_k) + \sin(\delta_i - \delta_k)]. \end{aligned} \tag{B.10}$$

Therefore:

$$\begin{aligned} P_i &= \sum_{k=1}^{N} |V_i||V_k|[G_{ik}\cos(\delta_i - \delta_k) + B_{ik}\sin(\delta_i - \delta_k)] \\ Q_i &= \sum_{k=1}^{N} |V_i||V_k|[G_{ik}\sin(\delta_i - \delta_k) - B_{ik}\cos(\delta_i - \delta_k)]. \end{aligned} \tag{B.11}$$

The optimal power flow determines the real and reactive power dispatch from the generators at each bus that minimises the operating cost, while meeting system operating constraints. This is done by minimising the objective function, f_i, while satisfying (B.11) as equality constraints and satisfying operating limitation constraints on the voltage, the real and reactive output by each generator and the limitations of the transmission circuits. The AC optimal power flow is then defined as:

$$\min_{\underline{P}_g} \sum_{i=1}^{N} f_i(P_{gi})$$

subject to

$$\begin{aligned} P_i = & \sum_{k=1}^{N} |V_i||V_k|(G_{ik}\cos(\delta_i - \delta_k) + & B_{ik}\sin(\delta_i - \delta_k)) \\ Q_i = & \sum_{k=1}^{N} |V_i||V_k|(G_{ik}\sin(\delta_i - \delta_k) - & B_{ik}\cos(\delta_i - \delta_k)) \\ P_{gi,min} & \leq P_{gi} & \leq P_{gi,max} \\ Q_{gi,min} & \leq Q_{gi} & \leq Q_{gi,max} \\ V_{i,min} & \leq V_i & \leq V_{i,max} \\ & |F_{ik}| & \leq F_{ik,max} \end{aligned} \tag{B.12}$$

where $\underline{P}_g$ is the set of generator power outputs, f_i is the cost function for generator at bus i, P_{gi} is the power generated from generator i. $P_{gi,min}$ and $P_{gi,max}$ are the minimum and maximum real output power of generator i. $Q_{gi,min}$ and $Q_{gi,max}$ are the minimum and maximum complex output power of generator i, where Q_{gi} is the complex power output of generator i. $V_{i,min}$ and $V_{i,max}$ are the minimum and maximum voltage magnitudes at bus i. F_{ik} is the power flow between bus i and bus k. $F_{ik,max}$ is the maximum safe amount of power that can flow through the circuit connecting bus i to bus k. This is also known as the circuit rating.

For each bus in the network, we know two out of the following four variables: $P_i, Q_i, |V_i|$ and δ_i, so that for each bus, there are two equations available for two unknowns. This problem is one where we are required to solve simultaneous nonlinear

equations. Because most power systems are very large interconnections, with many buses, the number of power flow equations (and thus the number of unknowns) is very large. For example, a model of the UK power system has a few hundred buses.

The approach to solving the power flow problem, and the optimal power flow problem, is to use an iterative algorithm. The Newton-Raphson algorithm is the most commonly used algorithm in commercial power flow programs. This process involves starting with an initial guess. A linearised system of equations is then solved to find the next guess, using the initial guess. This method continues, using the previous guess to find the next guess, until a stopping criteria is met. Usually, this process requires 5-20 iterations to converge to a satisfactory solution. For large networks, it is computationally intensive. In the case where we want to re-run simulations for deterministic security analysis, such as $N-1$, we would need to look at using parallel computing to do the computation in a satisfactory time. A more detailed discussion of power flow computation can be found in [58] which was used as the source for this derivation.

B.2 Derivation of Direct Current (DC) Optimal Power Flow

To compensate for the computational burden of the AC power flow we can linearise these equations. We can then apply the linear equations to an optimisation function which will make computation of the optimal power flow much more time efficient. This is called a DC optimal power flow. Making DC approximations to the power flow equations consists of using the following three observations [44]:

1. The resistance, r_{ik}, of transmission circuits is significantly less than the reactance, x_{ik}. For a given transmission circuit the conductance and susceptance is defined in (B.9). If r_{ik} is small compared to x_{ik}, then G_{ik} is small compared to B_{ik}. We approximate G_{ik} and B_{ik} as:

$$\begin{aligned} G_{ik} &= 0 \\ B_{ik} &= \tfrac{-1}{x_{ik}}. \end{aligned} \tag{B.13}$$

From this (B.11) become:

$$\begin{aligned} P_i &= \sum_{k=1}^{N} |V_i||V_k|(B_{ik}\sin(\delta_i - \delta_k)) \\ Q_i &= \sum_{k=1}^{N} |V_i||V_k|(-B_{ik}\cos(\delta_i - \delta_k)). \end{aligned} \tag{B.14}$$

2. For most systems, the difference in angles between bus i and k is small. We use this to approximate $\cos(\delta_i - \delta_k) = 1$. It then seems logical to approximate $\sin(\delta_i - \delta_k) = 0$. However, a better approximation is $\sin(\delta_i - \delta_k) = \delta_i - \delta_k$. Applying this (B.14):

$$\begin{aligned} P_i &= \sum_{k=1}^{N} |V_i||V_k|(B_{ik}(\delta_i - \delta_k)) \\ Q_i &= \sum_{k=1}^{N} |V_i||V_k|(-B_{ik}). \end{aligned} \tag{B.15}$$

Expanding B_{ik}:

$$\begin{aligned} B_{ik} &= -b_{ik} && \text{if } i \neq k \\ B_{ii} &= b_{ii} + \sum_{\substack{k=1 \\ k\neq i}}^{N} b_{ik} && \text{if } i = k \end{aligned} \tag{B.16}$$

Substituting (B.16) into (B.15) obtains:

$$\begin{aligned} P_i &= \sum_{k=1}^{N} |V_i||V_k|(B_{ik}(\delta_i - \delta_k)) \\ Q_i &= -|V_i|^2 b_{ii} + \sum_{k=1}^{N} |V_i||b_{ik}|(|V_i| - |V_k|) \end{aligned} \tag{B.17}$$

3. In per unit systems the numerical values of voltage magnitudes $|V_i|$ and $|V_k|$ are very close to 1.0. Typical range under most operating conditions is 0.95 to 1.05. Given this we can approximate $|V_i| = |V_k| = 1$. However, we can not approximate $|V_i| - |V_k| = 0$ as the difference of two numbers close to 1 can range significantly. Substituting this into (B.17) we obtain

$$\begin{aligned} P_i &= \sum_{k=1}^{N} (B_{ik}(\delta_i - \delta_k)) \\ Q_i &= -b_{ii} + \sum_{k=1}^{N} |V_i||b_{ik}|(|V_i| - |V_k|) \end{aligned} \tag{B.18}$$

The reactive power flow equation is proportional to the circuit susceptance and the difference in voltage phasor magnitudes. The maximum difference in voltage phasor magnitudes will be on the order of 1.05-0.95=0.1. The real power flow equation is proportional to the circuit susceptance and the difference in voltage phasor angles. The maximum difference in voltage phasor angles will be, in radians, about 0.52. From this we can assume:

$$P_i \gg Q_i. \tag{B.19}$$

Finding the absolute value of (B.6), we can rewrite as:

$$|I_i| = \frac{\sqrt{P_i^2 + Q_i^2}}{|V_i|}. \tag{B.20}$$

Using approximation of (B.19):

$$|I_i| \approx \frac{\sqrt{P_i^2}}{|V_i|} = \frac{|P_i|}{|V_i|} \approx |P_i| \tag{B.21}$$

Therefore we neglect Q_i in (B.18)

We have eliminated the reactive power terms in (B.12) and we have linearised the real power flow equation. We can neglect the reactive power constraint and the voltage magnitude constraint. The transformation from the AC power flow (B.12) to DC evaluates to:

$$\begin{aligned} &\min_{\underline{P}_g} \sum_{i=1}^{N} f_i(P_{gi}) \\ &\text{subject to} \\ &\qquad P_i = \quad \sum_{j=1}^{N} (B_{ij}(\delta_i - \delta_k)) \\ P_{gi,min} \leq \quad &P_{gi} \quad \leq P_{gi,max} \\ &|F_{ik}| \quad \leq F_{ik,max} \end{aligned} \tag{B.22}$$

which is much simpler to solve than (B.12) as we can use linear programming techniques.

Appendix C

Maximum Likelihood Estimation

Let $x_1, x_2, \ldots, x_n$ be a sample of independent and identically distributed observations, coming from a distribution with unknown probability density function $f_X(x;\theta)$ where θ is an unknown parameter and referred to as the *true value* of the parameter. We can find an estimation of θ by using the maximum likelihood method. This estimation is denoted $\hat{\theta}$.

The likelihood function of an independent and identically distributed sample is the joint density function and is a function of the unknown parameter θ, with the values x_i seen as fixed parameters:

$$\mathcal{L}(\theta; x_1, \ldots, x_n) = \Pi_{i=1}^{n} f_{X_i}(x_i; \theta). \tag{C.1}$$

The maximum likelihood of θ is the value of θ that maximises $\mathcal{L}(\theta; x_1, \ldots, x_n)$, or for simplicity, maximises $\ln \mathcal{L}(\theta; x_1, \ldots, x_n)$, where ln is the natural logarithm. Moreover, in the case where the logarithm of (C.1) is differentiable (as is the case for the Weibull distribution and Normal distribution), we find the value of $\hat{\theta}$ by finding the solution of:

$$\frac{d \ln \mathcal{L}(\theta; x_1, \ldots, x_n)}{d\theta} = 0 \tag{C.2}$$

where θ can be a vector of parameters. Since the logarithm function is strictly increasing then the values which maximise the likelihood will also maximise its logarithm. To examine is the solution unique we must examine the second derivative of the likelihood. If it is negative we can conclude the value of $\hat{\theta}$ we found is the unique maximum.

C.1 Maximum Likelihood Estimation for Weibull Distribution

To solve for the Weibull parameters $f_X(x;\theta)$ takes the form of (2.8). Therefore $\theta = [\lambda \quad \beta]^T$, where superscript T denotes the transpose. (C.1) takes the form:

$$\mathcal{L}(\lambda,\beta;x_1,\ldots,x_n) = \Pi_{i=1}^{n}\Big(\frac{\beta}{\lambda}\Big)\Big(\frac{x_i}{\lambda}\Big)^{\beta-1}\exp\Big((\frac{x_i}{\lambda})^{\beta}\Big). \tag{C.3}$$

Taking the logarithm of (C.3) and differentiating with respect to λ and β we obtain:

$$\begin{aligned} \frac{\partial \ln \mathcal{L}}{\partial \lambda} &= -\frac{n}{\hat{\lambda}} + \frac{1}{\hat{\lambda}^2}\sum_{i=1}^{n}\ln x_i^{\hat{\beta}} &= 0 \\ \frac{\partial \ln \mathcal{L}}{\partial \beta} &= \frac{n}{\hat{\beta}} + \sum_{i=1}^{n}\ln x_i - \frac{1}{\hat{\lambda}}\sum_{i=1}^{n} x_i^{\hat{\beta}}\ln x_i &= 0 \end{aligned} \tag{C.4}$$

where $\hat{\lambda}$ and $\hat{\beta}$ are the maximum likelihood estimates of λ and β respectively. Rearranging (C.4) we can set:

$$\begin{aligned} \hat{\lambda} &= \frac{\sum_{i=1}^{n}\ln x_i^{\hat{\beta}}}{\lambda} \\ 0 &= \frac{\sum_{i=1}^{n} x_i^{\hat{\beta}}\ln x_i}{\sum_{i=1}^{n} x_i^{\hat{\beta}}} - \frac{1}{\hat{\beta}} - \frac{1}{n}\sum_{i=1}^{n}\ln x_i \end{aligned} \tag{C.5}$$

We can then use an iterative method to solve for $\hat{\beta}$, such as the Newton-Ramphson method. Upon evaluation, we can use simple substitution to arrive with an answer for $\hat{\lambda}$.

C.2 Maximum Likelihood Estimation for Normal Distribution

To solve for the gaussian parameters $f_X(x;\theta)$ takes the form of (3.7). Therefore $\theta = [\mu \quad \sigma^2]^T$, where superscript T denotes the transpose. (C.1) takes the form:

$$\mathcal{L}(\mu,\sigma^2;x_1,\ldots,x_n) = \Big(\frac{1}{2\pi\sigma^2}\Big)^{\frac{n}{2}}\exp\Big(-\frac{\sum_{i=1}^{n}(x_i-\mu)^2}{2\sigma^2}\Big) \tag{C.6}$$

Taking the logarithm of (C.6) and differentiating with respect to μ and σ^2 we obtain:

$$\begin{aligned} \frac{\partial \ln \mathcal{L}}{\partial \mu} &= \frac{\sum_{i=1}^{n}(x_i-\hat{\mu})}{\sigma^2} &= 0 \\ \frac{\partial \ln \mathcal{L}}{\partial \sigma^2} &= -\frac{n}{2\sigma^2} + \frac{\sum_{i=1}^{n}(x_i-\hat{\mu})^2}{2\sigma^4} &= 0. \end{aligned} \tag{C.7}$$

where $\hat{\mu}$ and $\hat{\sigma}^2$ are the maximum likelihood estimates of μ and σ^2 respectively. We can then solve for $\hat{\mu}$ and $\hat{\sigma}^2$ by first solving for $\hat{\mu}$:

$$\hat{\mu} = \frac{\sum_{i=1}^{n} x_i}{n} \tag{C.8}$$

and then solving for $\hat{\sigma}^2$:

$$\hat{\sigma}^2 = \frac{\sum_{i=1}^{n} (x_- \hat{\mu})^2}{n} \tag{C.9}$$

and substituting the value of $\hat{\mu}$ found in (C.8) into (C.9). We could also solve first for $\hat{\sigma}^2$ by substituting (C.8) into (C.9):

$$\hat{\sigma}^2 = \frac{1}{n} \sum_{i=1}^{n} x_i^2 - \frac{1}{n^2} \sum_{i=1}^{n} \sum_{j=1}^{n} x_i x_j. \tag{C.10}$$

Appendix D

Nomenclature for Chapter One

A	Area of conductor per unit length.
B_{ij}	Susceptance of the circuit between bus i and bus j.
C_i	Load curtailed in system state i.
D	Diameter of the conductor.
$EDLC$	Expected duration of load curtailment.
$EDNS$	Expected demand not supplied.
$\underline{f}_0(\cdot)$	Cost function vector.
$f_i(\cdot)$	Cost function for generator i.
F_{ij}	Power flow between bus i and bus j.
$F_{ij,max}$	Maximum safe amount of power that can flow through the circuit connecting bus i to bus j.
G_{ij}	Conductance of the circuit between bus i and bus j.
$\underline{g}_k(\cdot)$	Power flow equality equations.
H_c	Altitude of the sun.
$\underline{h}_k(\cdot)$	Power flow inequality equations.
I	Current.
I_{max}	Maximum safe operating current.
I_N	Normal conductor rating corresponding to I_{max}.
$Im(\cdot)$	Impact.
K_{angle}	Wind direction factor.
k_f	Thermal conductivity of air.
N_B	Number of buses.

P_{di}	Real power demand at bus i.
$\underline{P}_g$	Vector of real power outputs.
P_{gi}	Real power generated from generator i.
P_i	Real power injection at bus i.
p_i	Probability of being in state i.
PLC	Probability of load curtailment.
$Q_c(\cdot)$	Forced convection.
$P_{gi,max}$	Maximum real output power of generator i.
$P_{gi,min}$	Minimum real output power of generator i.
$Q_{ch}(\cdot)$	Convection during high wind speeds.
$Q_{cl}(\cdot)$	Convection during low wind speeds.
$Q_{cn}(\cdot)$	Convection during zero wind speed.
$Q_{di}(\cdot)$	Reactive power demand at bus i.
Q_{gi}	Reactive power generated from generator i.
$Q_{gi,max}$	Maximum reactive output power of generator i.
$Q_{gi,min}$	Minimum reactive output power of generator i.
Q_i	Reactive power injection at bus i.
Q_s	Solar heat gain due to radiation from the sun.
Q_{se}	Total solar and sky radiated heat flux rate elevation corrected.
$R(\cdot)$	Resistance of conductor.
$Risk(\cdot)$	Risk index.
$RiskC_{ij}$	Expected risk of circuit ij
$RiskV_k$	Expected risk of bus k.
S	Set of all system states.
$\underline{u}_k$	Control variables.
V_i	Voltage at bus i.
$V_{i,max}$	Maximum voltage at bus i.
$V_{i,min}$	Minimum voltage at bus i.
$\underline{x}_k$	State variables.
W_s	Wind Speed.
$\underline{z}$	Set of weather parameters.
Z_c	Azimuth of the sun.

Z_l	Azimuth of the line.
α	Solar absorbability of the conductor.
β	Temperature coefficient of resistance.
δ_i	Voltage angle at bus i.
η	Hazard Rate.
θ_a	Ambient temperature.
θ_c	Conductor temperature.
θ_{max}	Maximum safe operating temperature.
ω	Weighting coefficients.
μ	Repair rate.
μ_f	Dynamic viscosity of air.
ρ_f	Density of air.
ϕ	Angle at which the wind meets the conductor.

Appendix E

Nomenclature for Chapter Two

A	Bus adjacency matrix.
$\mathbf{B}'$	Nodal admittance matrix.
B_{ij}	Susceptance of the circuit between bus i and bus j.
$\mathbf{C}$	Connection matrix.
$\mathbf{D}$	Adjacency (node-arc) matrix.
$f_i(\cdot)$	Cost function for generator i.
$f(t)$	Probability density function.
$F(t)$	Cumulative distribution function.
F_{ij}	Power flow between bus i and bus j.
$F_{ij,max}$	Maximum safe amount of power that can flow through the circuit connecting bus i to bus j.
G_{ij}	Conductance of the circuit between bus i and bus j.
$g(\cdot)$	Load curtailment cost function.
$\mathbf{I}$	Identity matrix.
I_{max}	Maximum safe operating current for conductor.
I_t	Current flowing through conductor at time t.
L_i	Load demanded in run i.
l_i	Load delivered in run i.
N_B	Number of buses.
$\underline{P}$	Vector of power injections.
$\underline{P}_B$	Vector of line flows.
$\underline{P}_{B,max}$	Vector of line ratings.

P_{di}	Real power demand at bus i.
$\underline{P}_g$	Vector of real power outputs.
P_{gi}	Real power generated from generator i.
$P_{gi,max}$	Maximum real output power of generator i.
$P_{gi,min}$	Minimum real output power of generator i.
P_i	Real power injection at bus i.
$R(t)$	Reliability (survival) function.
t_a	First failure time corresponding to "aging" hazard rate.
t_c	First failure time corresponding to constant "random" hazard rate.
t_{derate}	First failure time to derate state.
t_{down}	First failure time to down state.
t_f	First failure time. $t_f = \min(t_{down}, t_{derate})$.
t_r	First time to repair.
V_i	Voltage at bus i.
β	Shape parameter for Weibull Distribution.
δ_i	Voltage angle at bus i.
η_c	Constant hazard rate for exponential distribution.
η_{down}	Hazard rate for transition from up to down state
η_{derate}	Hazard rate for transition from up to derate state
$\eta_t/\eta(t)$	Time dependent hazard rate.
$\eta_t^{\beta>1}$	Increasing time dependent hazard rate corresponding to $\beta > 1$ in Weibull Distribution.
$\eta_t^{\beta=1}$	Constant hazard rate corresponding to $\beta = 1$ in Weibull Distribution.
$\eta_t^{\beta<1}$	Decreasing time dependent hazard rate corresponding to $\beta < 1$ in Weibull Distribution.
η_t^o	Observed time dependent hazard rate for bathtub curve.
$\underline{\theta}$	Vector of bus voltage angles.
θ_a	Ambient temperature of conductor.
θ_{max}	Maximum safe operating temperature of conductor.
θ_t	Absolute temperature of conductor at time t.
Θ_t	Relative temperature of conductor at time t.
λ	Scale parameter for Weibull Distribution.
μ	Constant repair rate for exponential distribution.

τ	Thermal time constant.

Appendix F

Nomenclature for Chapter Three

a_t	Planning value for time t for one period model.
a_t^*	Optimal planning value for time t for one period model.
$a_t^{(1)}$	First period planning value for time t for two period model.
$a_t^{(2)}$	Second period planning value for time t for two period model.
$a_t^{(p)\prime}$	p^{th} period optimal planning value for time t for unconstrained model for two period model.
$a_t^{(p)\prime\prime}$	p^{th} period optimal planning value for time t for that satisfies constraint (3.23) for two period model.
$a_t^{(p)*}$	p^{th} period optimal planning value for time t for that satisfies constraint model, i.e (3.23) and (3.25), for two period model.
$\mathbf{a}_t$	Set of planning values for time t containing a_{X_t} and a_{Y_t} for one period model.
$\mathbf{a}_t^*$	Set of optimal planning values for time t containing $a_{X_t}^*$ and $a_{Y_t}^*$ for one period model.
a_{X_t}	Planning value at time t corresponding to random variable X_t for one period model.
a_{Y_t}	Planning value at time t corresponding to random variable Y_t for one period model.
$a_{X_t}^*$	Planning value at time t corresponding to random variable X_t for one period model.
$a_{Y_t}^*$	Planning value at time t corresponding to random variable Y_t for one period model.
B_{ij}	Susceptance of the circuit between bus i and bus j.
CLC	Cost of load curtailment.
CLC_{max}	Maximum cost of load curtailment accepted by system operator.
C_g	Generator output cost vector.

$c(x_k, a_t)$	Cost function using sample x_k and planning value a_t.
$f_i(\cdot)$	Cost function for generator i.
F_{ij}	Power flow between bus i and bus j.
$F_{ij,max}(x_k)$	Maximum safe amount of power that can flow through the circuit connecting bus i to bus j calculated using ratings with weather parameters x_k.
$F_{ij,max}(a_t)$	Maximum safe amount of power that can flow through the circuit connecting bus i to bus j calculated using ratings with weather parameters a_t.
$f_{X_t}(\cdot)$	Probability density function with random variable X_t.
L	Load demanded.
l_i	Load delivered in state i.
l_{x_i,a_t}	Load delivered when the random variable X_t takes value x_i using planning value a_t.
IL	Interruptible load.
$ILC(\cdot)$	Interruptible load function.
M	Number of discrete values when discretising X_t.
N_B	Number of buses.
$\underline{P}$	Vector of power injections.
$\underline{P}_B$	Vector of line flows.
$\underline{P}_{B,max}$	Vector of line ratings.
P_{di}	Real power demand at bus i.
$\underline{P}_g$	Set of real power outputs.
P_{gi}	Real power generated from generator i.
$P_{gi}^{a_t}$	Power generated from generator i when ratings $\underline{F}_{max}(a_t)$ are used.
$P_{gi,max}$	Maximum real output power of generator i.
$P_{gi}(a_t)$	Generation from generator i associated to planning value a_t and is set by first running an optimal power flow with ratings $\underline{F}_{max}(a_t)$ and maximum generation $P_{gi,max}$
P_i	Real power injection at bus i.
$P(X_t = x_i)$	Probability random variable X_t takes value x_i.
p_i	Probability of being in system state i
p_{max}	Maximum probability of load curtailment accepted by system operator.
t_0	Initial starting time.

u_t	Normal random variable at time t with mean zero and variance 0.5.
V_t	Minimum expected cost function at time t.
$V_t(a_t)$	Expected cost function using planning value a_t, and the t^{th} forecast X_t.
x_k	Sample k from random variable X_t.
X_t	Random variable at time t that follows probability distribution $f_{X_t}(\cdot)$.
$X_t^{(1)}$	Random variable at time t for first period of two period model.
$X_t^{(2)}$	Random variable at time t for second period of two period model.
$\mathbf{X}_t$	Set of random variables at time t containing X_t and Y_t.
Y_t	Random variable at time t that follows probability distribution $f_{Y_t}(\cdot)$.
β	Shape parameter for Weibull Distribution.
$\Gamma(\cdot)$	Gamma function.
δ_i	Voltage angle at bus i.
Δg_{max}	Maximum ramp rate.
$\Delta g(a_{t-1}, a_t)$	Change in generation output between times $t-1$ and t using planning values a_{t-1} and a_t.
$\Delta g(a_t^{(1)}, a_t^{(2)})$	Change in generation output between first and second period at time t using planning values $a_t^{(1)}$ and $a_t^{(2)}$.
ϵ_t	Standard normal random variable at time t.
$\epsilon_t^{(1)}$	Standard normal random variable at time t for first period scale parameter in two period model.
$\epsilon_t^{(2)}$	Standard normal random variable at time t for second period scale parameter in two period model.
ζ_t	Standard normal random variable at time t.
λ_0	Initial scale parameter for Weibull Distribution.
Λ_t	Random scale parameter for Weibull Distribution at time t.
$\Lambda_t^{(1)}$	Random scale parameter for Weibull Distribution at time t for one period forecast in two period model.
$\Lambda_t^{(2)}$	Random scale parameter for Weibull Distribution at time t for two period forecast in two period model.
μ	Mean parameter for normal distribution.
μ_0	Initial mean parameter for normal distribution.
μ_t	Random mean parameter for normal distribution at time t.
σ	Standard deviation of normal distribution.
σ^2	Variance of normal distribution.

Bibliography

[1] K. Anderson. RESNET: Resilient electricity networks for Great Britain. http://www.arcc-cn.org.uk/wp-content/pdfs/RESENET.pdf. Accessed: December 2012.

[2] W. Li. *Risk Assessment Of Power Systems: Models, Methods, and Applications*. John Wiley & Sons, May 2005.

[3] P. Smith, D. Hutchison, J.P.G. Sterbenz, M. Scholler, A. Fessi, M. Karaliopoulos, C. Lac, and B. Plattner. Network resilience: a systematic approach. *IEEE Communications Magazine*, 49(7):88 –97, July 2011.

[4] J.D. McCalley, V. Vittal, and N. Abi-Samra. An overview of risk based security assessment. In *Power Engineering Society Summer Meeting, 1999. IEEE*, volume 1, pages 173 –178 vol.1, July 1999.

[5] R. Billinton and W. Li. *Reliability Assessment of Electrical Power Systems Using Monte Carlo Methods*. Springer, November 1994.

[6] M. MacDonald. Capacity mapping and market scenarios for 2010 and 2020. www.berr.gov.uk/files/file23772.pdf. Accessed: December 2012.

[7] B. S Howington and G. J Ramon. Dynamic thermal line rating summary and status of the state-of-the-art technology. *IEEE Transactions on Power Delivery*, 2(3):851–858, July 1987.

[8] D. Roberts, P. Taylor, and A. Michiorri. Dynamic thermal rating for increasing network capacity and delaying network reinforcements. In *SmartGrids for Distribution, 2008. IET-CIRED. CIRED Seminar*, pages 1–4. IET, June 2008.

[9] L. Trigeorgis, editor. *Real Options and Business Strategy: Applications to Decision Making*. Risk Publications, 1 edition, December 1999.

[10] R. Billinton and R. N. Allan. *Reliability Assessment of Large Electric Power Systems*. Springer, March 1988.

[11] A. R. Bergen. *Power systems analysis*. Prentice-Hall, 1986.

[12] D.I. Sun, B. Ashley, B. Brewer, A. Hughes, and W.F. Tinney. Optimal power flow by newton approach. *IEEE Transactions on Power Apparatus and Systems*, PAS-103(10):2864 –2880, October 1984.

[13] J. J. Grainger and W. D. Stevenson. *Power system analysis*. McGraw-Hill, January 1994.

[14] Co-ordination and specification of plant thermal ratings. National Grid: Policy Statement (Transmission) Note 060 Issue 3, June 2011.

[15] Current ratings for overhead lines. National Grid: Technical Guidance Note 26 Issue 3, April 2001.

[16] W.S. Wadman, G. Bloemhof, D. Crommelin, and J. Frank. Probabilistic power flow simulation allowing temporary current overloading. http://homepages.cwi.nl/ wadman/work/137.pdf, June 2012.

[17] IEEE standard for calculating the current-temperature of bare overhead conductors. *IEEE Std 738-2006 (Revision of IEEE Std 738-1993)*, pages c1 –59, 2007.

[18] D. A Douglass, D. C Lawry, A. A Edris, and E. C. Bascom. Dynamic thermal ratings realize circuit load limits. *IEEE Computer Applications in Power*, 13(1):38–44, January 2000.

[19] J.W. Jerrell, W.Z. Black, and T.J. Parker. Critical span analysis of overhead conductors. *IEEE Transactions on Power Delivery*, 3(4):1942 –1950, October 1988.

[20] D. A Douglass and A. A Edris. Field studies of dynamic thermal rating methods for overhead lines. In *1999 IEEE Transmission and Distribution Conference*, volume 2, pages 842–851 vol.2. IEEE, April 1999.

[21] K. E Holbert and G. T Heydt. Prospects for dynamic transmission circuit ratings. In *The 2001 IEEE International Symposium on Circuits and Systems, 2001. ISCAS 2001*, volume 3, pages 205–208 vol. 2. IEEE, May 2001.

[22] H. T Yip, C. An, G. J Lloyd, P. Taylor, A. Michiorri, S. Jupe, and M. Bartlett. Dynamic thermal rating and active control for improved distribution network utilisation. In *Managing the Change, 10th IET International Conference on Developments in Power System Protection (DPSP 2010)*, pages 1–5. IET, April 2010.

[23] A. Michiorri and P. Taylor. Forecasting real-time ratings for electricity distribution networks using weather forecast data. In *20th International Conference and Exhibition on Electricity Distribution - Part 1, 2009. CIRED 2009*, pages 1–4. IET, June 2009.

[24] A. Piccolo, A. Vaccaro, and D. Villacci. Thermal rating assessment of overhead lines by affine arithmetic. *Electric Power Systems Research*, 71(3):275–283, November 2004.

[25] P. Pytlak, P. Musilek, and E. Lozowski. Precipitation-based conductor cooling model for dynamic thermal rating systems. In *2009 IEEE Electrical Power & Energy Conference (EPEC)*, pages 1–7. IEEE, October 2009.

[26] B. Pouckovic and Z. Djurisic. Current carrying capacity of overhead line that connects wind power plant to the grid. In *2011 10th International Conference on Environment and Electrical Engineering (EEEIC)*, pages 1 –4, May 2011.

[27] F.R. McElvain and S.S. Mulnix. Statistically determined static thermal ratings of overhead high voltage transmission lines in the rocky mountain region. *IEEE Transactions on Power Systems*, 15(2):899 –902, May 2000.

[28] R. Billinton and R.N. Allan. Power-system reliability in perspective. *Electronics and Power*, 30(3):231 –236, March 1984.

[29] R. N. Allan and R. Billinton. *Reliability Evaluation of Power Systems*. Springer, August 1996.

[30] B. Stott, O. Alsac, and A.J. Monticelli. Security analysis and optimization. *Proceedings of the IEEE*, 75(12):1623 – 1644, December 1987.

[31] H. Wan, J. D McCalley, and V. Vittal. Increasing thermal rating by risk analysis. *IEEE Transactions on Power Systems*, 14(3):815–828, August 1999.

[32] W. Fu and J.D. McCalley. Risk based optimal power flow. In *Power Tech Proceedings, 2001 IEEE Porto*, volume 3, page 6 pp. vol.3, 2001.

[33] H. Wan, J.D. McCalley, and V. Vittal. Risk based voltage security assessment. *IEEE Transactions on Power Systems*, 15(4):1247 –1254, November 2000.

[34] A.P. Meliopoulos, A.G. Bakirtzis, and R. Kovacs. Power system reliability evaluation using stochastic load flows. *IEEE Transactions on Power Apparatus and Systems*, PAS-103(5):1084 –1091, May 1984.

[35] Y. Li and J.D. McCalley. Risk-based optimal power flow and system operation state. In *Power Energy Society General Meeting, 2009. PES '09. IEEE*, pages 1 –6, July 2009.

[36] M.A. Rios, D.S. Kirschen, D. Jayaweera, D.P. Nedic, and R.N. Allan. Value of security: modeling time-dependent phenomena and weather conditions. *IEEE Transactions on Power Systems*, 17(3):543 – 548, August 2002.

[37] JF. Moon, JC. Kim, HT. Lee, CH Park, and SY. Yun. Reliability evaluation of distribution system through the analysis of time-varying failure rate. pages 668 – 673 Vol.1, 2004.

[38] J. He, L. Cheng, D.S. Kirschen, and Y. Sun. Optimising the balance between security and economy on a probabilistic basis. *IET Generation, Transmission Distribution*, 4(12):1275 –1287, December 2010.

[39] J. Bai, H.B. Gooi, L.M. Xia, G. Strbac, and B. Venkatesh. A probabilistic reserve market incorporating interruptible load. *Power Systems, IEEE Transactions on*, 21(3):1079 –1087, August 2006.

[40] C.S. Chen and J.T. Leu. Interruptible load control for taiwan power company. *IEEE Transactions on Power Systems*, 5(2):460 –465, May 1990.

[41] Met Office. http://www.metoffice.gov.uk/about-us. Accessed: December 2012.

[42] P. D. Jones, C. G. Kilsby, C. Harpham, V. Glenis, and A. Burton. UK climate projections science report: Projections of future daily climate for the UK from the weather generator. *University of Newcastle, UK*, 2009.

[43] Weather generator. http://ukclimateprojections.defra.gov.uk/23261. Accessed: December 2012.

[44] J. McCalley. Lecture in Steady-State Analysis: The DC Power Flow Equations. http://home.eng.iastate.edu/ jdm/ee553/DCPowerFlowEquations.pdf. Accessed: December 2012.

[45] Cai D.W.H. Tan, C. W. and X. Lou. DC optimal power flow: Uniqueness and algorithms. *IEEE Smart Grid 2012 Workshop*, July 2012.

[46] National grid: Metered half-hourly electricity demands. http://www.nationalgrid.com/uk/Electricity/Data/Demand+Data/. Accessed: December 2012.

[47] MATLAB. *version 7.12.0 (R2011a)*. The MathWorks Inc., Natick, Massachusetts, 2011.

[48] R.D. Zimmerman, C.E. Murillo-Sanchez, and R.J. Thomas. MATPOWER: steady-state operations, planning, and analysis tools for power systems research and education. *Power Systems, IEEE Transactions on*, 26(1):12 –19, February 2011.

[49] MathWorks united kingdom - solve linear programming problems - MATLAB. http://www.mathworks.co.uk/help/optim/ug/linprog.html. Accessed: December 2012.

[50] L. Koralov and Y. G. Sinai. *Theory of Probability and Random Processes*. Springer, November 2007.

[51] B. S. Everitt and A. Skrondal. *The Cambridge Dictionary of Statistics*. Cambridge University Press, August 2010.

[52] Xlpe land cable systems user's guide. Accessed: December 2012.

[53] A. Shapiro, D. Dentcheva, and A. Ruszczynski. *Lectures on Stochastic Programming: Modeling and Theory*. SIAM, October 2009.

[54] B. Safari and J. Gasore. A statistical investigation of wind characteristics and wind energy potential based on the weibull and rayleigh models in rwanda. *Renewable Energy*, 35(12):2874–2880, December 2010.

[55] British atmospheric data centre (BADC). Accessed: December 2012.

[56] M. A Al-Fawzan. Methods for estimating the parameters of the weibull distribution. *King Abdulaziz City for Science and Technology, Riyadh, Saudi Arabia*, 2000.

[57] J. Sun and L. Tesfatsion. DC optimal power flow formulation and solution using quadprogj. *ISU Economics Working Paper No. 06014*, July 2010.

[58] Hadi Saadat. *Power System Analysis Third Edition*. PSA Publishing, THIRD EDITION edition, June 2010.